IMPERIAL COLLEGE OF SCIENCE, TECHNOLOGY AND MEDICINE

Oil and Natural Gas Division,

Department of Earth Resources Engineering

THE KINETICS OF CALCIUM CARBONATE PRECIPITATION AND THE APPLICATION TO OILFIELD SCALING PROBLEMS

by

YUPING ZHANG

A thesis submitted for the degree of doctor of Philosophy of the University of London, and the Diploma of Membership of the Imperial College.

London May 1997

本文谨献给我的父母亲

This thesis is dedicated to my parents

ABSTRACT

This thesis is concerned with the kinetics of calcium carbonate precipitation and scaling from oilfield formation waters. When water is produced during oil production scale formation often occurs and causes expensive production problems. Calcium carbonate, $CaCO_3$, is one of the most common scale components found in oilfield production wells and surface facilities. It is important to know where, when and how much $CaCO_3$ scale will be deposited during oil and water production. Many computer models have been developed to predict the thermodynamic tendency of scaling, but the kinetics have usually been neglected due to a lack of a reliable kinetic model to predict how fast the scale will build-up.

The aims of this work have been to study the kinetics of $CaCO_3$ precipitation, including the nucleation which controls when scaling will start, and the crystal growth rate which determines how fast the scale will build-up. The effects of supersaturation, temperature, pH, ionic strength and the presence of Mg^{2+}, organic acids and a gas-liquid interface on the calcite growth kinetics have been examined. $CaCO_3$ precipitation experiments were conducted at temperatures up to 70°C and one atmosphere by a pH-free-drift method and visual observation inside a glass micromodel. The calcite growth rates have been determined from solution pH changes during calcite growth in a closed system and by the observation of the crystal size change in a solution with a constant supersaturation and constant flow velocity in a glass micromodel. Analysis of carbonate species when organic acids are present has also been developed.

The major results from this study include:

- A analytical method to analyse both carbonate species and organic acids has been developed using acid titration by an automatic titrator and some mathematical data treatment.
- The presence of a gas phase increases the $CaCO_3$ nucleation rate. This is one of the important reasons why most field $CaCO_3$ scale starts after the liquid bubble point has been reached.
- The presence of Mg^{2+} inhibits the calcite growth rate and also modifies the morphology of the crystals due to the Mg^{2+} density on newly formed surfaces being higher than on the original surfaces. The distribution of Mg^{2+} ions on the calcite surfaces will be not stable at the initial stage of calcite growth when calcite seeds are used.
- The $CaCO_3$ scaling rate of oilfield produced waters can be estimated from the kinetic data and the rate equation obtained from this study.

$$R_L = k_p (S^{0.5} - 1)^2$$

$$\log k_p = 0.1257(IS)^{0.5} - 2504/T - 2.03$$

CONTENTS

NOMENCLATURE

Symbol	Name	*Unit* / eqn. No.
a	area	m^2
a_i	activity of *i*th species	$mol\ kg^{-1}$, eqn. 2.17
$\mathring{a}$	ion size	*pm*
A	constant from Kebye-Hückel equation	$(l/mol)^{1/2}$, eqn.2.19
A_2	a constant (2-D nucleation rate)	eqn. 2.55
A_a	Arrhenius constant	eqn. 2.16
A_C	percentage of ion consumed inside micromodel	eqn. 6.6
A_j	a constant	eqn. 2.46
A_j'	a constant	eqn. 2.48
A_m	Madelung constant	eqn. 2.52
Alk_C	carbonate alkalinity	eq kg^{-1}, eqn. 2.12
Alk_T	total alkalinity	eq kg^{-1}, eqn. 2.11
B	factor from Kebye-Hückel equation	$(l/mol)^{1/2}/pm$
Bs	a constant of the BCF rate equation	eqn. 2.56
$B_{\pm}^{\gamma}$	Pitzer's constant	eqn. 2.22
C_i	the concentration of *i*th species	$mol\ kg^{-1}$
Cs	the BCF rate constant	eqn. 2.56
C_{T1}	total carbonic acid	eqn. 2.7
C_{T2}	total organic acids	eqn. 3.4
$C_{\pm}^{\gamma}$	Pitzer's constant	eqn. 2.22
D	diffusion coefficient	$m^2\ s^{-1}$
e	elementary charge	$1.602\times10^{-19}\ C$
E_a	activation energy	J
EP	equivalent point	Figure 3.1
F	Faraday constant	$9.6485\times10^{4}\ C/mol$
F_1 - F_4	Gran functions	eqn.s 3.18 - 3.21
f_g	gas fugacity	eqn. 8.4

f^{γ}	Pitzer's constant	eqn. 2.22
G	free energy	eqn. 2.43
H^{o}_{r}	standard reaction enthalpy	eqn. 2.40
IAP	activity products	eqn. 2.37
IS	ionic strength	$mol\ kg^{-1}$, eqn. 2.18
J	nucleation rate	$s^{-1}m^{-3}$, eqn. 2.46
J'	2-D nucleation rate	$s^{-1}m^{-2}$, eqn. 2.55
k	Boltzmann constant	$1.381\times10^{-23}\ JK^{-1}$
K	equilibrium constant	
K'	stoichiometric equilibrium constant	
K_1	the first dissociation constant of carbonic acid	eqn. 2.5
K_2	the second dissociation constant of carbonic acid	eqn. 2.6
K_a	the equilibrium constant of organic acids	eqn. 3.3
k_{DJ}	the rate constant of the Davies and Jones model	eqn. 2.60
k_f	rate constant of forward reaction	eqn. 2.61
K_H	the Henry's Gas Law constant for CO_2	eqn. 2.4
K_{sp}	solubility product	
K_w	the ionic product of water	$mol^2\ l^{-2}$, eqn. 2.3
p	pressure	atm
pCO_2	CO_2 partial pressure	atm
pH	$=log(a_H^+)$	eqn. 2.8
q_D	diffusion control index	eqn. 6.4
r	radius	m
R	general gas constant	$8.3144\ JK^{-1}\ mol^{-1}$
R_D	diffusion controlled crystal growth rate	eqn. 6.5
R_L	crystal layer growth rate	$m\ s^{-1}$, eqn. 4.15
R_m	crystal mass growth rate, eqn. 4.1	$mmol\ m^{-2}\ h^{-1}kg^{-1}$
s	surface area	m^2
S	saturation ratio	eqn. 2.38
SI	saturation index (= logS)	eqn. 2.39
t	time	$second$

t_{ind}	induction period	*second*, eqn. 2.47
T	absolute temperature	*Kelvin*
U	electronic potential	*voltage*
U_{cell}	electronic potential of a electrochemical cell	*voltage*, eqn. 2.30
u_i	mobility of ith species	eqn. 2.35
U_1, U_2	defined in equation 2.35	eqn. 2.35
V	volume	m^3
V_1' V_2'	defined in equation 2.35	eqn. 2.35
V_m	molecular volume	$m^2\ mol^{-1}$
X_a	the fraction of total organic acids	eqn. 3.11
W	weight	g
z_i	electric charge of *i*th item	
α_0	mole fraction of $H_2CO_3^*$ in total carbonic acid species	eqn. 9
α_1	mole fraction of HCO_3^- in total carbonic acid species	eqn. 10
α_2	mole fraction of CO_3^{2-} in total carbonic acid species	eqn. 11
β	buffer capacity	eqn. 3.1
Δ	difference	
$\gamma_\pm$	mean activity coefficient	
γ_i	the activity coefficient of *i*th species	
γ^s	solid surface energy	$J\ m^{-2}$
φ	angle	
μ	lattice energy	eqn. 2.52
ν	the numbers of ions or and molecules	
θ	contact angle	
ρ	density	$kg\ m^{-3}$
σ	relative saturation (= S - *1*)	
σ_F	surface energy	
ψ_i	the work required to break the chemical bonds	eqn. 2.53
Ψ	work needed to break a chemical bond	eqn. 2.53

Subscripts:

aq	aqueous
c	calculated
C	carbonate
crit	critical value
eq	value at equilibrium
e	end point or equilibrium state
g	gas
i	initial
i	*i*th component
i	initial
j	junction
het	heterogeneous
hom	homogeneous
m	measured
R	reference
s	solid
S	standard
t	the value at time *t*
Total	total
x	position
+	positive charged
-	negative charged
numbers, 1, 2, 3 ...	sequence numbers

Superscripts

+	positive charged
-	negative charged
o	ion pair
O	standard value

ACKNOWLEDGEMENTS

I would like to express my deepest thanks and appreciation to my supervisor, Dr. Richard A. Dawe, for his support, guidance, encouragement and understanding through out this study.

A special thanks to my colleagues in the petroleum Engineering Section of Imperial College and the members of EU Joule III QC-Scale project group for their advice and help, in particular Carlos Grattoni, Bill Harman, Ron Walker, Paul Ravenscroft, Harry Shaw and Sean Mulshaw.

I am also grateful to the Stephen & Anna Hui Fellowship (Imperial College) and the EU Joule III QC-Scale project for financial support.

Finally I would like to thank my husband Zhao Jinming and my parents as well as my son for their encouragement and support during my study.

Yuping Zhang

CHAPTER 1

INTRODUCTION AND OBJECTIVES

1.1 Introduction

Many oilfield waters contain large quantities of dissolved calcium ions and carbonate species (e.g. HCO_3^- and CO_3^{2-}) which can precipitate as $CaCO_3$ scale. Scale formation will cause increasingly difficult problems during the production life of an oilfield as more water is produced with the oil and gas. The scaling may occur downhole or in the surface facilities. Scale deposition within production systems associated with the production of brine can impact field economics and result in the costly cleaning or the restimulation of wells, replacement of equipment, lost oil production or even in the total shutdown of a field. For example, during 1995 around 1.4m barrels of production were lost as a result of scaling in the Magnus Field, one of BP's oilfields in North Sea, despite £2m being spent on inhibition and removal (Anonymous, 1997). Therefore the accurate prediction of where, when and how much precipitation will occur has been a major challenge to the oil industry.

Carbonate scale, mainly calcium carbonate scale ($CaCO_3$), is the most common scale in oilfields. As opposed to most sulphate scales ($BaSO_4$, $SrSO_4$ and $CaSO_4$), the prediction of carbonate scales requires not only the consideration of pressures, temperatures and water compositions, but also the knowledge on the chemical reactions within the brine and CO_2 in the gas phase. Most oilfield reservoirs contain carbonate mineral cements and carbon dioxide, therefore the formation water is normally saturated with calcium carbonate under reservoir conditions where the temperature can be as high as 200°C and the pressure up to 700 bar. As the formation water is produced with the oil and gas from the reservoir to the surface, the pressure falls so that degassing can occur which will lead to the removal of CO_2 from the formation water, an increase in the pH and carbonate (CO_3^{2-}) concentration, and the water can then become supersaturated.

Many field observations show that even if a water is supersaturated with scaling ions, precipitation may not occur or the amount of precipitation is much smaller than that

predicted from thermodynamic calculation when the water reaches the surface (Osborne et al, 1994 and Wright et al, 1994) because of the kinetic reasons, including the kinetics of degassing, scale crystals nucleation and growth. Clearly the kinetics of the processes are extremely important from the practical point of view. Unfortunately, the most available computer models for scale prediction are mainly based on thermodynamics and limited solubility data, and can only predict the potential or tendency to form scale. Kinetic and transport factors are normally ignored. This is because the kinetics of precipitation of calcium carbonate has not been extensively studied, particularly under oilfield conditions, so that the relevant available kinetic data are limited. Only a few computer models found in the published literature have been concerned with the kinetic factors, such as the model by Granbakken et al. (1989) in Norway, Haarberg et al., (1989) and the OSPMOD model (Yeboah et al., 1993), but this is still not valid for calcium carbonate scaling because no reliable kinetic model available for the prediction of $CaCO_3$ growth rate. There are a number of rate laws for describing crystal growth from supersaturated solutions (Bennema, 1967; Davies and Jones, 1955; Granbakken et. al., 1989; Plummer et. al., 1978; Reddy and Nancollas, 1971; Reddy et. al., 1981), however no reliable rate law for the $CaCO_3$ precipitation over the wide range of solution pH, temperature and pressures of oilfield reservoir conditions is available. This is because the complex three phase kinetics related to the $CaCO_3$-H_2O-CO_2 system for the precipitation of carbonate are not well understood. Also, most $CaCO_3$ and water reaction kinetic studies have concentrated on the $CaCO_3$ dissolution reactions rather than precipitation, and some of the equations of $CaCO_3$ precipitation rate were simply modified from the dissolution rate (Plummer et al, 1978). The experimental conditions have been mostly based on the conditions of natural water (e.g. seawater) rather than reservoir brine which can have much higher ionic strength (e.g. ≥1mol/kg), low pH (pH ≤ 5) and contain inhibitor ions, e.g. Mg^{2+}. Hence the calcium carbonate precipitation mechanisms and precipitation rates under the conditions of oilfield reservoirs are still unclear.

Experimental technique is a most important part in any study of $CaCO_3$ precipitation kinetics in aqueous solution, because the chemical reactions involved are multi-phase and heterogeneous, including solid-liquid and liquid-gas reactions. Many factors have to be considered, such as solution saturation state, CO_2 partial pressure, pH, involvement of a

gas phase, the mass transport from solution to the solid surface, seed surface properties, solution ionic composition and any inhibition as well as the hydrodynamics. The stirred suspension of calcite ($CaCO_3$) powder at steady state has been widely used for the study of $CaCO_3$ precipitation (Berner and Morse, 1974; Plummer and Wigley, 1976; House, 1989; Kazmlerczak et al., 1982; Morse, 1974a; and Zhong and Mucci, 1989 and 1993). However, most of these methods are difficult to operate and the system hydrodynamics are poorly defined (e.g. simply change the stirring rate) so that the crystal surface property changes during precipitation are hard to follow.

A study of the kinetics of scaling also requires a reliable calculation of the thermodynamic states of the flowing water at any stage of the precipitation and any position within the flowpath. An accurate evaluation of the thermodynamic state of an aqueous solution during carbonate scale precipitation significantly depends on the accuracy of water analysis, the water pH and the concentration of carbonate species under downhole conditions. The downhole water pH is difficult to measure directly and is normally calculated from a water composition, CO_2 partial pressure, thermodynamic data, temperature and pressure. Actually many thermodynamic data for carbonate species are not available under downhole conditions, so that the downhole pH predicted from many models cannot be satisfied.

The concentration of carbonate species is normally obtained from alkalinity analysis using acid titration. Analysis of oilfield waters shows that considerable quantities of carboxylic acids may be present (as high as 80 mmol/l, Barth, 1987). These carboxylic acids can affect the analysis of carbonate species by acid titration because the carboxylic acids interfere with the normal titration end points of bicarbonate. As a result of an unclear end point, part of the concentration of carboxylic acid anions is considered as bicarbonate. As a consequence, an overestimation of carbonate scaling tendency and consequent unnecessary treatments can occur. However there is no simple accurate way of analysing for carbonate species when organic acids are also present in the solution. Without an accurate analysis of carbonate species and organic acids, an accurate prediction of downhole pH is impossible.

1.2 Objectives

The motivation for this study is to provide the knowledge for the understanding of the kinetics of calcium carbonate precipitation and scaling from water solutions similar to oilfield formation brines. The fundamental processes governing calcium carbonate precipitation, including the understanding of the distribution of carbonate and organic acids species, pH as well as ionic complexes in a high ionic strength solution (> 1mol/kg), need to be considered. The objectives of this thesis include:

(i) to develop a simple and accurate analytical method to determine carbonate species when organic acids are also present in a water solution and to detect whether there are organic acids present and in what quantity;

(ii) to find out under what reservoir conditions $CaCO_3$ nucleation starts and what is the mineralogy of the nuclei;

(iii) to establish a reliable kinetic model which can describe the calcite growth rate for oilfield formation brines;

(iv) to understand the influence of inhibitor ions, such as Mg^{2+}, on calcite growth rate and crystal morphology;

(v) to understand the influence of mass transport on carbonate scaling rate and the reaction mechanisms.

1.3 Approach

The chemical reaction defining $CaCO_3$ precipitation can be described by:

$$Ca^{2+} + 2HCO_3^- = CaCO_3 + CO_2 + H_2O\,. \qquad (1.1)$$

When a solution is supersaturated with $CaCO_3$ (the amount of dissolved $CaCO_3$ in the solution is above its solubility), precipitation (including nucleation and growth) may occur. In a closed water system, (there is no mass exchange between the water system and the gas phase) the bulk solution pH will fall once $CaCO_3$ precipitation occurs. The solution pH changes is related only to the $CaCO_3$ precipitation. The $CaCO_3$ precipitation rate can then be determined by following the bulk solution pH change as a function of time. The $CaCO_3$ crystal growth rate has been known to be proportional to the solution

supersaturation (Burton et al., 1951; Davies and Jones, 1955; Reddy and Nancollas, 1971; Plummer et al., 1978 and Nielsen and Toft, 1984), hence a mathematical relationship between the crystal growth rate and supersaturation can then be established to describe the crystal growth rate at any supersaturation state. The $CaCO_3$ growth rate is also proportional to the total crystal surface area which is very difficult to measure accurately. The crystal growth rate can be determined by observing and measuring individual crystal size change as a function of time at a constant solution composition and hydrodynamic state. This visual observation also makes it possible to examine many factors which may influence the crystal precipitation. For example, the mass transport influence can be examined by changing the water flowing rate, so that the crystal morphology changes during crystal precipitation can be observed. In this way the influence of the initial property of crystal seeds on the determination of crystal kinetics can be reduced to the minimum.

1.4 Thesis outline

Chapter 2 is concerned with the basic knowledge of the CO_2 - H_2O system, solution equilibrium and calcium carbonate precipitation. The previous work related to the kinetics of calcium carbonate precipitation has also been reviewed.

In Chapter 3 an acid titration method using an automatic titrator to analyse carbonate species and organic acid species has been developed. The acid titration data often needs mathematical manipulation to obtain the separate concentrations of carbonate species and organic acid species present in a solution.

In Chapter 4 two experimental methods, developed for experimentally detecting the thermodynamic precipitation tendency and the kinetics of $CaCO_3$ precipitation.

In Chapter 5 the nucleation and morphology of the calcium carbonate precipitation have been examined. The critical saturation for $CaCO_3$ nucleation at different temperatures has been determined.

Chapters 6 and 7 present the experimental results concerning the $CaCO_3$ crystal growth mechanisms and growth rates. Many factors which may influence the $CaCO_3$ precipitation, such as pH, alkalinity, ionic strength, the presence of Mg^{2+} ion, mass transport rate as well as temperature, have been examined.

Chapter 8 demonstrates how the kinetic model developed in this study can be used to predicate calcite scaling profile within an oilfield tubing surface. A calcium carbonate scaling case reported in open literature has been tested. Chapter 9 summarises the work in Chapters 3 to 8. The conclusions from this work and suggestions for further studies are given.

CHAPTER 2

BACKGROUND KNOWLEDGE AND LITERATURE REVIEW

2.1 Introduction

Scaling is a process of a solid precipitating from a liquid onto surfaces. The condition necessary for scale formation on a surface immersed in a liquid is that the solution is supersaturated with respect to the scaling compounds. The initial stage of scale formation is nucleation of scale-forming crystals onto an exposed surface. For this to happen a minimum supersaturation with respect to the scale-forming compound must be established. Nucleation onto a surface proceeds mostly by heterogeneous mechanisms under conditions where it may not take place within the bulk solution (Hasson et. al., 1968 and Nancollas and Reddy, 1974). The rate of this initial scale formation stage is determined by the level of supersaturation, the temperature, the pressure, the presence of inhibitor ions, a gas-liquid interface and the providing hydrodynamic conditions. Factors determining scale adhesion to the surface, such as the surface material and surface roughness, also have a significant influence.

To study the kinetics of the $CaCO_3$ precipitation, knowledge of the thermodynamics of solutions and crystallisation is important. It is also essential to understand the physical and chemical properties of the solution, such as the equilibrium of the CO_2-H_2O system and the solubility of the precipitating component (Ca^{2+} and CO_3^{2-}) at given conditions. In this chapter the basic knowledge of equilibrium and thermodynamics of solutions and crystallisation, especially in a CO_2-H_2O system, have been discussed. The previous work related to the kinetics of calcium carbonate precipitation has been reviewed.

2.2 Carbonic acid system

2.2.1 Dissolved carbon dioxide

CO_2 gas ($CO_{2(g)}$) in the atmosphere can dissolve into water to form aqueous CO_2, ($CO_{2(aq)}$), which associates to some extent with water molecules to form carbonic acid, H_2CO_3:

$$CO_{2(g)} + H_2O \leftrightarrow H_2CO_3 \quad (2.1)$$

Carbonic acid can dissociate in two steps, releasing one proton in each step. In fact more than 90% of the dissolved carbonic acid is aqueous CO_2 (Morse and Mackenzie, 1990), thus the form $H_2CO_3^*$ is usually used,

$$H_2CO_3^* \leftrightarrow CO_{2(aq)} + H_2CO_3 \quad (2.2)$$

The relevant mass reactions and reaction constants which are needed to calculate the composition of the solution are given in Table 2.1,

Table 2.1 Equilibrium constants form dissolved CO_2 species at 25°C (Appelo and Postma, 1993).

Chemical reaction	Equilibrium	Equilibrium constant	Equations
$H_2O \leftrightarrow H^+ + OH^-$	$K_W = C_{H^+} C_{OH}$	$K_w = 10^{-14.00}$	(2.3)
$CO_{2(g)} \leftrightarrow H_2O + H_2CO_3^*$	$K_H = C_{H_2CO_3^*} / pCO_2$	$K_H = 10^{-1.47}$	(2.4)
$H_2CO_3^* \leftrightarrow H^+ + HCO_3$	$K_1 = C_{H^+} C_{HCO_3} / C_{H_2CO_3^*}$	$K_1 = 10^{-6.35}$	(2.5)
$HCO_3 \leftrightarrow H^+ + CO_3^{2-}$	$K_2 = C_{H^+} C_{CO_3^{2-}} / C_{HCO_3}$	$K_2 = 10^{-10.33}$	(2.6)

where C_i refers to the concentration of *ith* species, (concentration in equations 2.3 - 2.6 can only be used in an infinitely dilute solution, otherwise activity should be used, which will be discussed shortly), K_w is the ionic product of water, K_H is the Henry's Gas Law constant for CO ,, K_1 and K_2 are the first and the second dissociation constants of carbonic acid, and pCO_2 is the CO_2 partial pressure. The concentration of total carbonate, C_{T1}, is defined as:

$$C_{T1} = C_{H_2CO_3^*} + C_{HCO_3} + C_{CO^{2+}} \quad (2.7)$$

2.2.2 Fractional concentration factors

The symbol "pH" is defined as the negative logarithm of the hydrogen ion concentration, i.e.

$$pH = -log(C_{H^+}), \tag{2.8a}$$

where the concentration of hydrogen ions, C_H^+, can only be used for an infinitely dilute solution, otherwise activity should be used, i.e.

$$pH = -log(a_{H^+}), \tag{2.8b}$$

where a_{H^+} is the activity of hydrogen ion. The carbonate species play an important role in influencing the solution pH. When considering how the concentrations of the *i*th species change as a function of pH, it is convenient to deal with carbonate species in terms of fractional concentration factors which are defined as:

$$\alpha_0 = \frac{C_{H_2CO_3^*}}{C_{T1}} = \frac{1}{1 + K_1/10^{-pH} + K_1K_2/10^{-2pH}} \tag{2.9}$$

$$\alpha_1 = \frac{C_{HCO_3}}{C_{T1}} = \frac{1}{1 + 10^{pH}/K_1 + K_2/10^{pH}} \tag{2.10}$$

$$\alpha_2 = \frac{C_{CO^2}}{C_{T1}} = \frac{1}{1 + (10^{pH})^2/K_1K_2 + 10^{-pH}/K_2} \tag{2.11}$$

where α_0, α_1 and α_2 are the fractional concentration factors of carbonic acid, bicarbonate and carbonate, respectively and $\alpha_0 + \alpha_1 + \alpha_2 = 1$.

With equations 2.7 - 2.11 we can easily calculate the percentage of carbonate species as a function of pH as shown in Figure 2.1. As we can see, at the pHs between pH 7 and 10 which are the most common pH of natural waters, most carbonate species are in the form of bicarbonate. The concentration of each carbonate species can be obtained from its

concentration fraction factor and total carbonate, for example, the concentration of carbonate can be obtained from $C_{CO_3^{2-}} = \alpha_2 C_{T1}$.

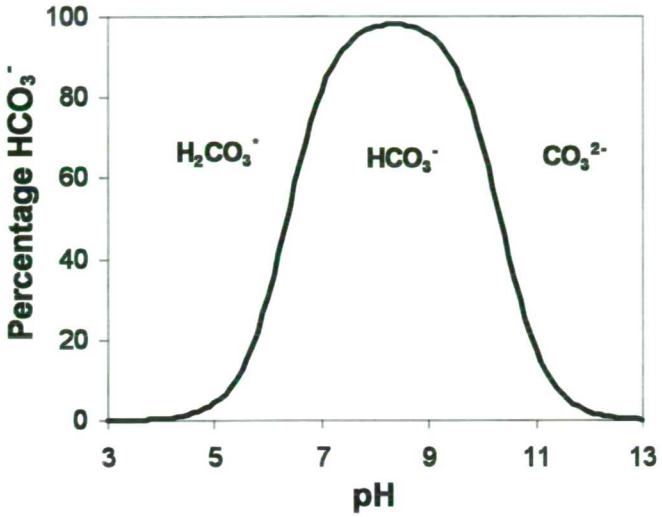

Figure 2.1 Percentage of HCO_3^- in total carbonate as a function of pH

The total carbonate (C_{T1}) in a closed system is constant. A closed water system here defined as a system without a gas phase being present. In an open water system, the CO_2 partial pressure is fixed so that the total carbonic acid (C_{T1}) will change with pH. Figures 2.2 and 2.3 show the concentrations of carbonate species as a function of pH in a closed system (2.2) and an open system (2.3).

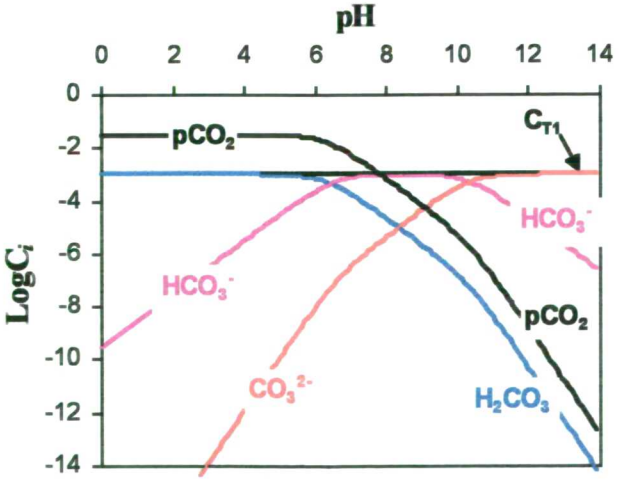

Figure 2.2 The concentrations of carbonate species as a function of pH in a closed system, $C_{T1} = 10^{-3}$ mol/kg.

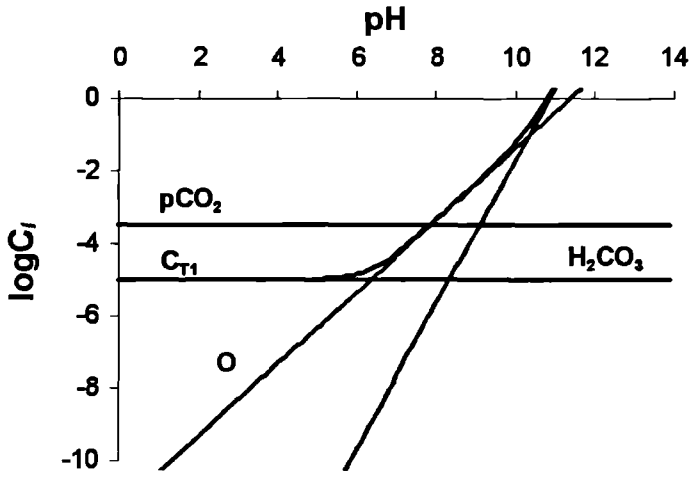

Figure 2.3 The concentrations of carbonate species as a function of pH in an open system, $pCO_2 = 10^{-3.5}$ atm.

From Figures 2.2 and 2.3 we can easily work out which carbonate species are dominant at different solution pHs in a closed or an open water system. The distribution of carbonic acid species at different pHs is needed for the prediction of carbonate scaling. It is important to note that although there is no gas phase present in a closed water system, it is common for significant amounts of CO_2 species to be present. It is convenient to have a value for pCO_2 that can be used in variety of needed equations. This can be handled by defining an "in- situ pCO_2" for closed system. Consider a beaker of water that is shown in Figure 2.4a. Above the water there is an essentially an infinitely large gas phase containing some $CO_{2(g)}$. Obviously, for this open system, we can use all of the open system equations involving pCO_2. If we take a syringe to remove some of the water from the beaker, a closed water system is produced as shown in Figure 2.4b. The concentrations of the various dissolved species remained constant during the transfer from the beaker to the syringe. Application of a knowledge of $[H_2CO_3]$ in the syringe together with the values of K_H will produce a value for pCO_2 that is exactly the same as the pCO_2 value above the beaker. Thus, while there is no actual gas phase in equilibrium with the water in the syringe, thermodynamically, the system is characterizable by a perfectly well defined pCO_2. This is "in-situ" pCO_2. Use of an in-situ pCO_2 and with the pH will produce perfectly correct values for HCO_3^-, CO_3^{2-}, etc.

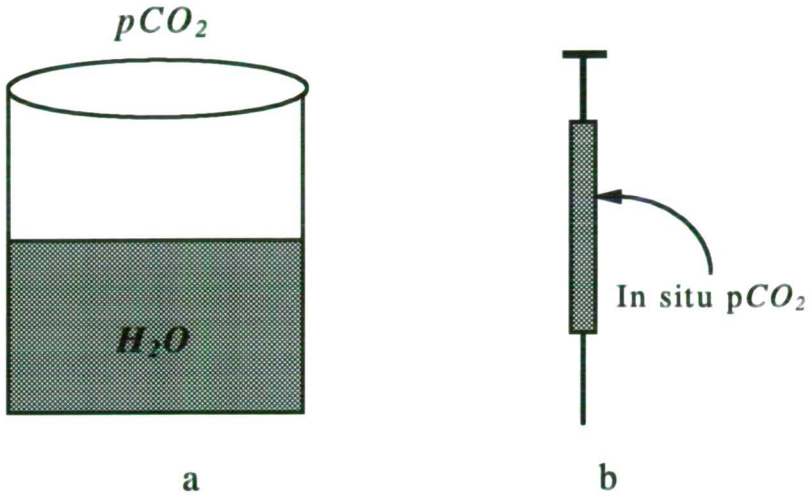

Figure 2.4 (a) Open system in equilibrium with an essentially infinitely large gas phase containing a constant pCO_2.
(b) Closed system (no gas phase) containing water that has been removed from the beaker in Figure 2.4a; the chemical composition of the water in the syringe is identical to that in the beaker.

2.2.3 Alkalinity

Another important measurement of a carbonic acid-water system is alkalinity. Alkalinity is the acid neutralisation capacity of a solution in moles of protons. It can be divided into two parts: the alkalinity associated with the carbonic acid system (Alk_C), and the alkalinity associated with all the other solution components, which have a neutralisation capacity of protons,

$$Alk_T = Alk_C + \sum Alk_i \tag{2.11}$$

where Alk_T is the total alkalinity and Alk_i is the alkalinity contributed by the components other than carbonate, such as boric acid, hydrogen sulphide and organic acid anions. Carbonate alkalinity can be obtained from:

$$Alk_C = C_{HCO_3^-} + 2C_{CO_3^{2-}} \quad . \tag{2.12}$$

If carbonic acid is the only dissolved weak acid in a solution, the total alkalinity can be obtained from:

$$Alk_T = C_{HCO_3} + 2C_{CO_3^2} + C_{OH} - C_{H^+} \quad . \tag{2.13}$$

Now we have four parameters describing a CO_2-H_2O system: pH, pCO_2,, C_{TI} and Alk_T. If any two of these four parameters are known, the other two can be calculated from equations 2.7 to 2.13.

2.3 Solutions and equilibria

If we put some calcite ($CaCO_3$) crystals into distilled water, they will dissolve into the water to a certain extent. The reaction involved is:

$$CaCO_3 \xleftrightarrow{H_2O} Ca^{2+} + CO_3^{2-} \tag{2.14}$$

In a closed system we have:

$$C_{Ca^{2+}} = C_{CO_3^2} \tag{2.15}$$

and therefore

$$K_{sp} = (C_{Ca^{2+}})^2 \tag{2.16}$$

where K_{sp} is the solubility product of calcite. The solubility of calcite can be obtained by measuring the concentration of calcium ions in the water when equilibrium has been reached. The value of K_{sp} obtained in this way is $10^{-8\,3}$ at 25°C (Appelo and Postma, 1993). However, it was found that when a solution contained neutral salts, such as sodium chloride ($NaCl$), the solubility product obtained by measuring the concentration of Ca^{2+} at equilibrium is much higher (can be 100 times) than the value with distilled water. The difference is caused by the effect of

- electrostatic interaction between ions of opposite charge,
- ionic hydration, water concentration becomes less than 1,

- ion pairing (or ion pairing) from cation-anion interaction.

The electrostatic interaction and ionic hydration can be corrected by a term of activity coefficient, and the ion pairing can be corrected by the relationship of multiple ion association (Loewenthal and Marais, 1984).

2.3.1 Concentration and activity

The interaction between the ions within the solution restricts the mobility of the ions to such an extent that considerable deviations from ideal behaviour can occur. However the activity of an ion approaches its molar concentration as the concentrations of all the solutes approach zero. A correction term, the activity coefficient, is used to correct the deviation of the concentration from dissolved ions,

$$a_i = \gamma_i C_i \tag{2.17}$$

where a_i is the activity of the ith species and γ_i is the activity coefficient (dimensionless). In an infinitely dilute solution, $\gamma_i = 1$, so that under this condition, $a_i = C_i$. Activity coefficients can be calculated from the ionic strength which is a measurement of the overall concentration of ions in a solution. The more highly charged ions exert a greater influence on ionic interactions. The ionic strength is defined as (Söhnel and Garside, 1992):

$$IS = 0.5\Sigma C_i z_i^2 \tag{2.18}$$

where IS is ionic strength, z_i is the electric charge for the ith species. The unit of ionic strength is the same as the unit of C_i. Table 2.1 gives a number of equations to calculate the activity coefficient, γ_i. For high ionic strength solutions ($1 < I < 6$ eq/kg), such as oilfield formation brines, the most widely used model is the Pitzer equation. The Pitzer equation is based on an ion-interaction or viral-coefficient model where the effects of ion association are implicitly incorporated into the stoichiometric activity coefficients calculated by a viral expansion of the Debye Hückel theory (Pitzer, 1973a, 1973b, 1981

and Silvester and Pitzer, 1978). This method provides an excellent interpolative framework for molecular activity coefficients and accurate predictions of mineral sequences in very concentrated brines at low temperatures.

Table 2.1 Equations for activity coefficient, after Pankow (1991)

Name	Equation for calculation of activity coefficient	Ionic Strength Range (eq/kg)	
Debye-Hückel	$Log\gamma_i = -Az_i^2\sqrt{IS}$	$IS<10^{23}$	(2.19)
Extended-Debye Hückel	$Logg_i = -Az_i^2[\sqrt{IS}/(1+\mathring{a}B\sqrt{IS})]$	$IS<10^{10}$	(2.20)
Davies	$Log\gamma_i = -Az_i^2[\sqrt{I}S/(1+\mathring{a}B\sqrt{IS})]-0.2IS$	IS<0.5	(2.21)

where, $\mathring{a}$ is a size parameter for the ith ion, A and B are constants for the Debye Hückel equation and A = 0.51, B = 0.33 at 25°C.

The generalised form of Pitzer's equation (Pitzer, 1973a, 1973b) for mean activity coefficients ($\gamma_{\pm}$) in a mixture of electrolytes is:

$$ln\gamma_{\pm} = |z_+z_-|f^{\gamma} + m\left(\frac{2\nu_+\nu}{\nu}\right)B_{\pm}^{\gamma} + m^2\left[\frac{2(\nu_+\nu)^{1.5}}{\nu}\right]C_{\pm}^{\gamma} \qquad (2.22)$$

where $f^{\gamma}, B_{\pm}^{\gamma}, C_{\pm}^{\gamma}$ are the Pitzer constants, m is the molality (mole per kg of water) of the species, ν_+ ν_- and ν are the numbers of cation, anion and molecules, respectively. The problem is that this method relies on the availability of data and is applicable only over the range of the fitted data. There does not appear to be any reasonable correlation for the Pitzer coefficients which extends the fit to outside the range of the experimental dataset (Pitzer and Mayorga, 1973; Pitzer and Silvester, 1977, 1978).

In low ionic strength waters (< 0.025 eq/kg), generally only the electrostatic effects are of importance. However, as ionic strength of the solution increase, the ion pairing and/or ion pairing effects become of increasing importance and eventually dominate over the electrostatic effect.

2.3.2 Ion pairs (or complexes)

Considering the charge and the size of the metal ions it is obvious that in solution they cannot exist "freely", but that they are associated with the counter ions or other components of the solution having non-bonding electron pairs, i.e. forming aqueous ion pairs. Therefore, apart from electrostatic shielding, the reactivity of ions in solution is further reduced by the presence of aqueous ion pairs and/or ion pairs. Examples of aqueous ion pairs are $CaCO_3^o$ (a subscript o represents an ion pair to be differ from solid $CaCO_3$), $CaHCO_3^+$, $NaCO_3^-$ etc. The formation of aqueous ion pairs can be described by equilibria of the type:

$$Ca^{2+} + CO_3^{2} \leftrightarrow CaCO_3^o. \tag{2.23}$$

The equilibrium constant of reaction 2.23 can be simply obtained from

$$K_{CaCO_3^o} = \frac{C_{Ca^2}\, C_{CO_3^2}}{C_{CaCO_3}} \tag{2.24}$$

Considering the various possible aqueous ion pairs of Ca^{2+}, the total amount of Ca^{2+} in solution is described by a mass balance equation of the type:

$$(C_{Ca^{2+}})_T = C_{Ca^{2+}} + C_{CaCO} + C_{CaHCO_3} + C_{CaOH^+} + C_{CaSO_4^o} + \cdots \tag{2.25}$$

here $(C_{Ca^{2+}})_T$ is the total Ca^{2+} in the solution and can be determined by chemical analysis. $C_{Ca^{2+}}$ is the *free* Ca^{2+} concentration in a solution. So now an accurate calcite solubility product can be obtained by considering both activity and ion pairs,

$$K_p = a_{Ca^{2+}} a_{CO_3^2} = C_{Ca^{2+}} C_{CO_3^2}\, \gamma_{Ca^+} \gamma_{CO_3^2} \tag{2.26}$$

After the concentrations of free Ca^{2+} and CO_3^{2} ions are corrected for both activity coefficients and ion pairs, the calculated solubility product of calcite from the measured

ion concentration in a calcite equilibria solution is in good agreement with the solutions with various ionic strengths, and is $10^{8.48}$ at 25°C (Sass et al, 1983). We can see that this value is slightly smaller than the value from the calcite dissolution experiment in distilled water without any activity and ion pairing corrections ($10^{8.3}$).

2.3.4 Stoichiometric equilibrium constant

For the calculations of mass precipitation, the concentrations instead of activities of the species are normally convenient to use, especially when the solution compositions are relatively constant, such as for seawater. The term of activity coefficient is included in the equilibrium constant which is called the stoichiometric equilibrium constants (concentration equilibrium constants), e.g. K_1', K_2' and K_{sp}',

$$K_1' = \frac{10^{-pH} C_{HCO_3}}{C_{H_2CO_3^*}} = K_1 \frac{\gamma_{H_2CO_3^*}}{\gamma_{HCO_3}} \tag{2.27}$$

$$K_2' = \frac{10^{-pH} C_{CO_3^{2}}}{C_{HCO_3}} = K_2 \frac{\gamma_{HCO_3}}{\gamma_{CO_3^{2}}} \tag{2.28}$$

$$K_{sp}' = C_{Ca^{2+}} C_{CO_3^{2}} = \frac{K_{sp}}{\gamma_{Ca^{2+}} \gamma_{CO_3^{2}}} \tag{2.29}$$

The free ion concentration should be used for equations 2.27 to 2.29. It is important to note that for the calculation of the concentration of fractional factors (α_i in equations 2.9 - 2.11) of carbonate species in a finite dilute solution, the stoichiometric equilibrium constants, K_1', K_2' should be used.

2.3.5 Measurement of pH in a high ionic strength solution

The measurement of a solution pH seems very simple. A pH meter with a glass electrode and a reference electrode (or one combined electrode) should be sufficient. For ionic strengths $0.01 < IS < 0.1$, the measurement of pH from a glass electrode gives a reliable value of the activity of H^+, i.e. $pH = -\log(a_H^+)$. The electrode system is standardised

against low salinity aqueous NBS buffers (Bates, 1964). However, outside this range of ionic strengths, an error is inherent in the pH readings due to residual liquid junction effects from the reference electrode. A liquid junction potential (or diffusion potential) is set up in the transition zone between the measured solution and internal reference electrolyte of the electrode. Figure 2.5 shows the principle of how a glass electrode measures a solution pH.

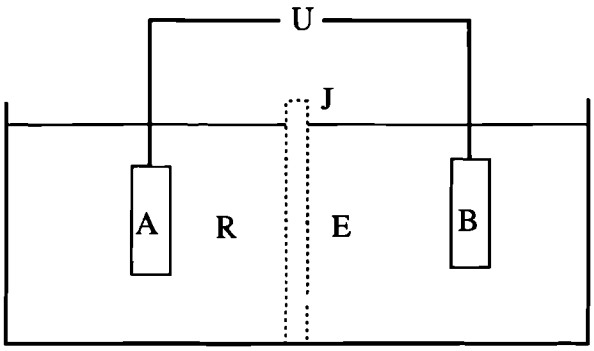

Figure 2.5 Electrochemical cell with liquid junction. A and B, electrodes, J, separator, R and E, electrolytes, U, cell in emf.

The left hand of the cell is filled with a concentrated *KCl* solution (e.g. 3 mol/l) with a reference electrode in it; the right side is the test solution for the pH measurement with a glass electrode. The electronic potential of the cell, U_{ell}, is the sum of three individual potentials; U_E for the pH electrode, U_R for the potential of the reference electrode, and U_J for the potential across the liquid junction boundary between the measured solution and the concentrated *KCl* solution. When the standard solution (an NBS buffer) is in the right hand cell, the cell potential, $U_{ell\,S)}$, is given as follows:

$$U_{ell\,S)} = U_R^o - U_E^o + U_{J\,S} - \frac{RT}{F} ln((a_H)_S (a_{Cl})_R) \tag{2.30}$$

where superscript o beside U refers to standard potential, subscripts R and S refer to reference and the standard solutions. The pH of the standard solution is:

$$pH_S = (U_{ell(S)} - U_R^o - U_{J\,S)} + U_E)\frac{F}{RT\,ln10} + log(a_{Cl})_R \tag{2.31}$$

When the test solution is in the right hand of the cell, the cell potential $U_{ell(x}$, is:

$$U_{ell\ x)} = U_R^o - U_E^o + U_{J\ x)} - \frac{RT}{F} ln((a_{H^+})_x (a_{Cl^-})_R) \tag{2.32}$$

and the pH of the test solution can be obtained from:

$$pH_{(x)} = (U_{cell(x)} - U_R^o - U_{J(x)} + U_H^o) \frac{F}{RT\,ln10} + log(a_{Cl^-})_R \tag{2.33}$$

Subtracting equation (2.31) and (2.33) gives the relationship linking the pH of the test solution to the cell potentials and liquid junction potentials in the standard and test solutions, i.e.

$$pH_{(x)} = pH_{(S)} + \frac{(U_{ell\ x} - U_{ell\ s})F}{RT\,ln10} - \frac{(U_{J(x} - U_{J(S)})F}{RT\,ln10} \tag{2.34}$$

From equation 2.34 we can see that the pH of the test solution is independent of the activity of the Cl^- in the saturated KCl solution. The residual liquid junction potential is the liquid junction potential difference between an NBS buffer and the measured solution, reflected by the last term of equation 2.34. This is the error of the pH measurement coming from (Galster, 1991) and can be minimised by using a number of calibration buffers and measured solutions with a similar ionic strength and pH. The ionic strengths of the NBS buffers are low (0.01-0.05 eq/l). When the ionic strength of a test solution are much higher than these values, the error can be significant. There are two options to solve this problem:

1. evaluate the residual liquid junction potential and estimate the true pH from the operational pH or
2. re-evaluate all the equilibrium constants for a particular solution in terms of operational values.

The second option is to use water with similar ionic composition, for example, seawater. The first option allows the analysis to be general for all waters. The residual liquid junction potential can be determined experimentally (Bates, 1964, Loewenthal and Marais, 1984). There are also some theoretical approaches to estimate the residual liquid junction potential. In this study, a theoretical approach (Henderson equation) has been used (Galster, 1991). The liquid junction potential between the reference and measured solutions can be calculated from

$$U_J = \frac{RT}{F}\frac{(U_1 - V_1) - (U_2 - V_2)}{(U_1' - V_1') - (U_2' - V_2')} lg \frac{U_1' - V_1'}{U_2' - V_2'} \qquad (2.35)$$

where the subscript numbers 1 and 2 in equation 2.35 refer to the reference solution and the test solution; $U_1 = \sum u_i^+ C_i$, $V_1 = \sum u_i^- C_i$, $U'_1 = \sum u_i^+ C_i z_i$, $V'_1 = \sum u_i^- C_i z_i$ and u_i^+ and u_i^- refer to the mobility of the positive and negative ions in a solution. The residual liquid junction potential, ΔU_j, is the liquid junction potential difference between the standard buffer solution and the test solution:

$$\Delta U_j = U_{j(R)} - U_{j(x)} . \qquad (2.36)$$

2.4 The prediction of carbonate mineral precipitation tendency

To predict the precipitation tendency for an aqueous system, a simple way is to compare the ionic activity products (IAP) of precipitated ions with their thermodynamic solubility products. For calcium carbonate:

$$IAP = a_{Ca^{2+}} a_{CO_3^{2-}} \qquad (2.37)$$

if

	$IAP < K_{sp}$	undersaturated, precipitation is impossible,
	$IAP = K_{sp}$	saturated, the system is in equilibrium,
	$IAP > K_{sp}$	supersaturated, precipitation is possible.

A common representation of how far away a water system is from the equilibrium state is the supersaturation ratio (*S*) or saturation index (*SI*),

$$S = a_{Ca^{2+}} a_{CO^2} \ / K_{sp} \tag{2.38}$$

and

$$SI = Log\ (S)\ . \tag{2.39}$$

S and SI can also be called the thermodynamic driving force for crystal growth. The larger the value of S or SI for a solution, the higher the possibility of precipitation. When S = 1 (SI = 0), the system is in equilibrium.

2.4.1 Carbonate minerals and their solubilities

The carbonate minerals which commonly form chemical scale include calcite, aragonite, vaterite, magnesite and siderite. The solubility of these carbonate minerals change with the solution composition, ionic strength, pH, CO_2 partial pressure and temperature, but their thermodynamic solubility products are constant at a given temperature and pressure. Table 2.2 summarises some of the physical properties of these common carbonate scaling minerals.

Table 2.2 The chemical composition of carbonate minerals (25°C), after Appelo and Postma (1993).

Minerals	Formula	- $LogK_{sp}$	Density (g/cm^3)	Crystal system
calcite	$CaCO_3$	8.48	2.71	Rhombohedral
aragonite	$CaCO_3$	8.34	2.93	Orthorhombic
vaterite	$CaCO_3$	7.91	2.54	Hexagon
magnesite	$MgCO_3$	8.24	2.96	Rhombohedral
siderite	$FeCO_3$	10.89	3.80	Rhombohedral

2.4.2 Influence of temperature and pressure

The influence of temperature and pressure variations on the precipitation tendency of carbonate minerals is mainly caused by the influence of temperature and pressure on the distribution of carbonic acid chemical species in the natural water systems, as well as on

the carbonate mineral solubility, i.e. on K_H, K_1, K_2 and K_p. The equation representing the influence of temperature on an equilibrium constant (K_t) is:

$$\frac{d \ln K_t}{dT} = \frac{\Delta H_r}{RT^2} \tag{2.40}$$

where ΔH^o_r is the enthalpy of the reaction, R is the gas constant. An empirical equation can be used to calculate the K_t changes with temperature (Morse and Mackenzie,1990):

$$\ln K_t = a_1 + a_2/T + a_3 \ln T + a_4 T + a_5/T^2 \tag{2.41}$$

where a_1 to a_5 are experimentally determined constants. The values of these constants are given in Table 2.3

Table 2.3 The constants of equation 2.41, after Plummer and Busenbery (1982)

K_t	a_1	a_2	a_3	a_4	a_5	T(°C) range
K_H	249.570	-15932.9	-40.452	0.0457	1541279	0-250
K_1	-820.438	50275.8	126.834	-0.1403	-3879685	0-250
K_2	-248.421	11862.5	38.925	-0.0749	-1298007	0-250
K_{sp} (calcite)	-395.832	6537.8	71.595	-0.1796	0	0-90
K_{sp}(aragonite)	-395.995	6685.1	71.595	-0.1796	0	0-90

The effect of pressure on equilibrium constants is given by equation 2.42 (Morse and Mackenzie, 1990):

$$\ln\left(\frac{K_t^P}{K_t}\right) = \left(\frac{-\Delta V}{RT}\right)p + 0.5\left(\frac{\Delta K}{RT}\right)p^2 \tag{2.42}$$

where ΔV is the change in volume associated with the reaction, K_t is the value of K_t at one atmosphere and K_t^P is K_t at the given pressure. The part of the equation involving ΔK_t is a correction for the influence of pressure on ΔV. Both ΔV and ΔK_t are temperature and pressure dependent.

The solubility of $CaCO_3$ decreases rapidly with an increase in temperature. Compared with the effects of temperature on K over the wide range of surface and oilfield formation conditions, the effect of pressure is small and can usually be neglected (Kharaka et al., 1988). However if there is gas present, any pressure change will affect the CO_2 partial pressure and consequently affect the $CaCO_3$ saturation index. At a constant temperature, the solubility of $CaCO_3$ increases with an increase in CO_2 partial pressure.

2.4.3 Computer modelling

Many computer programs are available to calculate the thermodynamic properties of electrolyte solutions, including the activity coefficient, mass balance, temperature and pressure dependency of equilibrium constants. The reliability of the calculations depends on the reliability of the thermodynamic models and the database. Some of these programs include Aspen Plus, COMICS, CHEMEQUIL-2, ECHEM, EQUILIB, EQ3/EQ6, ProChem/ESP, Solmineq88, WATEQ4F and more (Sandler, 1994).

In this study, Solmineq88 (Kharaka et al., 1988) has been used in the thermodynamic calculations. This is a computer model for monitoring and predicting geochemical reaction and changes in formation water chemistry as well as for calculating the amount of a mineral precipitated or dissolved from a given solution. The effect of temperatures up to 350°C, pressures up to 1000bar and ionic strengths up to 6 eq/kg can also be calculated. There are two options in Solmineq88 for calculating the activity coefficients; the ion pair (extended-Debye Hückel equation and ion pairing model) and the Pitzer equation. This computer model has been used in this study for the calculation of a solution thermodynamic properties.

2.5 The kinetics of crystal nucleation

The kinetics of calcite precipitation can be divided into two stages; nucleation and crystal growth. When a solution is supersaturated (S >1), precipitation is possible, but for kinetic reasons, precipitation may not occur. The kinetics of precipitation is an essential tool in determining the conditions and the rate of the scaling.

The first step of scaling is nucleation which determines where or when scale will start to form. Two types of nucleation can be identified; homogeneous nucleation, in which the formation of the solid phase is not brought about by the presence of any solid phase and heterogeneous nucleation, where the formation of new solid phase particles is catalysed by the presence of a foreign solid phase.

2.5.1 Homogeneous nucleation

When a solid phase is formed from a solution, the overall excess free energy, (ΔG_{hom}) is equal to the sum of the surface excess free energy (ΔG_S), and the volume excess free energy, (ΔGv), i.e.,

$$\Delta G = \Delta G_S + \Delta G_V = 4\pi r^2 \gamma^s + \tfrac{4}{3}\pi r^3 \Delta G_v \tag{2.43}$$

where γ^S is the solid surface energy (for calcite, γ^S = 0.097 Jm^{-2}, Söhnel and Garside, 1992), and r is the size of nuclei. The tendency of these two terms of excess energy are shown in Figure 2.6. The maximum value (ΔG_{crit}) which corresponds to the critical size of a nucleus (r_c) is the barrier for forming the new phase,

$$\Delta G_{rit} = \frac{16\pi(\gamma^s)^3}{3(\Delta G_v)^2} = \frac{4\pi\gamma\ r^2}{3} \tag{2.44}$$

and

$$\Delta G_v = \frac{2\gamma^s}{r} = \frac{kT\ln S}{V_m} \tag{2.45}$$

where k is the Boltzmann constant (1.38×10^{-23} JK^{-1}), V_m is the molecular volume.

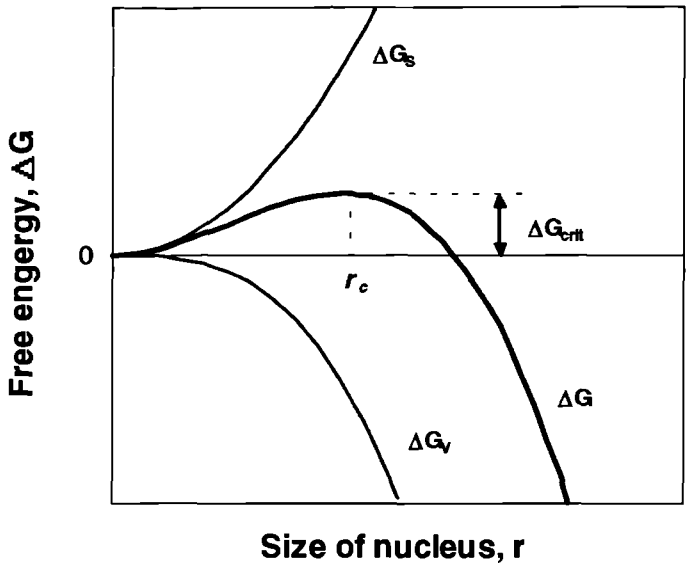

Figure 2.6 Free energy diagram for nucleation explaining the existence of the "critical nucleus".

The rate of homogeneous nucleation (i.e. the number of nuclei formed per unit time per unit volume) can be calculated from the critical free energy (Mullin, 1994):

$$J = A_j \exp(-\frac{\Delta G}{kT}) = A_j \exp\left[-\frac{16\pi(\gamma^s)^3 V_m^{\ 2}}{3k^3T^3(\ln S)^2}\right] \tag{2.46}$$

where J is the nucleation rate ($s^{-1}m^{-3}$) and A_j is a constant. The time needed for the formation of the new phase is called the induction period, t_{ind}, and this can be experimentally determined by following a change in a physical property, such as a decrease in the solution conductivity or pH. The induction period can also be calculated by:

$$t_{ind} = 1/J \ , \tag{2.47}$$

where t_{ind} is the induction period (s). Figure 2.7 shows the nucleation rate of calcite as a function of the supersaturation ratio at different temperatures.

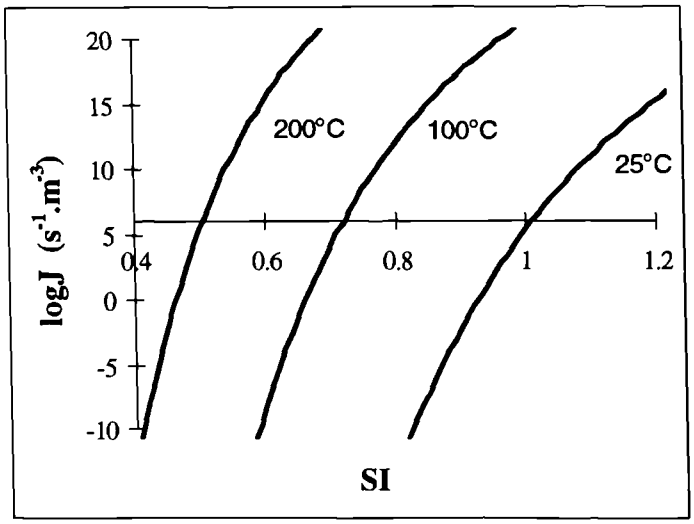

Figure 2.7 The nucleation rate of calcite as a function of the supersaturation ratio at the temperatures of 25°, 100° and 200°C

We can see from Figure 2.7 that the nucleation rate rapidly increases within a very narrow range of supersaturation ratios. This region of supersaturation is usually defined as the critical supersaturation ratio (S_{crit}) at which the nucleation rate $J \approx 10^6 s^{-1} m^{-3}$. Hence the critical supersaturation ratio, S_{crit}, of calcite can be calculated from:

$$ln S_{nt} = \left[\frac{16\pi\gamma^{S3}V_m^2}{3k^3T^3 ln A_j}\right]^{1/2} = A_j T^{-3/2} \qquad (2.48)$$

where

$$A_j' = \left[\frac{16\pi\gamma^{S3}V_m^2}{3k^3 ln A_j}\right]^{1/2}$$

If the critical supersaturation ratio at a temperature is known, the critical supersaturation ratios at other temperatures can be calculated by rearranging equation 2.48:

$$ln S_{nt2} = ln S_{nt1}\left(\frac{T_1}{T_2}\right)^{3/2}, \qquad (2.49)$$

where S_{nt1} and S_{nt2} are the critical supersaturation ratios at the temperatures T_1 and T_2, respectively.

2.5.2 Heterogeneous nucleation

Formation of new crystals by homogeneous nucleation is feasible only under specific conditions. Much more frequently the formation of a new solid phase is governed by the presence of another solid phase within the system. This new phase appears as a result of heterogeneous nucleation. Particles of a foreign solid phase can act as a catalyst for the nucleation. The Gibbs energy needed for heterogeneous nucleation can be represented by (Söhnel and Garside, 1992):

$$\Delta G_{het} = \Delta G_{hom} f(\theta)_v \tag{2.50}$$

and

$$f(\theta) = (2 - 3\cos\theta + \cos^3\theta)/4 \tag{2.51}$$

where θ is the contact angle between the liquid and the solid. For liquids wetting the surface of the solid phase $\theta < 90°$, then $f(\theta) < 1$ and therefore $\Delta G_{het} < \Delta G_{hom}$. The foreign solid phase then makes nucleation easier and serves as a nucleation catalyst so that nucleation occurs at a lower supersaturation than without the foreign surface being present. If the solid phase is not wetted by the liquid, i.e. $\theta = 180°$, then $f(\theta) = 1$ and according to equation 2.50, $\Delta G_{het} = \Delta G_{hom}$. In this case, nucleation will not be influenced by the foreign solid phase.

2.6 Crystal growth theories

2.6.1 Equilibrium structure of crystal surfaces

To understand the crystal growth mechanisms, the analysis of the energy distribution on the crystal surface needs to be examined. Supposing a crystal is built-up with cubic lattices. If the crystal grows by one layer forming on top of another, the new layer could start from the centre (Figure 2.8, lattice *c*), the edges (lattice *a*) or the corners (lattice *b*) of a flat surface.

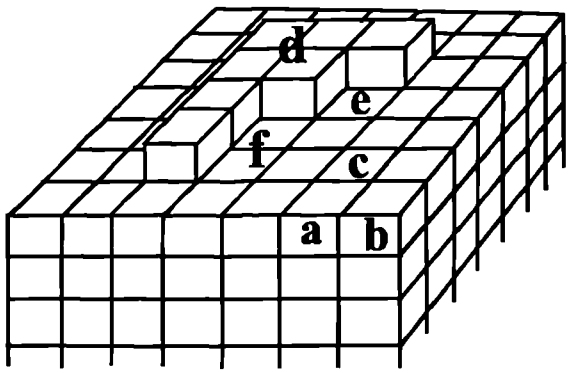

Figure 2.8 A new layer starts from a flat crystal surface. *c*, a lattice in the centre; *a*, in edge; *b*, in the corner; *d*, the first lattice grown on the flat surface; *e*, kink and f, step.

For an ionic crystal, the lattice energy can be defined as the energy liberated when the crystal is formed from widely separated ions. If a pair of ions is considered as point charges Z_1e and Z_2e a distance r apart, the lattice energy can be simply represented as (Evans, 1966),

$$\mu = A_m Z_1 Z_2 e^2 / r \tag{2.52}$$

where A_m is termed the Madelung Constant. When a lattice ion is adsorbed onto a flat crystal surface, the opposite charged ions in the crystal bulk will attract the new incoming ion. To determine the specific surface energy we should take into account the ionic bonds between the first, second and third nearest neighbour ions. The value of the surface energy will be equal to the total work required to break the bonds divided by double the area of the contact surfaces. For a flat surface, the surface energy is (Markov, 1995)

$$\sigma_F = \frac{\Psi}{2b^2} = \frac{\psi_1 + 4\psi_2 + 4\psi_3}{2b^2}, \tag{2.53}$$

where σ_F is the surface energy, ψ_1, ψ_2 and ψ_3 are the work required to break the bonds between the first, second and third nearest neighbours, respectively, and b^2 is the area per ion, where b is the interionic distance. Normally the work contributed by the second nearest neighbours is about 10% of the total work and the work from the third nearest

neighbours will be negligible (Markov, 1995). When a lattice start to form at the positions *c*, *a* and *b* in Figure 2.8, the total work for breaking the ionic bonds will be $\psi_1 + 4\psi_2$, $\psi_1 + 3\psi_2$ and $\psi_1 + 2\psi_2$, respectively. It is clear, from the thermodynamic point of view, a new layer will start from the centres of a flat crystal surface rather than from the edges or corners because the energy gain to form a lattice is the highest at the position *c* compared to the positions at *b* and *a*,

Once a new layer starts to be formed with one lattice (e.g. lattice *d*), the energy gain for incorporating another lattice (e.g. lattice *f*) next to lattice *d* will be high $2\psi_1 + 4\psi_2$, so that the growth rate will be faster than that for the first lattice. As we can see the highest energy gain point is *e* at which the lattice energy is $3\psi_1 + 6\psi_2$; this point has been defined as a "kink" site. From the energy distribution of a crystal surface we can expect that the more the kink sites on a crystal surface, the faster the crystal grows.

2.6.2 The crystal growth mechanism

Many reports about calcite precipitation kinetics show that the mechanism of calcium carbonate precipitation from supersaturated solutions is surface reaction controlled (Mucci and Morse, 1983; Nielsen, 1984; Reddy and Gaillard, 1981; Reddy and Nancollas, 1971, 1973). There are two main theories to describe surface reaction controlled crystal growth theory: two-dimensional nucleus (Markov, 1995) and screw dislocation theory (Gratz et al., 1993).

The Gibbs-Volume theory - Two-dimensional nucleus.

The Gibbs-Volume theory is based on thermodynamic reasoning. When units of the crystallising substance arrive at the crystal face they are not immediately integrated into the lattice, but merely loose one degree of freedom and are free to migrate over the crystal face (surface diffusion). There will, therefore, be a loosely adsorbed layer of integrating units at the interface, and a dynamic equilibrium is established between this layer and the bulk solution. The Gibbs-Volume theory is also called a two-dimensional nucleus. Figure 2.9 (a) shows that a new layer will start from a flat surface by a 2-D nucleus. The building of a new layer is particularly difficult at the beginning of the new layer formation. The excess Gibbs free energy of 2-D nucleation can be written as:

$$\Delta G = \alpha\gamma + \nu\Delta G_v \tag{2.54}$$

and the rate of two-dimensional nucleation, J', can be expressed by

$$J' = A_2 \exp(-\frac{\Delta G}{kT}) = A_2\left[\exp(-\frac{\pi h\gamma^2 \upsilon}{k^2 T^2 \ln S})\right] \tag{2.55}$$

where A_2 is a constant. Once a new layer starts to be formed with a 2-D nucleus or nuclei on the surface, the energy required for incorporating another lattice will be lower, so that the growth rate will be faster than the rate of formation of the 2-D nuclei. Therefore if a crystal grows by the 2-D nucleus mechanism, the entire crystal growth rate should be controlled by the rate of formation of the 2-D nuclei but not be affected by the crystal size. The calculated free energy required for a 2-D nuclei from equation 2.55 is equivalent to the saturation ratio of around 2. However, the crystal growth has been observed at much lower supersaturations (S = 1.01, Mullin, 1994). To explain this phenomenon, another theory of crystal growth has been developed which is called the screw dislocation theory.

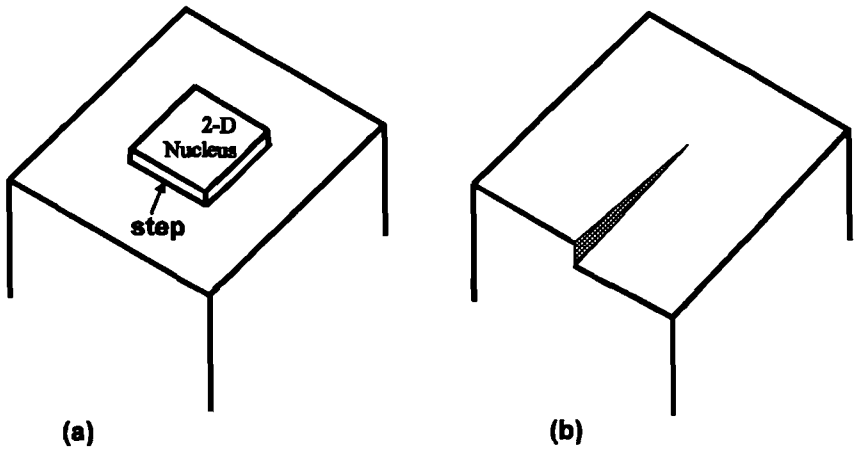

Figure 2.9 The illustration of calcite growth on a flat surface (a) by a the 2-D nucleus and (b) by a screw dislocation mechanisms.

Screw dislocation theory.

The emergence of a screw dislocation on a crystal face results in the formation of a growth step on an smooth crystal surface, as illustrated in Figure 2.9 (b). In the simplest case, this step will develop as an Archimedian spiral which rotates about its axis during growth. Interactions of this spiral with other growth steps that have developed from other sources produce a complicated surface structure. The rate of the crystal surface growth is then determined by the strongest, or dominating, spiral. According to this theory, the energy required to form a new layer is very small and the crystal growth can progress as long as the solution is supersaturated. A theoretical treatment of screw dislocation growth was first given by Burton, Cabrera and Frank (1951). The BCF theory for a crystal growing from an aqueous solution has been developed as a rate law.

2.6.3 Review of crystal growth rate laws

Many crystallisation rate models have been developed to describe dissolution and/or precipitation kinetics under restricted sets of solution conditions. The most successful models are the BCF theory (Burton et al., 1951), Davies-Jones model (1955), Reddy and Nancollas' model (1971) and Plummer's model (1978).

Burton, Cabrera and Frank (BCF) theory

This model was developed by Burton, Cabrera and Frank (1951) for growth from the vapour phase. Later Bennema (1967) modified the model for crystals growing from aqueous solution and suggested that the crystal growth step is developed as an Archimedian spiral which rotates about its axis during growth. The rate at which the crystal surface grows is then determined by the strongest or dominating spiral. The crystal growth rate may be written as:

$$R_m = Cs\sigma^2/Bs \tanh(Bs/\sigma) , \qquad (2.56)$$

where Cs is a rate constant, σ is the relative saturation ($= S^{0.5} - 1$), Bs is a constant dependent on diffusion and temperature, is given by $Bs \propto 1/D^{1/2}T$ where D is the

diffusion coefficient. The BCF surface diffusion model may be simplified under certain conditions:

a. $\sigma << Bs$, then $R_m = Cs\,\sigma^2/Bs$ (parabolic) (2.57)

and

b. $\sigma >> Bs$ then $R_m = Cs\sigma$ (linear) (2.58)

Equations 2.57 and 2.58 shows that when the temperature and/or saturation of the lattice ions are low, the precipitation rate may follow a parabolic rate law, but as the temperature and/or saturation of lattice ions increases, the precipitation rate will tend to follow a linear rate law.

Davies and Jones model (parabolic rate law)

Davies and Jones (1955) developed a kinetic model from the adsorption layer model by assuming that there is a monolayer of hydrated ions covering the crystals in an aqueous solution and the hydration or dehydration of lattice ions at surface sites precedes dissolution or precipitation. The Davies and Jones model can be written as:

$$R_m = sk_{DJ}(C\text{-}C_e)^2\,, \tag{2.59}$$

where R_m is the mass precipitation rate, s is the surface area, k_{DJ} is the rate constant of the Davies and Jones model, and C and C_{eq} are the solution and equilibrium concentrations of the lattice ions. When this equation is applied to calcite precipitation, the equation takes the form:

$$R_m = sk_{DJ}\gamma^{s2}\left[(C_{Ca^{2+}})^{1/2}(C_{CO^2})^{1/2} - K_{sp}^{1/2}/\gamma^s\right]^2 \tag{2.60}$$

This equation is the same as the parabolic rate law form of the BCF theory, and has been used by Granbakken et al. (1989) in their reservoir scale prediction model.

Nancollas and Reddy rate model

In 1971 Nancollas and Reddy examined calcite crystallisation near pH 9 using a seeded growth technique and developed both a reaction rate law and a crystallisation mechanism. They suggested that calcite growth from a supersaturated solution is a second-order surface-controlled reaction. In this case, the rate equation of calcite growth is given by:

$$R_m = sk_f\gamma^{s2}(C_{Ca^{2+}}C_{CO_3^{2-}} - K_{sp}/\gamma^{s2}), \tag{2.61}$$

where k_f is a rate constant. The proposed second-order surface-controlled process is consistent with the observed lack of dependence of k_f on the stirring rate of the solution.

Plummer et al. mechanistic model

Plummer et al. (1978) established a mechanistic model which attempts to describe calcite dissolution and precipitation at any solution pH and pCO_2 value. It described three different dissolution mechanisms appropriate for different regions defined by pH. The overall dissolution rate was written as:

$$R_m = k_4 a_{Ca^{2+}} a_{HCO_3^-} - (k_1 a_{H^+} + k_2 a_{H_2CO_3^*} + k_3 a_{H_2O}) \tag{2.62}$$

where k_1, k_2 and k_3 were given by Plummer et al. as 0.051, 3.45×10^{-5} and 1.19×10^{-7} cm/sec at 25°C (Plummer et al, 1978), This model was established as a dissolution model where the experimental conditions were not designed to carefully measure precipitation rates (Inskeep and Bloom, 1985). Plummer et al. later attempted to modify the model to express the precipitation rate of calcite by using calcite precipitation rate data at low pCO_2 and pH > 8 (House, 1981 and Reddy et al., 1981). They believed that when the solution pH is high (> 8), the solution pH at the calcite surface is lower than that in the bulk solution. The constant for the precipitation (k_4) can be written as:

$$k_4 = \frac{K_2}{K_{sp}}\left[k_1 + \frac{1}{a_{H^+\,s}}(k_2 a_{H_2CO^*} + k_3 a_{H_2O})\right] \tag{2.63}$$

and $a_{H\ s}$ is the activity of hydrogen ion on the calcite solid surface, and which is much lower than the a_{H^+} in the bulk solution. k_1' is 10 to 20 times larger than k_1. When a_{H^+} $= a_{H^+}$ we have:

$$R_m = \gamma^{s2} K_w K_2^{-1} k_4 (C_{Ca^{2+}} C_{CO_3^{2-}} - K_{sp} / \gamma^{s2}) \tag{2.64}$$

which is identical to the Nancollas and Reddy model (1971) when Plummer's constant k_4' is related to k_f of the Nancollas and Reddy model by $k_4 = k_f K_2 K_w^{-1}$.

As we can see from the review of the crystal growth rate laws above, two general calcite growth rate equations can be represented as,

$$R_m = k_p (S^{0.5} - 1)^n \tag{2.65}$$

$$R_m = k_p (S - 1)^n \tag{2.66}$$

where n is defined as apparent reaction order for calcium and carbonate reaction. The BCF rate law is similar to the form of equation 2.65 with the apparent reaction order n of 1 or 2; the Davies and Jones rate model also has the same form as equation 2.65 with n of 2; the Nancollas and Reddy rate model and the Plummer et al model have the same form as equation 2.66 with n of 1.

All the rate equations mentioned above are based on experimental methods and conditions. Some experiments have been carried out by other workers to test these rate equations under different conditions. For example, Inskeep and Bloom (1985) used initial rate measurements and integral methods to test these precipitation rate equations. They concluded that the rate equations that posses a disequilibrium functional dependence, such as the Burton et al.'s dislocation model (1951), the Davies and Jones model (1955), and the model used by Reddy and Nancollas (1973), all have the form similar to equation 6.65, did not adequately describe the kinetics of calcite precipitation at pH's greater than

8 and pCO_2 less than 0.01 atm. Rate equations that describe independent dissolution and precipitation mechanisms with elementary reactions such as the equations presented by Plummer et al. (1978) and Nancollas and Reddy (1971) were more successful. Reddy and Gaillard (1981) used their experimental data to fit some available rate equations. Their results demonstrated that the Davies and Jones crystallisation rate equation satisfactorily describe calcite formation over the solid/solution range encountered in many geochemical and technical situations. A kinetic mode for describing the calcite growth rates at different water composition and conditions has not yet been well established.

2.7 Summary

In this chapter the basic knowledge for understanding the thermodynamics and kinetics of calcium carbonate precipitation has been reviewed. The thermodynamics of the carbon dioxide - water system is important for the study of the kinetics of calcium carbonate precipitation. In an infinitely dilute solution, the ions in solution do not interfere with each other and their behaviour can be described in term of the concentration. However, as the ionic strength increases, the interactions between ions increase too and their behaviour cannot be described in term of their concentrations but need a free ion activity to correct the deviation from non-ideal solution behaviour. The correct thermodynamic calculations are essential for obtaining correct kinetic data representations.

The kinetics of calcium carbonate precipitation has been studied by many workers, but there is as yet no reliable kinetic model available to estimate calcium carbonate scaling rates under oilfield reservoir conditions. This is partially because the determination of kinetic data for carbonate mineral growth is very laborious and depends critically on the solution composition, experimental technique and experimental conditions. Differences from different studies or even from the same study can be one order of magnitude (Zuddas and Mucci (1994), especially when the solutions contain inhibitor ion, such as Mg^{2+}. However, the reasons why these differences happen are not yet clear but is the main control of the kinetics of calcite growth.

CHAPTER 3

ANALYSIS OF CARBONATE SPECIES AND ORGANIC ACIDS

3.1 Introduction

Calcium carbonate scale tendency prediction needs accurate water compositions. The most important ions are calcium and carbonic acid species. The calcium ions can be determined by EDTA titration or AA (atomic absorption) analysis. Carbonate and bicarbonate ions are normally determined from the total alkalinity by acidmetric titration to end point pHs 8.3 and 4.5 using organic indicators (Arnold et al. 1992). As the pHs of most oilfield formation waters are lower than 8.0 (Warren and Smalley, 1994), the total alkalinity is normally assumed to be given by the bicarbonate concentration. When organic acid salts are also present, they also contribute to the solution alkalinity and affect the analysis results for the carbonic acid species. Consequently errors can occur in any geochemical prediction of formation water chemistry and carbonate scaling tendency from these analyses. Thus the conventional and widely practised ASTM titration technique (Arnold et al. 1992) using *HCl* for determining carbonate and bicarbonate ion concentrations in oilfield produced waters can be flawed.

There has been methods to determine the amount of organic acids by adding more *HCl* to the solution to about pH = 2, boiling or flushing with nitrogen to remove all the dissolved CO_2, and then back titration with *NaOH* (Oddo and Tomson, 1994, Day and Underwood, 1991 and Kaasa et al., 1997). It is obvious that short chain organic acids (< C_4) can also be evaporated and CO_2 cannot be removed completely. Therefore the amount of organic acids can only be roughly estimated by this method.

Analysis of a large number of formation waters from oil reservoirs shows that carboxylic acids are the major dissolved organic acids in the water phases (Barth, 1987, 1991 and 1992). Acetic acid is usually dominant. Thus in this work, acetate has mainly been used to quantify the influence of organic acids on carbonate analysis. The influences of acetic acid on the analysis of carbonic acid species are:

- to make the $H_2CO_3^*$ titration end point not clear and difficult to identify;
- over-estimate of bicarbonate concentration.

If it is known that there are organic acids present in an oilfield formation water, the carbonate alkalinity can be determined from the difference in the total alkalinity and the total concentration of organic acids. The total organic acids can be determined from gas chromatographic analysis (Arnold et al., 1992). However, the equipment required for a gas chromatographic analysis is expensive and requires a skilled operator to carry out the analyses and interpret the results. Even so the precision of this method is about ±10% (Warren and Smalley, 1994). It is therefore not feasible to use this technique to analyse accurately the dissolved organic acids in a formation water. The Gran titration method is another possible way to examine titration data and allows one to extract information concerning the location of the titration end point (Stumm and Morgan, 1996). Unfortunately, for the water system containing both carbonate and acetate, the Gran method also fails to identify them separately.

A method to analyse carbonate and acetate mixtures using an automatic titration has been developed during this project. The purpose was to study under what conditions the titration end point could be identified, as well as the effects of the solution total alkalinity, acetate concentration and ionic strength on the titration end point pH. The titration end point pH of carbonate water systems with and without acetate present have then been calculated from the equilibrium of carbonate and acetate water systems and examined by the experimental titration results. Therefore when the bicarbonate end point cannot be identified from a titration, the bicarbonate and acetate concentrations can be calculated from the total alkalinity and endpoint pH.

3.2 Titration and the titration end points

The alkalinity of a water system is normally determined from an acidmetric titration by adding volume increments of a strong acid (e.g. *HCl*) to a water sample. A titration curve can then be plotted as the volume of *HCl* added to a solution against the corresponding pH at each *HCl* increment. When the carbonate species are the only weak base in the water, the concentrations of carbonate and bicarbonate ions can be evaluated

from the amount of *HCl* used to neutralise the amount of carbonate and bicarbonate in the solution. The bicarbonate and the carbonic acid equivalent points are used to define the points at which carbonate and bicarbonate in the solution are neutralised. Figure 3.1 gives the definition of these equivalent points,

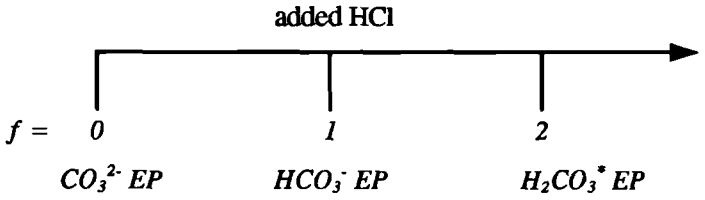

Figure 3.1 The definition of the equivalent points of a CO_2 water system

where f is the equivalent fraction of titrant. When the quantity of acid is added to the point where f equals 1, the carbonate ions in the solution are neutralised into HCO_3^-, therefore this point is called the HCO_3^- equivalent point (the HCO_3^- EP). At the point where f equals 2, the bicarbonate ions are neutralised into $H_2CO_3^*$ and this point is therefore defined as the $H_2CO_3^*$ equivalent point (the $H_2CO_3^*$ EP). The technique of the titration is to locate these equivalent points which are the titration end points. Figure 3.2 gives a typical titration curve of a water system with 0.005 mol/l Na_2CO_3 and titrated with 0.1 mol/l *HCl*.

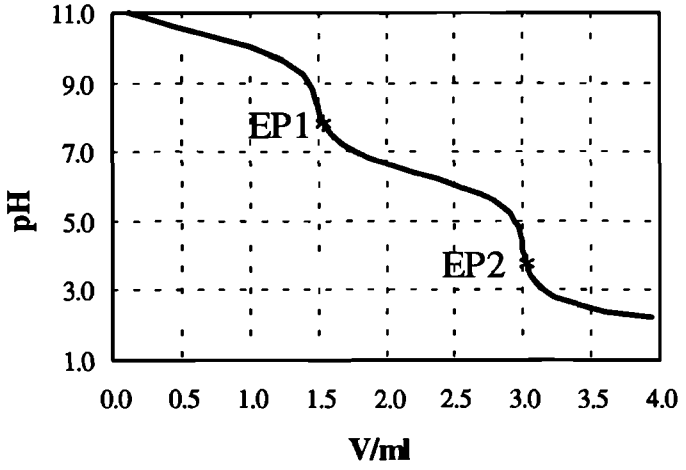

Figure 3.2 A titration curve for the carbonate water system 30 ml 0.005 mol/l carbonate, is titrated with 0.1 mol/l *HCl*. The carbonic acid and bicarbonate EPs are identified as the inflection points of the titration curve.

As we can see from Figure 3.2 both EPs are clearly identified by these inflection points, where a small volume of *HCl* causes a large pH change. An indication of how large a change in pH occurs for a specific incremental addition of strong acid or base is termed the buffer capacity (Pankow, 1991),

$$\beta = \frac{dC_i}{dpH} \tag{3.1}$$

where β is the buffer capacity. It is obvious that if the buffer capacity is low at an equivalent point, the titration accuracy is higher. Figure 3.3 shows the buffer capacity changes during the *HCl* acidmetric titration for the same water system used in Figure 3.2.

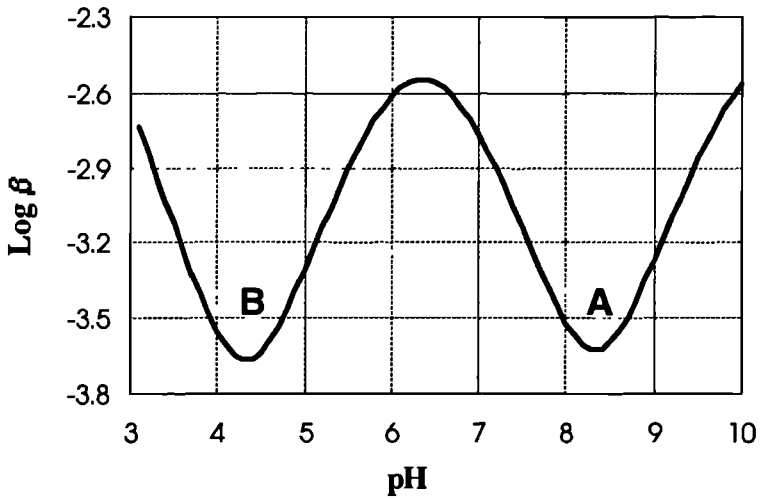

Figure 3.3 The buffer capacity of water system contain 0.005 mol/l of Na_2CO_3. At the points A and B, the buffer capacities reach their minimum values, and correspond to the HCO_3^- and $H_2CO_3^*$ EPs.

From Figure 3.3 we can see that the buffer capacity in a carbonate water system reaches lower level both at the HCO_3^- (point A) and the $H_2CO_3^*$ EP (point B) where the inflection points clearly appear on the titration curve of Figure 3.2. Thus the titration end points for carbonate and bicarbonate can be identified clearly using indicators at pHs 4.5 and 8.3 respectively.

When a water system contains organic acids, they will also contribute to the buffer capacity and alkalinity of the system. The organic acids in a solution can be represented as

$$CH_3(CH_2)_mCOOH \xleftrightarrow{K_a} H^+ + CH_3(CH_2)_mCOO^-, \tag{3.2}$$

$$K_a = \frac{C_{Ac^-}C_{H^+}}{C_{HAc}}, \tag{3.3}$$

where m is the number of CH_2 radicals (m = 0, 1, 2 ...), and HAc and Ac^- are used to represent organic acids and organic acid anions. For a system containing two weak acids or bases (e.g. carbonate and acetate), if the values for their acid dissociation constants, pK_a, do not differ by more than two pH units, there may be no separated inflection point at the equivalent points (Pankow, 1991). As the dissociation constant difference of acetic acid (pKa = 4.75 at 25°C) and carbonic acid (pK_1 = 6.35 at 25°C) is only 1.6, the $H_2CO_3^*$ and acetic acid EPs almost overlap. Figure 3.4 gives the titration curve for a water system containing both carbonate and acetate. As we can see from Figure 3.4, the inflection at the carbonic acid equivalent point (EP2) is much smaller than that in the system without acetate shown in Figure 3.2.

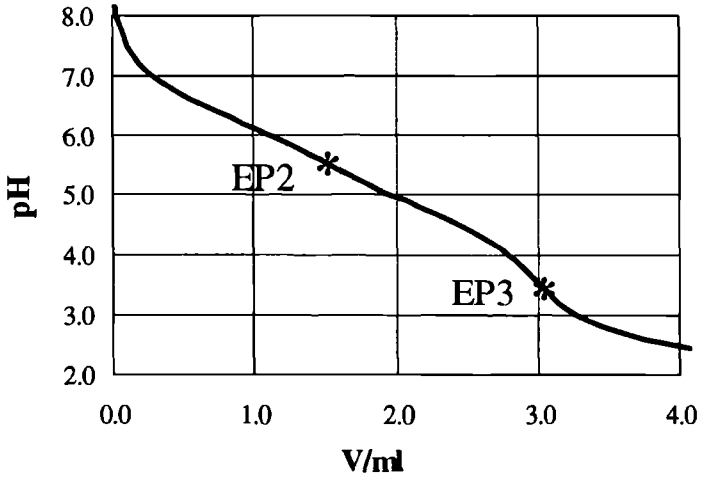

Figure 3.4 A titration curve for a carbonate water system. 30ml 0.005mol/l bicarbonate and 0.005 mol/l acetate is titrated by 0.1mol/l HCl.

As the result of carbonic acid and acetic acid EPs overlap, the buffer capacity at both EPs can be expected to be very small. Figure 3.5 is the plot of the buffer capacity change during the titration of the water system as shown in Figure 3.4.

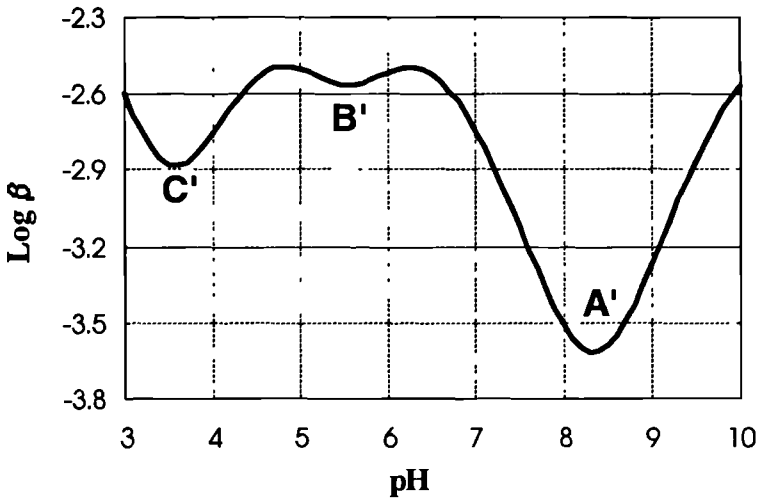

Figure 3.5 The buffer capacity of water system containing 0.005 mol/l of *NaHCO₃* and *NaAc* (*Ac⁻* represents acetate ion). At the points A', B' and C', the buffer capacities reach minimum values, and correspond to the *HCO₃⁻*, *H₂CO₃ and *HAc* EPs.**

As we can see, the buffer capacity reaches a minimum values at the bicarbonate EP (point A'), $H_2CO_3^*$ EP (point B') and the acetic acid EP (point C'), but the change at the $H_2CO_3^*$ end point is much smaller than that the buffer capacity change without acetate (Figure 3.3). This is the main reason why the $H_2CO_3^*$ EP has been found to be very difficult to identify when there are both carbonate and acetate species present in the water. Also, if an organic indicator (e.g. screened methyl orange, titration endpoint pH = 4.5) is used to determine the $H_2CO_3^*$ titration end point, the indicated bicarbonate concentration will be higher than its real value because this is now not its actual end point, as the solution contains some acetate neutralisation capacity. Furthermore, as the result of its lower buffer capacity, the indicator colour change is not sharp and so it is difficult to identify the end point, which can therefore cause error between different analysts.

3.3 The calculation of the H_2CO_3* and HAc equivalent points

The total dissolved organic acids (C_{T2}) are defined as,

$$C_{T2} = C_{HAc} + C_{Ac^-} \quad , \tag{3.4}$$

where C_{HAc} is the total organic acids and C_{Ac^-} is the total organic acid anions. The total alkalinity will be:

$$Alk_T = C_{HCO_3^-} + 2C_{CO_3^{2-}} + C_{Ac^-} + C_{OH^-} - C_{H^+} \quad . \tag{3.5}$$

The concentrations of carbonic acid species and acetic acid species as a function of pH in a closed system are shown in Figure 3.6.

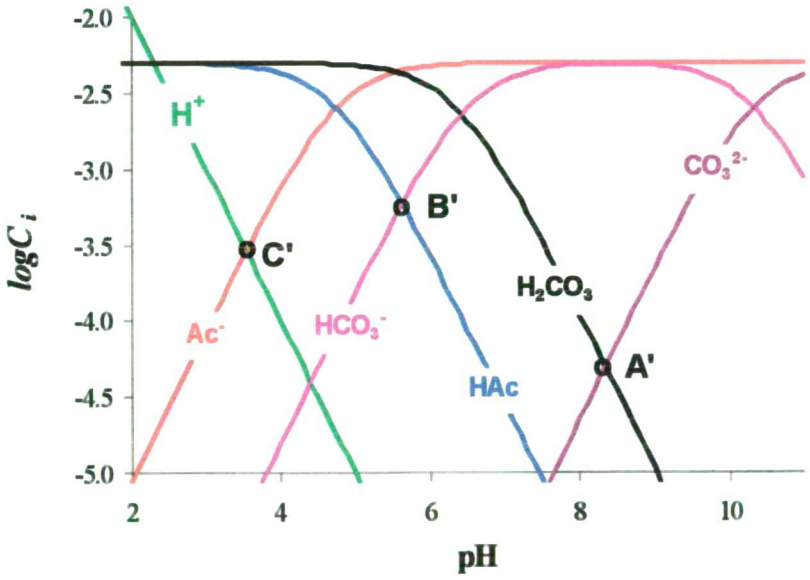

Figure 3.6 The concentrations of carbonate species and acetic acid species as a function of pH in a closed system, $C_{T1} = C_{T2} = 5\times10^{-3}$ mol/l.

Three equivalent points for the HCO_3^-, $H_2CO_3^*$, and *HAc* EPs are approximately at points A', B' and C', which correspond to the three EPs shown in Figure 3.5. The concentration distribution of all these species at different solution pHs are shown in Figure 3.6 and can help us to calculate these three equivalent points.

3.3.1 The $H_2CO_3^*$ EP pH

It is very common to use proton balance equations to accurately determine the equilibrium compositions in a water system containing both acids and bases (Pankow, 1991). A proton balance equation provides an account of the proton and hydroxide ions in the water system. For example, the proton balance equation for pure water is: $C_{H^+} = C_{OH}$. For the water system containing carbonate and acetate, the proton balance equation at the $H_2CO_3^*$ EP is:

$$C_{H^+} + C_{HAc} = 2C_{CO_3^{2-}} + C_{HCO_3} + C_{OH} \quad . \tag{3.6}$$

If the total carbonic acid C_{T1} and total organic acids C_{T2} are not too low (e.g. > 10^{-3} mol/l), the C_{H^+}, $C_{CO_3^{2-}}$ and C_{OH^-} are very small compared with C_{HAc} and $C_{HCO_3^-}$ (see Figure 3.6), and can be neglected, so $C_{HAc} \approx C_{HCO_3}$. As we can see, the same relationship can be obtained from Figure 3.6. From equations (2.9) and (3.3) we have:

$$\frac{C_{T1}}{1 + C_{H^+(e1)} / K_1 + K_2 / C_{H^+(e1)}} = \frac{C_{T2}}{1 + K_a / C_{H^+(e1)}} \quad . \tag{3.7}$$

$C_{H^+(e1)}$ is the hydrogen ion concentration at the $H_2CO_3^*$ EP,

so
$$C_{H^+(e1)} = \frac{(R_C - 1) + \sqrt{(R_C - 1)^2 - 4(K_2 - R_C K_a) / K_1}}{2 / K_1}$$

(3.8)

where R_C (= C_{T1}/C_{T2}) is the ratio of the total carbonate and the total acetate mole concentration. The pH at the $H_2CO_3^*$ EP, pH_{e1}, can then be calculated from,

$$pH_{e1} = -Log C_{H^+(e1)} \tag{3.9}$$

Equation (3.8) shows that the $H_2CO_3^*$ EP pH changes with R_C. If the $H_2CO_3^*$ equivalent point can be identified during a titration, we can calculate R_C by rearranging equation (3.7):

$$R_C = \frac{(C_{H^+(e1)})^2 / K_1 + C_{H^+ e1)} + K_2}{K_a + C_{H^+(e1)}} \quad . \tag{3.10}$$

The mole fraction of acetate (X_a) is,

$$X_a = \frac{C_{T2}}{C_{T1} + C_{T2}} = \frac{1}{1 + R_C} \quad . \tag{3.11}$$

If the $H_2CO_3^*$ EP cannot be found, equations (3.14)-(3.17) below can be used to obtain the concentrations of bicarbonate and acetate.

3.3.2 The acetic acid EP

At the acetic acid EP, the proton balance is,

$$C_{H^+} = C_{Ac^-} + C_{HCO_3^-} + 2C_{CO_3^{2-}} + C_{OH^-} \cdot \tag{3.12}$$

If both C_{T1} and C_{T2} are not so low (i.e. more than 10^{-3} mol/l) and of the same order of magnitude, then $C_{HCO_3^-}$, $C_{CO_3^{2-}}$ and C_{OH^-} can be neglected, i.e. $C_{H^+} \approx C_{Ac^-}$, and we can calculate the hydrogen ion concentration at the acetic acid EP by:

$$C_{H^+(e2} = \frac{-1 + \sqrt{1 + 4C_{T2} / K_a}}{2 / K_a} \, . \tag{3.13}$$

$C_{H^+ e2}$ is the hydrogen ion concentration at the acetic acid EP. From equation 3.13 we can see that the acetic acid EP pH depends on the total acetate concentration and the

acetic acid dissociation constant K_a only. However if C_{T2} is much smaller than C_{T1}, the error of the acetic acid EP pH calculated from equation 3.13 will be significant because the $C_{HCO_3^-}$ in equation 3.12 cannot then be neglected.

3.3.3 The estimation of bicarbonate concentration from the final end point pH

As already indicated, for some situations the $H_2CO_3^*$ EP may not be identified by titration. From equation 3.13 we can find that the final EP (the *HAc* EP) depends only on the total acetic acid. This means that if we obtain the final EP from a titration, the total acetic acid can be estimated by rearranging equation 3.13

$$C_{T2} = \frac{(C_{H^+(e2)})^2}{K_a} + C_{H^+(e2)} \tag{3.14}$$

and from,

$$K_a = \frac{C_{Ac}\, C_{H^+(i)}}{C_{HAc}} = \frac{C_{Ac}\, C_{H^+(i)}}{C_{T2} - C_{Ac}}, \tag{3.15}$$

the concentration of acetate (C_{Ac}-) can then be calculated by rearranging equation (3.15) to

$$C_{Ac^-} = \frac{C_{T2}}{1 + 10^{-pH_i} / 10^{-pK_a}} \quad . \tag{3.16}$$

where pH_i is the initial solution pH before the addition of any *HCl*. If only the two weak bases, carbonate and acetate, are present in a water system and the concentration of carbonate is not too low ($>10^{-3}$ mol/l), the carbonate alkalinity can be estimated from

$$Alk_c = Alk_T - C_A - \tag{3.17}$$

3.3.4 Limitation of the Gran's method

When we face the need to locate a difficult-to-detect EP, the "Gran Titration method" can often provide a solution. This method does not provide a different way to carry out the physical mechanics of a titration. Rather, it is a way to examine titration data (i.e., pH vs. volume of titrant data) that allows one to extract information concerning both the locations of the EP and acid dissociation K values for the acids involved in the titration. Based on the Gran titration method, four functions can be applied to locate the equivalence points f *1* and f *0*, respectively.

$$F_1 \quad (v_0 + v)10^{-pH} \tag{3.18}$$

$$F_2 \quad (v_2 - v)10^{pH} \tag{3.19}$$

$$F_3 \quad (v - v_1)10^{pH} \tag{3.20}$$

$$F_4 - (v_2 - 2v_1 + v)10^{pH} \tag{3.21}$$

where F_1 to F_4 are the Gran Functions and v is the volume of strong acid added, v_0 is the volume of the original sample and v_1, v_2 are the volumes of strong acid added corresponding to the equivalence points f *1* and f *0*, respectively. Figures 3.7 and 3.8 are plotted in terms of the Gran function.

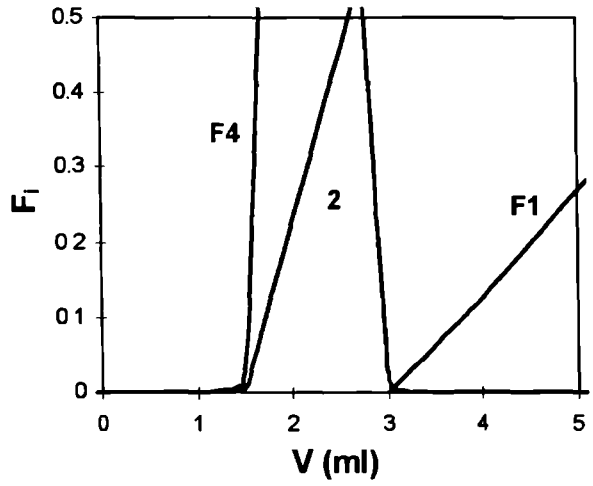

Figure 3.7 The titration curve in Figure 3.2 evaluated by the Gran method, the H_2CO_3* EP and HCO_3^- EP can be clearly identified.

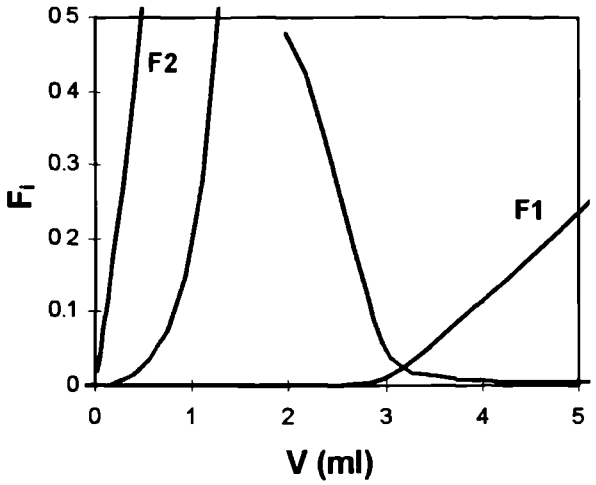

Figure 3.8 The titration curve in Figure 3.4 evaluated by the Gran method, the $H_2CO_3^*$ EP cannot be identified when acetate is present in the solution.

From the analysis using Gran's method we find that it cannot solve the problems of identifying the equivalent points for the solutions containing both carbonate and acetate. A practical but simple analytical method is necessary for obtaining the concentration of carbonate species and organic acid anion.

3.4 Analysis of carbonate and acetate by an acidmetric titration

A series of water sample titrations containing carbonate and acetate has been conducted to identify under what conditions the $H_2CO_3^*$ EP can be identified directly by an automatic titration, and to find out the effects of the total alkalinity, the fraction of total acetic acid, and the ionic strength on identifying the $H_2CO_3^*$ and *HAc* EPs, as well as estimating the accuracy of the calculated bicarbonate and acetate concentrations from equation 3 13 - 3.17 when the $H_2CO_3^*$ EPs cannot be identified directly during titration.

The titrations were carried out using an automatic titration (Metrohm 702SM) with computer software (Metrodata Menu Program) and a combined pH glass electrode (Metrohm 0081.0256). The concentration of each species was determined by the *HCl* volume used to the corresponding inflection points. The titration end points were located by the titration as a minimum slope of the titration curve. In order to find a small minimum inflection from a titration curve, a small signal drift (10 mv/min) and a *HCl* volume increment of $1/20V_{EP}$ were used. V_{EP} is the *HCl* titration volume at the final end

point (for the determination of total alkalinity). When the signal change is less than the set-up value (10 mv/min), the pH value is measured, and the next increment of *HCl* is added.

The pH electrode was calibrated by three NBS buffers; 0.01 mol/l borax (pH = 9.227, 20°C), a mixture of 0.025 mol/l potassium dihydrogen phosphate and 0.025 mol/l disodium hydrogen phosphate (pH=6.878, 20°C), and 0.05 mol/l potassium hydrogen phthalate (pH=3.999, 20°C) (Arnold, 1992).

In our experiments all the samples were prepared by mixing weighed quantities of sodium bicarbonate and sodium acetate solutions and titrated with 0.1 mol/l *HCl*. The titration errors were calculated by: error (%) = $(C_{i(m)}-C_{i(added)})/C_{i(added)}$, where $C_{i(m)}$ and $C_{i(added)}$ are the measured and the added concentrations of the ith species. In all of the calculations, the dilution created by adding the acid solution volume (0.1 mol/l *HCl*) has been taken into consideration, i.e. $C_i = C_{i(m)}V_{sample}/(V_{sample} + V_{HCl})$, where C_i is the real concentration of the *i*th species when a certain volume of *HCl* (V_{HCl}) has been added to the identical volume of water sample (V_{sample}) at each EP.

3.4.1 The effect of the total alkalinity

Table 3.1 gives the water titration results at different total alkalinities. The experiments show that over the wide range of total alkalinity (0.001 mol/l to 0.04 mol/l), the $H_2CO_3^*$ EPs could be identified when acetate is present in the solution. Over the range of total alkalinity from 0.006 to 0.02 mol/l (corresponding to 366 to 1220 ppm bicarbonate) the titration errors for the total alkalinity (from the HAc EP) were less than ±1%. The errors for the determination of carbonate alkalinity from the $H_2CO_3^*$ EP were estimated to be less than ±5%.

3.4.2 The effect of the fraction of total acetic acid, X_a

According to equations 3.8 and 3.11, the $H_2CO_3^*$ *EP pH* should change with the fraction of total acetic acid, X_a. The titration results for different fractions of total acetic acid are given in Table 3.2. Our experimental results show that titration end point pHs give the same change tendency as given by the calculations.

Table 3.1 The titration end point pH is affected by the total alkalinity (Alk_T) when the fraction of total acetic acid (X_a) equals 0.5

No	C_{HCO3}/(mol/l)		error	C_{Ac^-}/(mol/l)		error	Alk_T	error	pH_{e1}-	pH_{e2}-	pH_{e2}-	pH_{e2}
	measured	added	(%)	measured	added	(%)	(eq/l)	(%)	(c)	(m)	(c)	(c-m)
1	0.00049	0.00050	-2.0	0.00042	0.00050	-16.0	0.00091	-9.0	5.69	4.41	4.07	-0.34
2	0.00116	0.00100	16.0	0.00082	0.00100	-18.0	0.00198	-1.0	5.40	4.09	3.91	-0.18
3	0.00176	0.00200	-12.0	0.00220	0.00200	10.0	0.00396	-1.0	5.66	3.82	3.82	0.00
4	0.00288	0.00300	-4.0	0.00312	0.00300	4.0	0.00600	0.0	5.54	3.70	3.67	-0.03
5	0.00394	0.00400	-1.5	0.00409	0.00400	2.3	0.00803	0.4	5.50	3.63	3.61	-0.02
6	0.00504	0.00500	0.8	0.00492	0.00500	-1.6	0.00996	-0.4	5.38	3.48	3.56	0.08
7	0.00675	0.00667	1.0	0.00662	0.00667	-1.0	0.01337	0.3	5.43	3.46	3.50	0.04
8	0.00956	0.01000	-4.4	0.01050	0.01000	5.0	0.02008	0.4	5.56	3.37	3.42	0.05
9	0.02170	0.02000	8.5	0.01858	0.02000	-7.1	0.04028	0.7	5.29	3.29	3.31	0.02

pH_{e1}- (m) = the measured bicarbonate end point pH
pH_{e2}- (m) = the measured acetate end point pH
pH_{e2}- (c) = the calculated acetate end point pH
pH_{e2}- (c-m) = pH_{e2}(c) -pH_{e2}(m)

Table 3.2 The titration end point pH is affected by the fraction of total acetic acid (X_a) when the total alkalinity (Alk_T) equals 0.01 mol/l

No	C_{HCO3}	error	C_{Ac^-}	error	Alk_T	error	pH_{e1}-	pH_{e2}	pH_{e2}-	pH_{e2}-	X_a
	(mol/l)	(%)	(mol/l)	(%)	(eq/l)	(%)	(m)	(m)	(c)	(m)	
10	0.00997	-0.6			0.00997	-0.3	4.08				0
11	NEP[1]				0.00981	-1.9	NEP[1]	3.98	3.93	-0.05	0.1
12	NEP				0.00991	-0.9	NEP	3.74	3.77	0.03	0.2
13	0.00704	0.8	0.00283	-3.4	0.00987	-1.3	5.16	3.62	3.67	0.05	0.3
14	0.00605	1.1	0.00391	-1.8	0.00996	-0.4	5.34	3.61	3.61	0.00	0.4
15	0.00513	2.6	0.00482	-3.6	0.00995	-0.5	5.40	3.51	3.56	0.05	0.5
16	0.00367	-6.6	0.00634	6.8	0.01001	0.0	5.59	3.41	3.52	0 11	0 6
17	0.00273	-5.4	0.00719	3.8	0.00992	-0.8	5.65	3.34	3.48	0.14	0.7
18	-	-	0.01001	0.2	0.01001	0.0	-	3.30	3.41	0.11	1

[1] "NEP" means that this end point was not identified during the titration.

The results show that as X_a changed from 0 to 0.7, the $H_2CO_3^*$ *EP pH, pH_{e1},* increased from 4.08 to 5.65, and that the acetic acid titration end point *pH, pH_{e2},* decreased from 3.98 to 3.30. The significance of this point will be discussed later. When X_a was between 0.1 to 0.5, the difference between the calculated acetic acid end point pH (from equation 13) and the acetic acid EP pH recognised by the titration to be less than ±0.05 pH unit.

When X_a is higher than 0.7 or lower than 0.3, no separate titration end points could be identified for $H_2CO_3^*$ and *HAc*. In these cases the concentrations of bicarbonate and acetate could only be estimated by equations 3.14 - 3.17. For example for the sample No 12 in Table 3.2, the total alkalinity is 0.01 mol/l, X_a is 0.2, the initial pH is 8.51 and the final end point pH is 3.74; so that from equations 3.14 and 3.16,

$$C_{T2} = ((10^{-3.74})^2/10^{-4.75} + 10^{-3.74}) \times 33/30 = 0.00224(mol/l)$$

and

$$C_{Ac^-} = 0.00224/(1+10^{-8.51}/10^{-4.75}) = 0.00224(mol/l) \quad .$$

For the solutions with and without acetate there will be a difference between the end point pHs, but only when this difference is larger than the error of the measurement (0.05pH unit), can the estimations be regarded as sensible. Table 3.3 gives some examples of the calculated final EP pH, pH_{e2}, for the solutions with and without acetate.

Table 3.3 Comparing the titration end point pH in the solutions with and without acetate.

No	Alk_T (eq/l)	X_a	pH_{e2}-(c)	pH_{e2}-(m)	$pH_{e\text{-}HCO3}^-$	ΔpH_c	ΔpH_m
1	0.001	0.5	4.07	4.41	4.68	0.61	0.27
2	0.002	0.5	3.91	4.09	4.53	0.62	0.44
3	0.004	0.5	3.83	3.82	4.38	0.56	0.56
4	0.006	0.5	3.67	3.70	4.30	0.63	0.60
5	0.008	0.5	3.61	3.63	4.24	0.63	0.61
6	0.01	0.5	3.56	3.48	4.20	0.64	0.72
7	0.013	0.5	3.50	3.46	4.14	0.64	0.68
8	0.02	0.5	3.42	3.37	4.06	0.64	0.69
9	0.04	0.5	3.31	3.29	3.94	0.63	0.65
10	0.01	0	-	4.08	4.20	-	0.12
11	0.01	0.1	3.93	3.98	4.20	0.27	0.22
12	0.01	0.2	3.77	3.74	4.20	0.43	0.46
13	0.01	0.3	3.67	3.62	4.20	0.53	0.58
14	0.01	0.4	3.61	3.61	4.20	0.59	0.59
15	0.01	0.5	3.56	3.51	4.20	0.64	0.69
16	0.01	0.6	3.52	3.41	4.20	0.68	0.78
17	0.01	0.7	3.48	3.34	4.20	0.72	0.86
18	0.01	1.0	3.41	3.30	4.20	0.79	0.89

$pH_{e\text{-}HCO3}^-$ = the calculated bicarbonate EP pH at same total alkalinity when there is no acetate present
ΔpH_c = the difference between pH_{e2}-c and $pH_{e\text{-}HCO3}^-$.
ΔpH_m = the difference between pH_{e2}-m and $pH_{e\text{-}HCO3}^-$.

As we can see, the $H_2CO_3^*$ EP pH increase caused by the presence of acetate are significant, from 0.3 to 0.8 pH unit over the solution compositions used in this study, and much higher than experimental error. Therefore if a titration end point pH is more than 0.1 pH unit below the calculated EP pH, it suggests that acetate may be present in the solution. Because dissolved neutral salts, such as *NaCl*, can change a solution pH, we have to also consider their influence on the titration EP pH as discussed later.

3.4.3 The effects of dissolved salts

The effects of dissolved neutral salts on the titration end point are very complicated (Loewenthal and Marais, 1984). This is because dissolved salts affect the concentration dissociation constants of carbonic acid and carboxylic acids, and cause a high residual diffusion potential on a pH electrode.

To find out the effect of ionic strength on the titration end point pH, some titration experiments have been conducted for solutions at a fixed alkalinity but with different amounts of *NaCl* or with a brine representing seawater (Warren and Smalley, 1994). The test solutions contained 0.01 mol/l of bicarbonate and acetate (Alk_T = 0.02 eq/l). The composition of the brine was:

Ions	Concentrations (mol/l)
Na^+	0.573
K^+	0.00929
Mg^{2+}	0.0499
Ca^{2+}	0.00510
Cl^-	0.639
SO_4^{2-}	0.0269
ionic strength	0.740

Table 3.4 presents the measured titration pH at different ionic strengths. In general, as the ionic strength increased the titration end point pH decreased. When the solution contained concentrated NaCl (1.5 mol/l) or 100% of synthetic seawater, the H_2CO_3* EPs cannot be identified. Thus a significant error can be made if the bicarbonate

Table 3.4 The titration end point pH as a function of ionic strength when Alk_T equals 0.02mol/l and X_a equals 0.5

No	C_{HCO3^-} (mol/l)	error (%)	C_{Ac^-} (mol/l)	error (%)	Alk_T (eq/l)	error (%)	pH_{c1}- (m)	pH_{c2}- (m)	pH_{c2}- (c)	pH_{c2}- (c-m)	NaCl (mol/l)	Seawater[1] (%)	IS[2] (eq/l)	$C_{Ac^-(c)}$[3] (mol/l)	error (%)
19	0.00980	-2.0	0.01021	2.1	0.02001	0.0	5.57	3.44	3.42	-0.02	0.00		0.033	0.00912	-8.8
20	0.00991	-0.9	0.01008	0.8	0.01999	0.0	5.47	3.41	3.41	0.00	0.05		0.075	0.01015	1.5
21	0.00988	-1.2	0.01011	1.1	0.01999	0.0	5.45	3.41	3.41	0.00	0.10		0.116	0.00987	-1.3
22	0.00987	-1.3	0.01016	1.6	0.02003	0.1	5.42	3.39	3.39	0.00	0.20		0.200	0.01021	2.1
23	0.01002	0.2	0.01001	0.1	0.02003	0.1	5.31	3.37	3.38	0.01	0.30		0.283	0.01056	5.6
24	0.00983	-1.7	0.01013	1.3	0.01986	-0.2	5.25	3.35	3.36	0.01	0.50		0.449	0.01033	3.3
25	0.01007	0.7	0.00998	-0.2	0.02005	0.2	5.16	3.31	3.29	-0.02	1.00		0.866	0 00933	-6.7
26	NEP				0.02014	0.7	NEP	3.18	3.23	0.05	1.50		1.283	0.01265	26.5
27	0.01017	1.7	0.00986	-1.4	0.02003	0.1	5.37	3.40	3.41	0.01		20	0.156	0.01034	3.4
28	0.01019	1.9	0.00994	-0.6	0.02013	0.6	5.33	3.40	3.39	-0.01		40	0.280	0.00972	-2.8
29	0.00961	-3.9	0.01046	4.6	0.02007	0.4	5.24	3.38	3.38	0.00		60	0.403	0.01001	0.1
30	0.01084	8.4	0.00920	-8.0	0.02004	0.2	5.09	3.37	3.37	0.00		80	0.526	0.00985	-1.5
31	NEP				0.02006	0.3	NEP	3.35	3.35	0.00		100	0.650	0.01014	1.4

(1) Synthetic seawater (%) = volume of synthetic seawater/total volume of solution (10ml).
(2) The dilution by adding HCl has been concerned for the calculation of IS.
(3) $C_{Ac^-(c)}$ = calculated acetate concentration from equation 3.16.

concentration is now calculated from the titration end point pH. Therefore the influence of dissolved salts on the titration end point pH must be corrected.

From the EP pH changes with ionic strength shown in Table 3.4, a function has been established (equation 3.22) to correct the deviation of calculated EP pH with the measured values for solutions with high ionic strength.

$$pH_{(e)c} = pH_o - K(IS), \tag{3.22}$$

where $pH_{(e)c}$ and pH_o are the EP pH value with and without added neutral salts, K is a factor, IS is ionic strength with units of eq/l. From the experimental data we found that with the K values of 0.15 and 0.11 for $NaCl$ solution and seawater, a good prediction of end point pHs could be achieved. All the calculated EP in Tables 3.1 to 3.4 have been corrected by equation (3.22). The difference between the calculated EP pH and real measurements were smaller than ±0.02 pH units for high salinity solutions, whereas in dilute solutions at the same alkalinity and carbonate and acetate ratio, this difference can be as high as 0.08 pH units. This comparison indicates that the titration method is more suitable for high salinity waters, e.g. oilfield formation water, especially when the $H_2CO_3^*$ EP cannot be identified and the acetate concentration has to be estimated from the titration end point pH and total alkalinity.

3.4.4 The effect of other short chain carboxylic acids

As mentioned at the beginning of this chapter, the $H_2CO_3^*$ EP will be affected by any organic acid if its pK_a is within ±2 pH unit of the pK_1 of carbonic acid, (pK_1 = 6.35). Thus acetic acid (pK_{a2} = 4.75), propionic acid (pK_{a3} = 4.87) and butyric acid (pK_{a4} = 4.82) will have an effect but formic acid (pK_{a1} = 3.74) should not. Titrations have been carried out with a number of these acid anions. The measured titration end point pHs have a good match with the calculated values if the individual K_a of the organic acid is applied. The calculated EP pH values are shown in Figure 3.9.

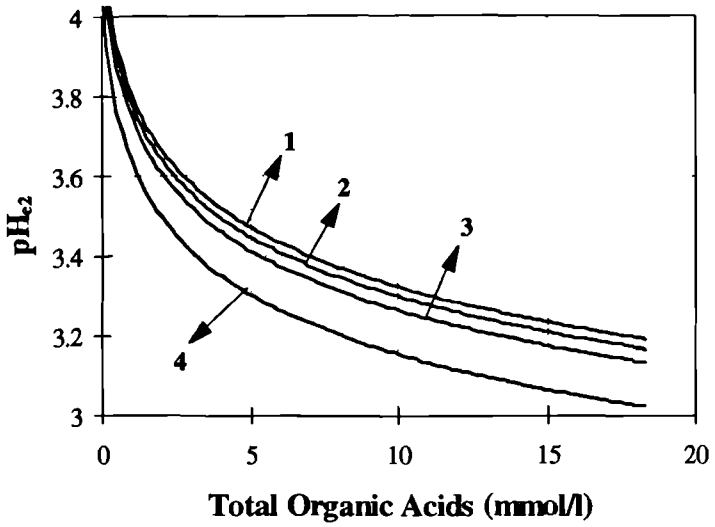

Figure 3.9 The effect of different carboxylic acids on the determination of EP pH. The EP pH (pH_{e2}) change with the concentration of carboxylic acids as well as the ionic strength in a closed water system at 25°C. (1) propionic acid (C_3), (2) butyric acid (C_4), (3) acetic acid (C_2), (4) acetic acid with 1 mol/l NaCl.

It can be seen clearly from Figure 3.9 that the differences of EP pH for these three carboxylic acids are very small. Thus for practical purposes for reservoir formation water at the wellsite, if the concentrations of other organic acids (C_{3+}) are much lower than acetate (C_2), the analysis errors will be very small even if all the organic acids are considered to be just acetic acid. Curve (4) in Figure 3.9 shows the EP pH for a solution containing the same concentration of acetate as that used for obtaining the data for curve (2) but at a high ionic strength (1 mol/l). The difference in the EP pH caused by the high ionic strength is much larger than those caused by the different type of organic acids used and so the ionic strength effect must be corrected using equation 3.22.

3.5 Suggestions for oilfield applications

3.5.1 How to handle water samples

This work has shown that the titration end points of $H_2CO_3^*$ can be difficult to identify when acetate is also present. The practical measurable range for identifying separated titration end points for bicarbonate and acetate respectively depends on the total alkalinity Alk_T, the fraction of total acetic acid X_a, and ionic strength. Thus for an

unknown sample if the $H_2CO_3^*$ *EP* cannot be found during the titration, the reasons could be that the total alkalinity is lower than 0.001 mol/l or higher than 0.04 mol/l, and/or the fraction of total acetic acid, X_a, is lower than 0.3 or higher than 0.7 and/or the ionic strength is higher than 1.0 mol/l NaCl. In these cases the acetate and bicarbonate concentration can be calculated from the titration final end point pH, the total alkalinity and ionic strength by using the equations 3.14 - 3.17. Alternatively, the fraction of total acetic acid could be adjusted to be close to 0.5 by adding either acetate or bicarbonate solution to the water sample and titrating the sample again. In this way a more reliable result should be obtained, because when the fraction of total acetic acid equals 0.5, the buffering capacity change at the $H_2CO_3^*$ EP is at its maximum compared to any other ratio (Figure 3.10).

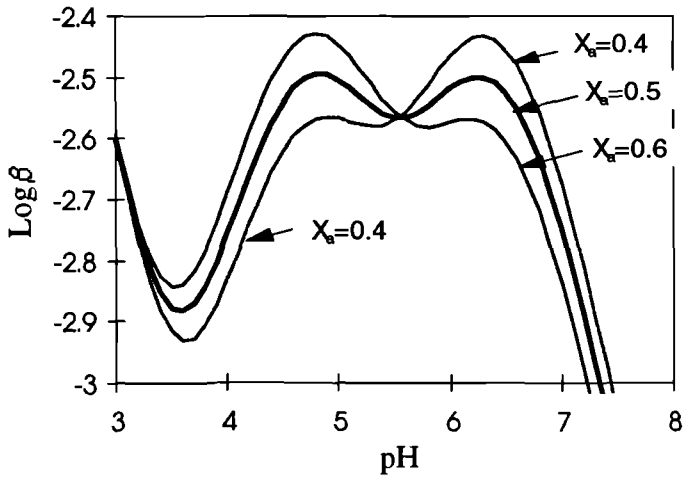

Figure 3.10 The buffer capacity (β) change with the mole fraction of total acetic acid (X_a = 0.4 - 0.6)

If the total alkalinity and/or ionic strength of a water sample is too high, the sample can be diluted with distilled water to the practical measurable range.

3.5.2 Suggested use of an automatic titration

An automatic titration or pH meter rather than organic indicator solutions must be used to analyse bicarbonate in water samples such as oilfield formation waters. During the titration, not only the volume of HCl used in the titration but also the titration endpoint pHs should be reported for each titration. In this way, the presence of carboxylic acids

can be detected at an early stage. Often even today, the alkalinity titrated to pH 4.5 by indicator is used to determine the concentration of bicarbonate, but as we have shown, if carboxylic acids are present, part of the neutralisation will be due to the effects of the carboxylic acids. This will cause errors in any application of the water analysis data, such as the calculation of $CaCO_3$ precipitation tendency (SI) and in-situ formation water pH estimations. Table 5 gives the calculated $CaCO_3$ precipitation tendency and the amount of $CaCO_3$ to be precipitated for two oilfield formation waters (Warren and Smalley, 1994). It can be seen from Table 5 that a significant overestimation of $CaCO_3$ precipitation occurred when the concentration of carboxylic acid anions is high compared to that of bicarbonate. Such errors can lead to incorrect estimation of oilfield scaling tendencies which could lead to an increase of unplanned wellbore workovers and sometimes even the provision of inappropriate production facilities.

Table 3.5 The errors of the calculated $CaCO_3$ precipitation tendency caused by using a normal water titration method

Oilfield	pH	Ionic strength (eq/l)	Using correct water analysis data including acetate SI	$CaCO_3$ Precipitated (mg/kg)	Carboxylic acid anions is reported as bicarbonate SI	$CaCO_3$ Precipitated (mg/kg)
Gryphon	6.0	1.20	0.202	96	0.524	444
Highland	6.0	0.82	0.088	30	0.244	113

3.6 Summary

Analysing for carbonate concentration by acid titration in a water system containing organic acids is always a problem because of the overlapping the titration end points. A practical method has been developed to accurately analyse carbonate species and organic acid anions by carrying out titrations using an automatic titration and by simple calculations.

For the identification of the $H_2CO_3^*$ EP of solutions containing both carbonate and acetate, the practical measurable ranges are: (a) the total alkalinity is from 0.006 to 0.02

mol/l when X_a is near 0.5; (b) the fractions of acetate are from 0.3 to 0.7; (c) the solution ionic strength is less than 1.0 mol/l. Even when the $H_2CO_3^*$ EP cannot be identified during the titration, the bicarbonate and acetate concentration of a solution can be calculated from the titration end point pH, the total alkalinity and solution ionic strength using equations (3.14) - (3,16). The calculated equivalent pH affected by dissolved salts can be corrected by an empirical equation (equation 3.22).

CHAPTER 4

THE METHODOLOGY FOR STUDYING THE KINETICS OF CALCIUM CARBONATE PRECIPITATION

4.1 Introduction

Experimental techniques always play an important role in the determination of the kinetics of $CaCO_3$ precipitation because the chemical reactions involved are influenced by many factors, such as solution saturation state, CO_2 partial pressure, pH, involvement of a gas phase, seed surface properties, solution ionic composition and any inhibitors as well as the hydrodynamics. Steady state methods, such as the "chemo-state" system (Mucci and Morse, 1983) and the "constant composition" system (Kazmlerczak et al., 1982), have been widely used in many studies (House, 1989; Kazmlerczak et al., 1982; Morse, 1974a; and Zhong and Mucci, 1989 and 1993), but they require complicated procedures and it is experimentally difficult to maintain constant conditions as a non-steady state period always exists at the beginning of an experiment. The effectiveness of any steady state method also depends on the rate at which CO_2 is produced in the solution by precipitation of calcium carbonate as compared to the rate of transport of the CO_2 produced during $CaCO_3$ precipitation (Arakaki and Mucci, 1995).

Free-drift methods to study the kinetics of calcite precipitation has also been reported (Weyl, 1958, House, 1989, Reeder et al., 1990 and Arakaki and Mucci, 1995). However, if an open system is used, the overall pH change from the initial state to the equilibrium state can be very small so that the calcite growth rate cannot be determined from the solution pH changes with sufficient accuracy, and the transformation of experimental data (pH vs. time) to give reaction curves (growth rate vs. time) can be complicated (Söhnel and Garside, 1992). It is also not usual practice to determine the calcite growth rate by monitoring the concentration of Ca^{2+} change by a Ca^{2+} sensitive electrode or water sampling for solutions with high ionic strengths (> 0.1 mol/kg) because of the small differential changes involved. Furthermore, the degree of transport for a mass reaction is generally determined from the effect of stirring rate on reaction rate, a lack of

stirring dependence being taken to imply a lack of transport control (Sjöberg and Rickard, 1983). It has been shown that in systems with poorly defined hydrodynamics, a lack of stirring dependence may not directly reflect the role of mass transport (Sjöberg and Rickard, 1983 and Nielsen, 1984). This makes both the interpretation of rate data and the comparison between independent studies dificult. There are also some attempts to examine the kinetics of the calcite - water reaction by observation of single crystal growth (Compton and Unwin, 1990, Higuchi et al, 1992 and Mullin, 1994), but most of them were designed for dissolution of calcite. In order to obtain satisfactory kinetic data, we have to keep the following questions in mind:

- Does the analytical method properly represent the extent of the reaction?
- Are the conditions of the experiment properly established and applicable?
- Are the data reproducible?

The aim of this chapter is to develop proper experimental methods in which all these questions are considered. Two experimental methods have been developed to study different aspects of the kinetics of calcite precipitation; the pH-free-drift method for the determination of the kinetic model over a wide range of saturation states in a closed water system and the visual observation method used for the determination of rate constant of $CaCO_3$ growth at different temperatures and transport rates in glass micromodels. The equations for converting the measured pH data to crystal growth rate data are also given.

4.2 The pH free drift method

When $CaCO_3$ precipitation occurs, the bulk solution pH falls. If the reaction is carried out in a completely closed water system without a gas phase present, there will be no CO_2 exchange between the solution and gas phase and the solution pH changes will be related only to the $CaCO_3$ precipition rate. The $CaCO_3$ precipitation rate can then be determined by following the bulk solution pH change as a function of time.

4.2.1 Materials and equipment

All chemicals used in the experiments were BDH AnalaR laboratory reagents. Calcite seeds were of BDH AnalaR $CaCO_3$ powder which contains more than 99% of calcite as determined by X-ray diffraction analysis (Figure 4.1). They had a specific surface area of 5.88 m^2/g as determined by a BET method using a Coulter Omnisorp 100, a volumetric adsorption instrument, and nitrogen gas as adsorbate at liquid nitrogen temperatures.

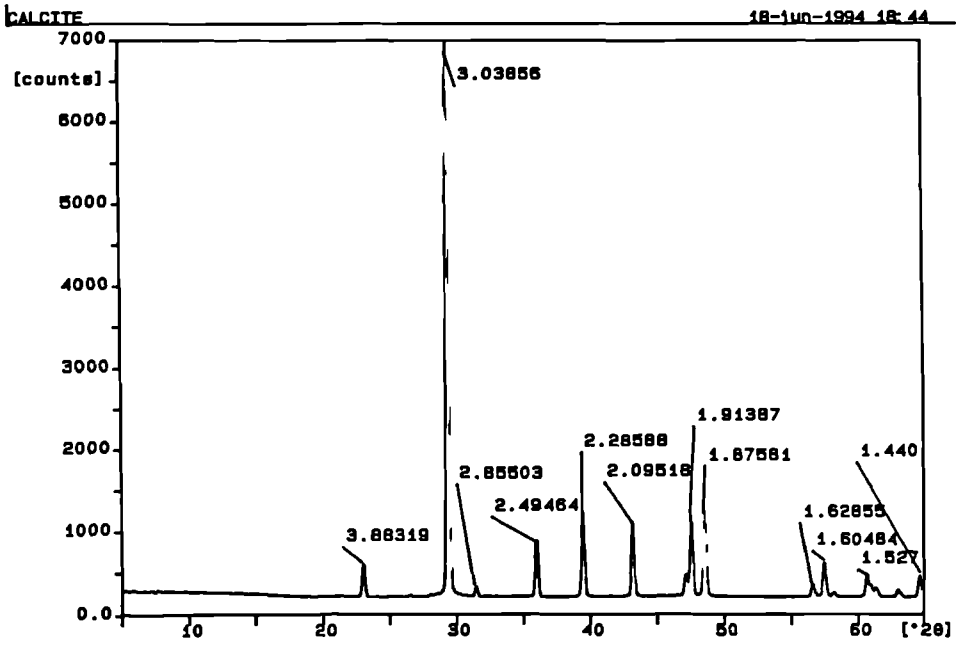

Figure 4.1 The result of an X-ray diffraction analysis of BDH AnalaR $CaCO_3$ powder.

The pH-free-drift experiments were conducted at selected constant temperatures in a 250ml double-walled vessel connected to a recirculating constant temperature bath. A schematic diagram of the pH-free drift equipment is shown in Figure 4.2. The vessel could be completely closed by a cover with four removable entry ports. A pH electrode was put into one of these ports and a thermometer in another. The solution in the reaction vessel was stirred with a magnetic stirrer at a constant rate. The temperature of the solution was held constant by circulating water from a constant-temperature bath. The pH electrode was calibrated in the same way as described in section 3.3. After each long time pH measurement (>8 hours), the electrode was checked by a pH buffer whose pH was nearest to the experimental solution's pH.

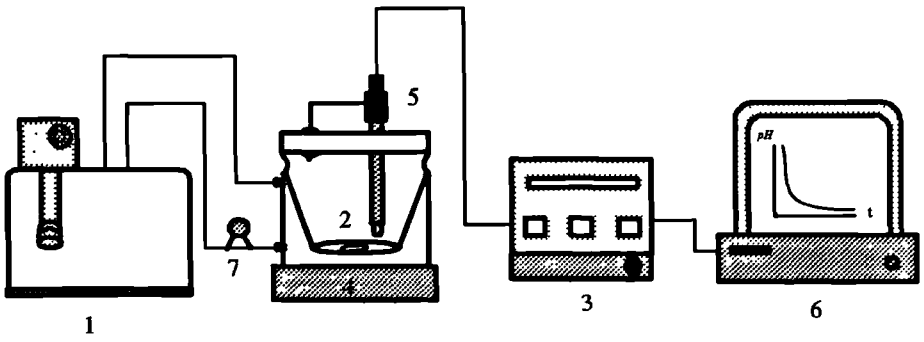

1 water bath, 2 magnetic stirrer, 3 titrator, 4 reaction vessel, 5 pH electrode, 6 computer, 7 pump

Figure 4.2 Schematic diagram of the pH-free drift equipment

4.2.2 The procedure of the pH free drift method

(i) The supersaturated calcium carbonate solutions were prepared by mixing equal volumes (200ml) of a $CaCl_2$ solution and $NaHCO_3$ which were each twice the desired final concentration. The desired pH was obtained by bubbling in CO_2 to lower the pH, or by bubbling in N_2 to increase the pH.

(ii) The prepared solution was placed into the reaction vessel, the vessel closed and one port opened to add calcite seeds. The water from the water bath was circulated to the vessel until the solution reached the designed temperature, and the solution pH recorded.

(iii) After the solution pH remained stable for half an hour, the required calcite seeds were weighed and added to the solution, the vessel was then completely closed by sealing the last port to ensure that there was no gas phase in the vessel.

(iv) The pH change accompanying the calcite growth was then recorded as a function of time immediately after the calcite seeds had been added to the $CaCO_3$ supersaturated solution.

(v) When the solution pH stopped decreasing, the solution was removed and filtered through a Millipore 0.22 μm filter to separate the solid calcite from the liquid. The calcium ion concentration in the solution was analyzed by EDTA titration by a Ca^{2+} ion-selective electrode and/or the alkalinity determined by acid titration, if the concentration ratios of Ca^{2+} and HCO_3^- ($C_{Ca^{2+}}/C_{HCO_3}$) were greater than 8.

4.2.3 The calculation of precipitation rate

The calcite precipitation rate is normally represented as the calcium concentration change as a function of time, i.e.

$$R_m \propto -dC_{Ca^{2+}}/dt \tag{4.1}$$

The rate data obtained from the experiments are solution pH changes as a function of time. As mentioned in chapter 3, the solution buffer capacity at different pH ranges is different, thus dpH/dt is not a linear function of $dC_{Ca^{2+}}/dt$. In other words, the same amount of precipitation will cause a different pH unit change for different water systems. To convert a pH change as a function of time (*dpH/dt*) to the calcium ion concentration changes ($dC_{Ca^{2+}}/dt$), the mass balance has been used. According to equation 1.1, forming one mole of $CaCO_3$ will result in two eq/kg alkalinity reduction and one mol/kg of total carbonate reduction. If the amount of $CaCO_3$ precipitate from a supersaturated solution at time t is $(PPT)_t$ mol/kg, the total alkalinity (defined by equation 2.13) at that time will be:

$$(Alk_T)_t = Alk_T - 2(PPT)_t = (C_{T1} - (PPT)_t)(\alpha_1 + 2\alpha_2) + C_{OH^-} - C_{H^+} \tag{4.2}$$

and the amount of $CaCO_3$ precipitate at time t can be obtained by rearranging equation (4.2),

$$(PPT)_t = \frac{Alk_T - C_{T1}/(\alpha_1 + 2\alpha_2) - C_{OH} + C_{H^+}}{2 - \alpha_1 - \alpha_2} \tag{4.3}$$

The concentration of the remaining ions in solution at time t can be calculated from,

$$(C_{Ca^{2+}})_t = (C_{Ca^{2+}})_i - (PPT)_t \tag{4.4}$$

$$(C_{CO_3^{2-}})_t = [(C_{T1})_i - (PPT)_t]\alpha_2 \tag{4.5}$$

where $(C_i)_t$ refers to the concentration of the ith species at time t. With equations 2.9 to 2.11 and 4.3 to 4.5, a measured solution pH change as a function of time can be converted to the amount of calcite precipitate as a function of time. Figure 4.3 gives an example of a measured solution pH changes as a function of time and the converted Ca^{2+} concentration change as a function of time.

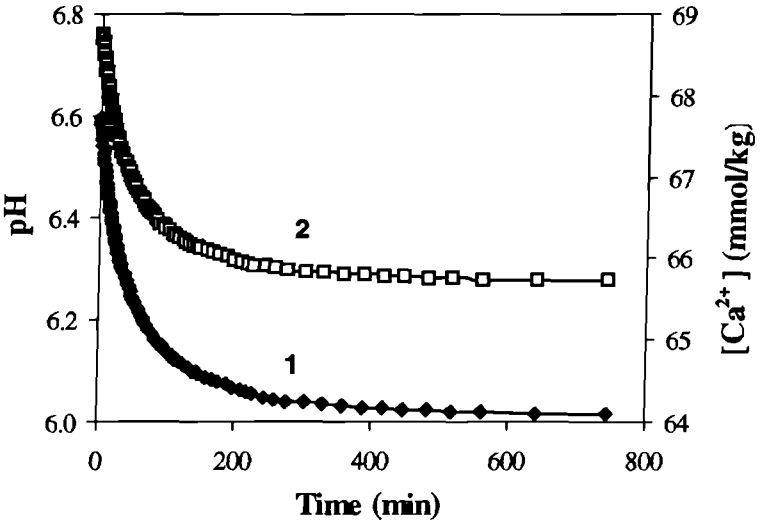

Figure 4.3 Converting the measured pH changes as a function of time (curve 1) to the Ca^{2+} concentration changes as a function of time (curve 2).

During calcite growth, the supersaturation ratio (S) will decrease with time. The supersaturation ratio at time t (S_t) can be obtained from

$$S_t = \frac{(a_{Ca^{2+}})_t (a_{CO_3^{2-}})_t}{K_{sp}} = \frac{(C_{Ca^{2+}})_t (C_{CO_3^{2-}})_t \gamma_{Ca^{2+}} \gamma_{CO_3^{2-}}}{K_{sp}} \tag{4.6}$$

We have demonstrated in chapter 2 that ion pairing is significant in a finitely dilute solution and affects the calculation of water chemistry so must not be ignored. The supersaturation of

the precipitated ions is obtained from the activity product of the free ions. Therefore a free ion concentraton should be used to calculate the saturation ratio at time t of $CaCO_3$ from equation 4.6. To determine the concentration of the free ions of Ca^{2+} and CO_3^{2-}, the stoichiometric equilibrium constants of all ion pairs associated with Ca^{2+} and CO_3^{2} must be determined. For the ion pair $CaCO_3^{o}$, we have

$$K'_{CaCO_3^o} = \frac{C_{Ca^{2+}} C_{CO_3^{2-}}}{C_{CaCO_3^o}} \quad . \tag{4.7}$$

and

$$C_{CaCO_3^o} = C_{Ca^{2+}} C_{CO_3^2} / K'_{CaCO_3^o} \quad . \tag{4.8}$$

The same treatment can be applied to the other calcium ion pairs, so that the concentration of total Ca^{2+} ion can be obtained from:

$$(C_{Ca^{2+}})_T = C_{Ca^{2+}} + C_{CaCO_3^o} + C_{CaHCO_3} + C_{CaOH^+} + C_{CaSO_4^o} + \cdots \tag{4.9}$$

i.e.

$$\begin{aligned}(C_{Ca^{2+}})_T = {} & C_{Ca^{2+}} + C_{Ca^{2+}} C_{CO_3^{2-}} / K'_{CaCO_3^o} + C_{Ca^{2+}} C_{HCO_3} / K'_{CaHCO_3} + C_{Ca^{2+}} C_{OH} K'_{CaOH^+} \\ & + C_{Ca^{2+}} C_{SO_4^2} K'_{CaSO_4^o} + \cdots\end{aligned} \tag{4.10}$$

so that the free Ca^{2+} ion cancentration can be obtained from:

$$C_{Ca^{2+}} = \frac{(C_{Ca^{2+}})_T}{1 + C_{CO_3^2} / K'_{CaCO_3^o} + C_{HCO_3} / K'_{CaHCO_3^-} + C_{OH} K'_{CaOH^+} + C_{SO_4^2} K'_{CaSO_4^o} + \cdots} \tag{4.11}$$

and similarly for CO_3^{2-} ions,

$$(C_{CO_3^2})_T = C_{CO_3^2} + C_{CaCO_3^o} + C_{MgCO_3^o} + C_{NaCO_3} + \cdots \tag{4.12}$$

so that the concentration of free CO_3^{2-} ion can be determined by

$$C_{CO_3^{2-}} = \frac{(C_{CO_3^{2-}})_T}{1 + C_{Ca^{2+}} / K'_{CaCO_3^0} + C_{Mg^{2+}} / K'_{MgCO_3^0} + C_{Na^+} / K'_{NaCO_3^-} + \cdots} \tag{4.13}$$

In this work, the ion pair influence has been considered for all the calculations.

As calcite crystals grow, the total surface area for growth increases. This has also to be considered in the calcite growth rate calculations. If we assume that all the calcite crystal surfaces have the same activity for growth, the total calcite crystal surface area at time t should be

$$A_t = A_i [(W_i + (PPT_t) \times 111) / W_i]^{2/3} \tag{4.14}$$

where A_i and A_t are the surface area of the calcite seeds at the beginning and at the time t, respectively; W_i is the initial seed weight in g/kg. From equations 4.3 - 4.14, the crystal growth rate as a function of the supersaturation ratio can be calculated. Figure 4.4 gives an example of the ploted rate data presented in Figure 4.3, using $(A_t / A_i d(C_{Ca^{2+}})_t / dt)$ against $(S_t^{0.5} - 1)$, so that the crystal growth rate as a function of supersaturation can be obtained .

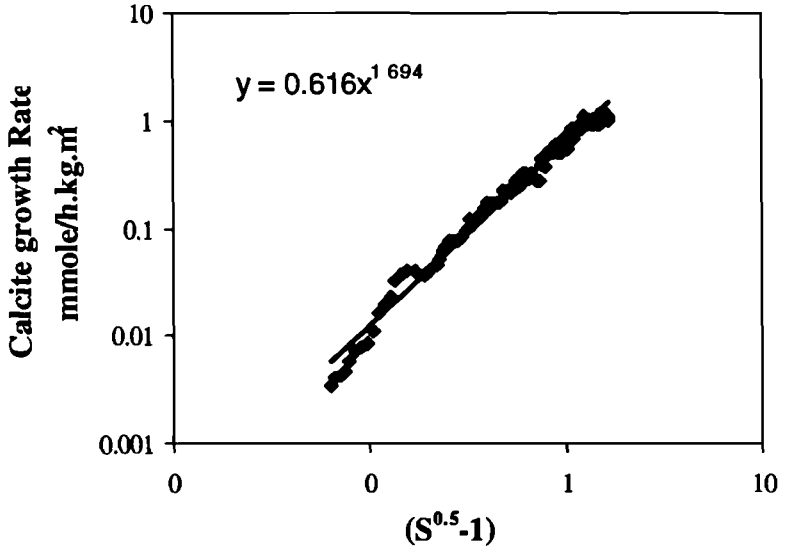

Figure 4.4 The calcite growth rate as a function of supersaturation ratio

4.2.4 The accuracy and reproducibility of $CaCO_3$ growth rate measurements

The advantages of using the pH drift method are that the experiments are simple and easy to control and repeat, and that the kinetics of $CaCO_3$ precipitation can be studied in detail over the saturation range from the initial supersaturation state to the equilibrium state in a single experimental run. The problems of this method (and other mass reaction methods) are that the pH measured by normal pH electrodes at a high ionic strength and high temperature may not represent the real hydrogen ion concentration because of the pH electrode free drift and residual liquid junction potential. Furthermore it can be difficult to obtain accurate values of the calcite seed surface area.

The electrode drift is caused by back diffusion of water into the internal reference electrolyte of the pH electrode, and is proportional to the concentration difference between the measured solution and the internal reference electrolyte. It is obvious that a high salinity solution can reduce the electrode pH free drift, but will increase the residual liquid junction potential (Bates, 1964). In this work, the solutions used for the precipitation experiments contained 1 mol/kg of *NaCl*, so that the deviation of pH measurement caused by the residual liquid junction potential is large. The Henderson equation (equations 2.35 and 2.36) has been used to estimate the pH deviation caused by the residual liquid junction potential. The values for the water systems with 1 mol/kg added *NaCl* at 25°C are 0.07 to 0.09 pH units.

During $CaCO_3$ precipitation, the system pressure may change slightly because there is no gas phase inside the reaction vessel to buffer the small volume change caused by releasing CO_2 during the calcite precipitation. This will also increase the liquid junction potential and in turn affect the pH measurement. To avoid this problem a plastic capillary tube of 0.5 mm diameter was used to connect the reaction vessel and electrode reference electrolyte chamber to maintain the pressure in the reaction vessel and electrode at the same level, and at same time to prevent the reference solution in the electrode evaporating.

After according for the residual liquid junction potential, the error of pH measurement is less than 0.02 pH unit. The total pH change from initial to the equilibrium state is about 0.7 - 0.8 pH units for a solution with an SI of 0.8. Thus the error will be less than 3%.

The reproducibility of the calcite growth rate data obtained from the pH-free-drift method has been examined by conducting a series of experiments with similar compositions and initial pHs. Table 4.1 shows the results.

Table 4.1 The reproducibility of the pH-free-drift method for determine calcite growth rate on the calcite seed*

No	pH_i	Alk_T (meq/kg)	$[Ca^{2+}]$ (mmol/kg)	SI	k_p	n
					$R_m = k_p (S^{0.5} - 1)^n$	
4i	7.68	10.9	5.40	0.733	0.742	1.86
4k*	7.75	10.6	5.52	0.795	0.764	1.87
4d	7.84	10.8	5.47	0.738	0.594	1.86
4f	7.70	10.4	5.48	0.740	0.689	1.95
4g	7.74	10.1	5.44	0.750	0.627	1.78

* calcite seed concentration was 0.78g/kg, for others, the seed concentration of 0.30g/kg was used.

The average rate from 5 rate measurements can be represented as

$$R_m = (0.68 \pm 0.09)\,(S^{0.5}-1)^{1.86\pm0.08}$$

We can see that the reaction order obtained from these experiments are very close, and that the rate constants are within 13% which shows a good reproducibility. Normally the reproducibility of the measured calcite growth rates within a factor of 2 has been considered as acceptable, because there are many factors influencing the measurement. The most important one is due to the uncertainty of the total surface area of the calcite seeds. To avoid the problem, a second experimental method - the visual observation method, has been developed.

4.3 The visual observation method

The $CaCO_3$ crystal growth rate can also be determined by measuring a single crystal size (edge) change over time intervals. The visual observation method therefore has be developed using glass micromodels. A solution supersaturated with $CaCO_3$ was continuously injected into a micromodel in which calcite seeds had been placed. The kinetics of the precipitation were studied by observing the crystal size change as a function of time at a constant solution composition, constant temperature and selected flow velocities.

4.3.1 Glass micromodel

The micromodels used in our experiments were produced by etching a pattern into a glass plate and sintering a flat glass plate onto them to make a permanent box. The micromodels have transparent flow channels and allow the process of crystal nucleation and growth to be observed and recorded. A micromodel can be designed with channel patterns of either regular or irregular dimension. Normally the sizes of the channels of a micromodel are 50-200μm in width and 30-100μm in depth (Dawe, 1990). A special micromodel with larger regular flow channels has been designed for studying the effect of the solution flowing velocity on the calcite growth rate. The sizes of the flow channels are 0.3, 0.6, 1.2 and 2.0 mm (millimeter) as shown in Figure 4.5.

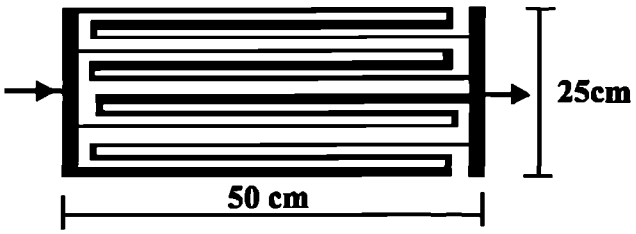

Figure 4.5 The pattern of the micromodel used for the calcite crystal growth rate measurements and flow rate effect.

The freshly prepared glass micromodels have a surface chemistry similar to that of quartz sandstones and are water-wet. The full procedures for producing glass micromodels can be found elsewhere (Dawe, 1990).

4.3.2 The experimental procedures

The chemicals used in this experiment are the same as those in 4.1.1. The experiments for following the $CaCO_3$ crystal nucleation and growth were conducted in the glass micromodels with either irregular or regular patterns. A schematic of the experimental system is given in Figure 4.6. The processes of the nucleation and growth were observed using a microscope which was connected to a video camera and TV.

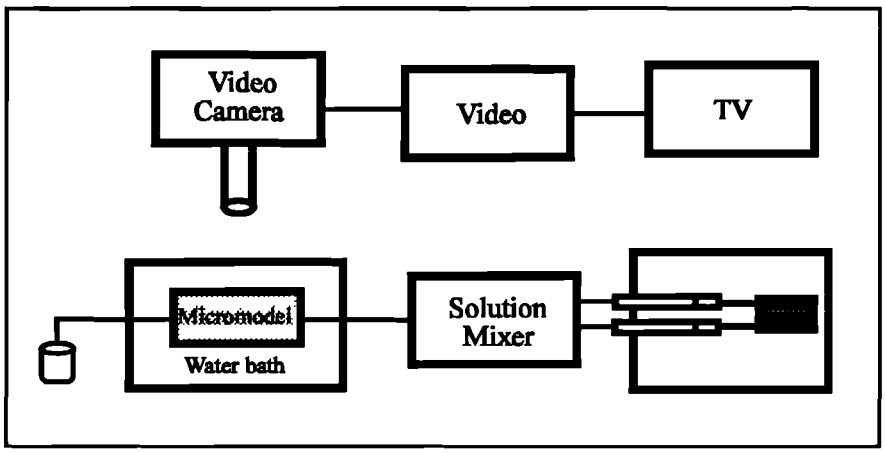

Figure 4.6 The schematic of the micromodel experimental system

The $CaCO_3$ supersaturated solutions were made by injecting two solutions from two parallel syringes fixed on a syringe injection pump. One solution contained twice the amount of the required calcium ion and the other twice the amount of carbonate alkalinity. These two solutions were mixed in another glass micromodel whose pattern is shown in Figure 4.7.

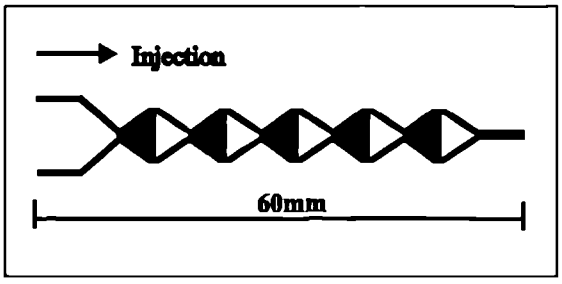

Figure 4.7 The pattern of the glass micromodel used for mixing two solutions.

The micromodel was initially saturated with distilled water, which was then displaced by the $CaCO_3$ supersaturated solution via the solution mixer. This was followed by the injection of a pore volume of solution containing calcite powder of 3 μm average size suspended in a calcite saturated solution to get a number of calcite seed crystals into the micromodel. The glass model was then immediately reconnected to the solution mixer by a plastic tube 0.5 metres long and 0.5 mm diameter, and the tube together with the micromodel placed in a waterbath at the required experimental temperature in order to pre-heat the supersaturated solution before it contacts the calcite seeds in the micromodel. The solution injection rate is determined from the number of calcite seeds placed inside the micromodel and the temperature is set to ensure that the calcite supersaturation inside the micromodel is maintained almost unchanged.

The solution pH at 25°C was determined separately after mixing the equal volumes of the two preheated solutions (25°C) in a bottle with only one port which can be sealed by the pH electrode itself to avoid degassing. The solution pHs at the temperatures above 25°C were calculated by Solmineq88 (Kharaka et al., 1988). The calculations have been based on the reaction vessel being completely closed so that the total carbonate ($CO_2 + H_2CO_3 + HCO_3^- + CO_3^{2-}$) does not change.

4.3.2 The calculation of the calcite growth rate

The crystal growth rate is expressed as the rate of displacement of a crystal face in the direction perpendicular to the linear face growth rate (Nielsen, 1984). Because our calcite crystals are sufficiently large to readily measure their size by microscope, a crystal face growth velocity can be represented by,

$$R_L \propto dx/dt, \tag{4.15}$$

where R_L is the crystal layer growth rate in m/s and dx is the length increase of the crystal equilibrium face at the time interval dt. The crystal growth rate as a function of the saturation ratio can be described by rate equation 2.65. The rate constant, k_p, is temperature dependent and can be given by (Stumm and Morgan, 1996)

$$k_p = A_a \exp(-E_a/RT), \tag{4.16}$$

where A_a is the Arrhenius constant, E_a is the activation energy and R is the gas constant. The parameters A_a and E_a can be determined by plotting $\log k_p$ against $1/T$ so that the slope gives $E_a/2.303R$ and the y-intercept $\log A$.

A crystal face growth velocity R_L (m/s) can be converted to a mass growth rate R_m (mmol/m^2.h.kg) by

$$R_m = \frac{1}{3}\frac{\rho_c R_L}{M} \tag{4.17}$$

where M is the molecular weight of calcite and ρ_c is calcite density. Figure 4.8 shows pictures taken during calcite growth inside a micromodel. Normally the crystals grow to 80μm. On a TV screen, they are magnified to about 4 - 5cm in length. The error of the measurement is less than 2mm, i.e. < 5%. Therefore the calcite growth rate determined in this way will be more reliable than the growth rate determined from a mass reduction in a reaction vessel.

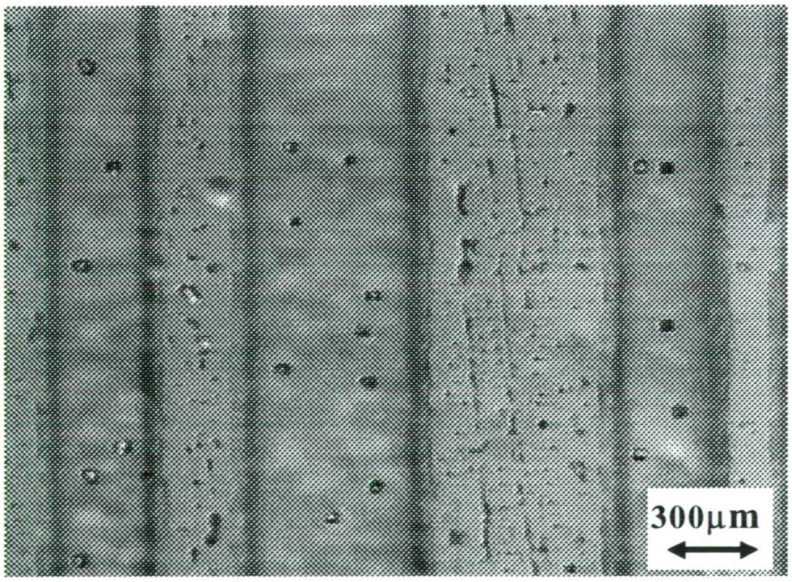

Figure 4.8 The calcite growth process inside a glass micromodel

4.4 The reliability of thermodynamic models

In order to obtain accurate kinetic data from the precipitation rate measurements, a reliable thermodynamic model is very important. In this work, the reliability of three thermodynamic models, Solmineq88, Oddo-Tomson's empirical saturation equation (Oddo and Tomson, 1982, 1994) and Langelier's saturation index model (Langlier, 1936) have been examined. For a closed water system, the saturation index and the solution pH at the equilibrium state can be calculated. The solution pH at the equilibrium state can also be measured experimentally. Therefore the reliability of the models can be determined by comparing the calculated and measured equilibrium pHs.

In this work, the pH at the equilibrium state of a $CaCO_3$ supersaturated solution was determined by continuously monitoring the solution pH after seeding until the solution pH became stable. The solution saturation index and the pH at the equilibrium state were calculated from the solution chemical composition and temperature. The calculation and experimental results are summarised in Table 4.2.

Table 4.2 The initial and equilibrium states of selected calcium carbonate water systems calculated from Solmineq88 (Sol) and Oddo-Tomson's (OT) thermodynamic models.

No	pH_i	IS	T (°C)	Ca^{2+} (mmol/kg)	Alk (meq/kg)	SI_{OT}	SI_{Sol}	$pH_{e(c)}$	$pH_{e(m)}$
6P	6.60	1.05	25	71.3	17.5	0.221	0.891	5.99	6.04
8H	8.63	1.01	25	7.81	1.89	0.103	0.894	7.70	7.76
2E	8.10	1.01	25	3.54	5.06	-0.087	0.749	7.46	7.48
3C	7.83	1.02	50	3.47	6.67	0.062	0.756	7.36	7.25
4E	7.73	1.02	70	3.47	6.67	0.325	0.643	7.26	6.98
Seawater	8.00	0.65	15	10.0	2.30	-0.210	0.382	-	-
Miller	5.89	1.33	121	25.0	34.3	0.880	0.809	-	-

SI_{OT} - the saturation calculated by Oddo-Tomson's equation.
SI_{Sol} - the saturation calculated by the Solmineq88.
$pH_{e(c)}$ - the solution pH at equilibrium state (with calcite) calculated by Solmineq88.

As we can see from Table 4.2, under ambient conditions, the differences between the measured solution pH at the equilibrium state and the calculated values from Solmineq88 were less than ±0.03pH units. This means that the calculations from Solmineq88 appear reliable at low temperatures. However, when the temperature was raised to above 50°C,

the calculated equilibrium pHs from Solmineq88 were much higher than the measured values, indicating that the saturation indexes should be higher than the calculated values at the temperature above 50°C. The test results also show that the reliability of Oddo-Tomson's equation is not as good as Solmineq88 even at low temperatures. The measured solution pHs indicates that the thermodynamic state of the solution is far away from its equilibrium state (No 2E, ΔpH = 0.60 units) where a minus SI is given by Oddo - Tomson's model. The calculated saturation index for seawater water by Solmineq88 is also more reasonable than that by Oddo-Tomson's equation, since it has long been known that seawater is supersaturated with calcite (Morse and Mackenzie, 1990). The measured pHs at the equilibrium state were about 0.1 pH unit lower at 50°C and 0.2 pH unit lower at 70°C than the calculated values when the initial pH was around 8.0 and the ionic strength was 1.0 eq/kg. This difference cannot be due to experimental error because the error of the pH-free-drift method is mainly from releasing CO_2 from the solution and electrode drift. The releasing of CO_2 from the solution will lead to a higher measured pH, and the electrode drift was less than 0.02pH unit. The major errors are therefore believed to be due to the ion pair-constants of carbonate species and/or the uncertainty of the activity coefficients which will be discussed later in Chapter 6.

Langlier's saturation model is the earliest model for calculating the $CaCO_3$ saturation index. Stiff and Davis (1952) adapted Langlier's model for oilfield operations. The basic form of the model is:

$$SI = pH_i - pH_e \tag{4.18}$$

where pH_i and pH_e are the solution pH at the initial and equilibrium states, respectively. As we can see this model requires the pH at the equilibrium state in order to obtain the saturation index. Therefore a comparison of the relationship between pH change and saturation index change during calcite precipitation obtained from the solutions with different initial pHs is given in Figure 4.9.

As we can see from Figure 4.9, at a high solution pH, the total pH change from the initial and the equilibrium states almost equals the saturation index change. However, for the

solutions with a low initial pH, the difference between the pH change and the saturation index change is about 0.2 pH unit. Comparing these three models, it is obvious that Solmineq88 is the most reliable model for the calculation of $CaCO_3$ saturation index.

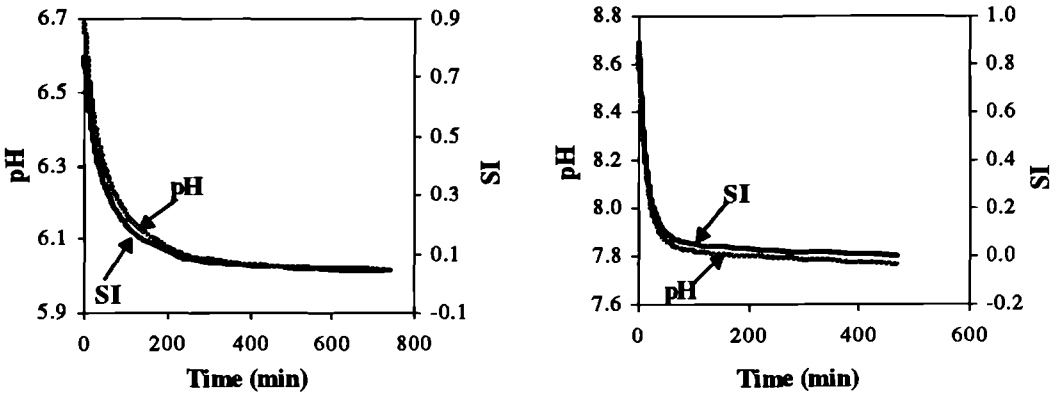

Figure 4.9 The solution pHs and saturation indexes change as a function of time obtained from two solutions with different initial pH, left, No 8H (ΔpH = 0.8), right, No 6P ((ΔpH = 0.6).

4.5 Summary

Two experimental methods have been developed to study different aspects of the kinetics of calcite precipitation; the pH-free-drift method for the determination of the kinetic model over a wide range of saturation states in a closed water system and the visual observation method used for the determination of rate constants of $CaCO_3$ growth under steady state using glass micromodels. The calcite growth rate can be determined by measuring the solution pH change which can more properly represent the extent of a reaction during the precipitation than by sampling and analysing the changes of the precipitating ions. The reproducibility of the rate data from the pH-free-drift is much better than most other methods. The visual observation method provides another way to obtain more reliable rate constants. Three thermodynamic models have been examined experimentally. Solmineq 88 is the most reliable model for the calculation of the $CaCO_3$ saturation index and will be used in this study of the kinetics of precipitating $CaCO_3$.

CHAPTER 5

THE KINETICS OF CALCIUM CARBONATE NUCLEATION

5.1 Introduction

Initially the surface of wellbore tubing and oil and water processing facilities are free of scale. Carbonate scale will not start to form even if the solution is supersaturated until nucleation has occurred (Nancollas and Reddy, 1974 and Vetter, 1980, 1987). It has been found that most field carbonate scales start to be deposited when the downhole pressure is below the oil bubble point and a gas phase starts to appear (Schmidt and Bentsen, 1992, and Vetter, 1980). The most common explanation of this phenomenon is that degassing can cause the solution pH to increase and in turn cause the solution saturation index to increase. When the saturation index is higher than a certain level (the critical saturation), spontaneous nucleation will start. Spontaneous nucleation here means that nucleation occurs without adding any seeds. It can be either homogeneous or heterogeneous nucleation.

Before any scale tendency prediction can be made, it is essential to know the mineralogy and morphology of the carbonate phases under different subsurface conditions. This is because there are three principal polymorphs of calcium carbonate ($CaCO_3$); calcite, aragonite and vaterite (Morse and Mackenzie, 1990); each of these minerals may also appear with different morphologies. Most studies assume that calcium carbonate scale is calcite because it is the thermodynamically most stable mineral ($K_{sp} = 10^{-8.48}$). However many factors can influence the mineralogy and morphology of carbonate precipitation, including saturation, temperature, impurities, ionic strength and solution flow velocity (Bischoff and Fyee, 1968; Folk, 1974; Gonzalez et al, 1992; Söhnel and Garside, 1992), so that a range of different scale minerals, including aragonite ($K_{sp} = 10^{-8.34}$), could be deposited under downhole oilfield conditions. Vaterite is the least thermodynamically stable of the calcium carbonate polymorphs and is seldom precipitated from solutions above about 30°C (George and Nancollas, 1980). Since no published data have been found to describe the connection between the water compositions and the mineralogy of

the carbonate scale under oilfield downhole conditions, carbonate scaling tendencies and deposit rates for oilfield practice cannot yet be predicted with confidence.

The critical saturation index is important for predicting when precipitation (scaling) may happen and is also useful for studying the kinetics of the crystallisation experimentally. This is because the occurrence of spontaneous nucleation can be avoided when calcite growth rates are being determined by measuring the solution pH change at constant seed concentration.

The objectives of this Chapter are:

- to observe the morphologies of the spontaneous nucleation inside a glass micromodel at temperatures between 25°C and 70°C and ionic strengths up to 1 mol/kg,
- to study the effects of the formation of gas bubbles on $CaCO_3$ nucleation,
- to experimentally determine the critical saturation index of $CaCO_3$ nucleation and compare with the calculated values from equation 2.48.

The nucleation time (or induction time) was determined by continuously measuring a solution pH in a closed system as a function of time. The time when the solution pH starts to drop is recorded as the nucleation time. If the solution pH remains constant for more than 24 hours, no spontaneous nucleation is considered to have occurred under the experimental conditions. The critical saturation index of calcite nucleation was determined by a series of nucleation time measurements at different saturation indexes. The critical saturation index was estimated to be at the point when the nucleation time changed sharply. The morphology of $CaCO_3$ nucleation was observed and recorded when a $CaCO_3$ supersaturated solution was injected into a glass micromodel and spontaneous nucleation occurred.

5.2 The morphology of the $CaCO_3$ precipitate

The mineralogy of the precipitate is normally determined by X-ray diffraction analysis, but in our case, the amount of precipitate inside the micromodel is too small to sample. However the shape of the $CaCO_3$ precipitate can be observed through the glass during the $CaCO_3$ precipitation experiments. Many studies have shown that there are some connections between the mineralogy of the $CaCO_3$ precipitate and their morphologies. For example among the three $CaCO_3$ minerals (calcite, aragonite and vaterite), only calcite has a rhombohedral morphology, whereas almost all aragonite appears as fibrous shapes (Gonzalez et al., 1992). When there is no inhibitor present in the solution, it is very unlikely that fibrous calcite will be formed (Gonzalez et al., 1992). When some inhibitor ions are present in the solution, such as Mg^{2+}, the rhombohedral crystal of calcite can change to steep rhombohedral forms or even fibrous shapes (Gonzalez et al., 1992, George and Nancollas, 1980). Therefore we can suggest the mineralogy of the $CaCO_3$ precipitate from their morphologies. In this work, rhombohedral nuclei have been considered to be calcite and fibrous precipitate to be aragonite if precipitation is from a simple water system without inhibitors

When a $CaCO_3$ supersaturated solution was injected into a micromodel and the saturation index was high enough (above the critical saturation index), spontaneous nucleation occurred. Normally rhombohedral crystals are the dominant morphology at a temperature of 25°C (Figure 5.1). When the temperature was below 70°C, and the supersaturation was not too high (SI $\leq$ 1), only rhombohedral crystals were found. The amount of crystals appearing inside the micromodel was proportional to the saturation and injection rate. This indicates that the nucleation is homogeneous dominant because according to equation 2.46, the number of nuclei formed from homogeneous nucleation is proportional to the saturation index. On the other hand, if heterogeneous nucleation occurs, the number of nuclei formed will depend on the available foreign solid (or suspended particles) in the solution.

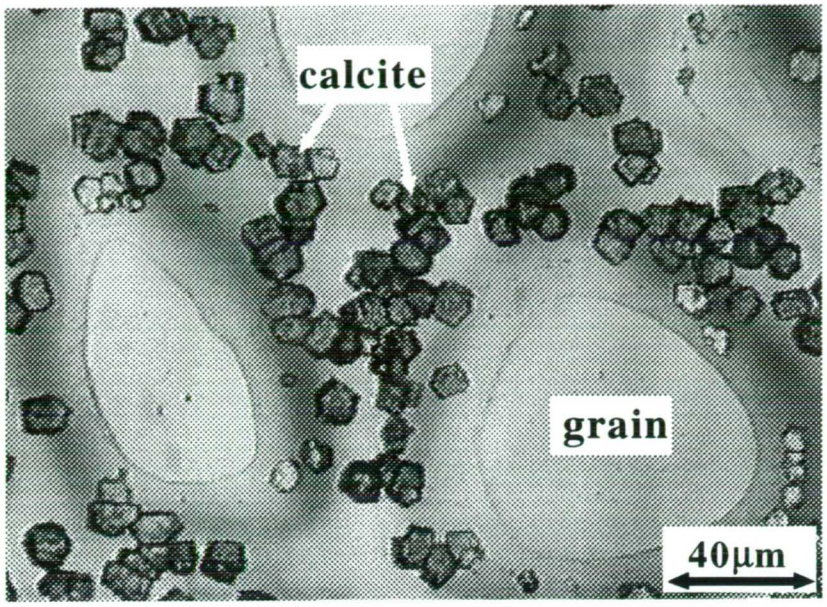

Figure 5.1 Spontaneous nucleation occurred inside a micromodel at 25°C, rhombohedral calcite was formed. Solution: pH = 7.8, IS = 1 eq/kg and SI = 2.0.

When the temperature was increased to 70°C with high supersaturation (above the critical values), three crystal morphologies were observed in the micromodel; rhombohedral, fibrous and plate crystals (Figure 5.2).

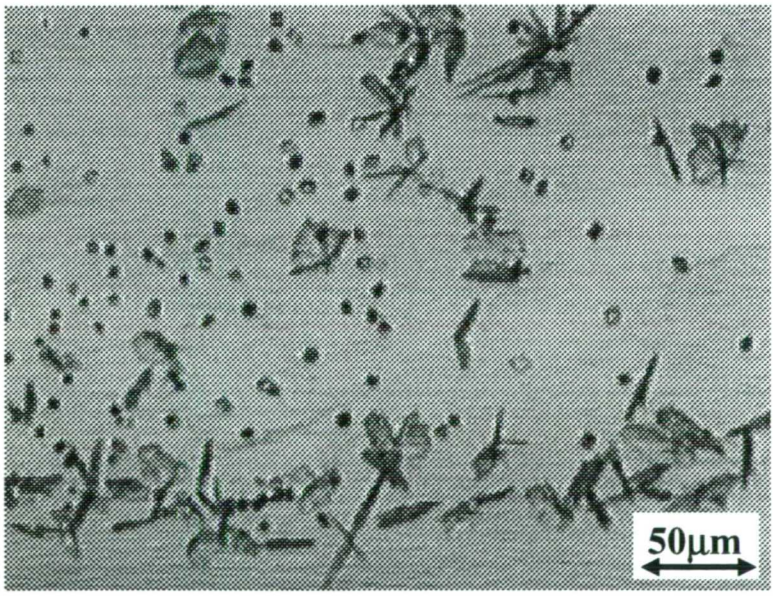

Figure 5.2 Spontaneous nucleation occurred inside a micromodel at 70°C, three morphologies: rhombohedral, fibrous and platy crystals were formed. Solution: SI = 0.76, pH = 7.8 and IS = 1 eq/kg.

At a lower ionic strength (0.1eq/kg), and high supersaturation and temperature (SI > 1, T = 70°C), fibrous nuclei were dominant (Figure 5.3).

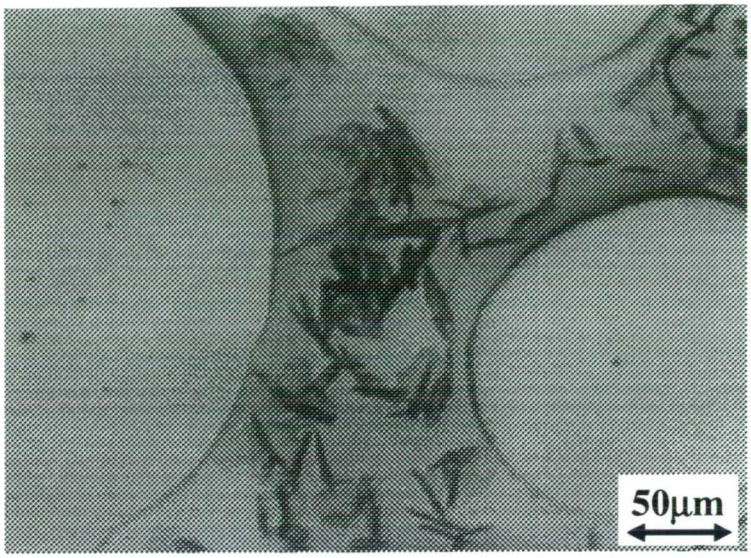

Figure 5.3 Spontaneous nucleation occurred inside a micromodel at 70°C, only fibrous morphology was formed. Solution: SI = 1.0, pH = 8.0 and SI = 0.1 eq/kg.

Heterogeneous nucleation is the common mechanism under industrial conditions. We have examined heterogeneous nucleation experimentally by observing the number of nuclei formed inside the micromodel when the saturation index of a solution was below the critical value. We found that when the temperature was below 50°C, nucleation did not occur within 4 days at a low supersaturation (less than the critical value). At temperatures above 70°C, spontaneous nucleation was observed at saturation indexes as low as 0.1 within 1 hour, but also the numbers of nuclei did not increase with SI significantly until the SI was above the critical value (0.71). This suggests that when the temperature was above 70°C heterogeneous nucleation occurred at supersaturations below the critical value. The morphology of the nuclei from heterogeneous nucleation was rhombohedron, i.e. calcite.

The experiments from Christ et al. (1974) show that the activation energies are 77 kJ/mol 42 kJ/mol for calcite and aragonite, respectively. This means that temperature has a stronger influence on the growth rate of aragonite than on calcite (see equation 4.16).

At a low temperature or high temperature with low saturation index, calcite may have the fastest growth rate because it has the lowest solubility among the three different minerals of $CaCO_3$. However, at a high SI and high temperature, the growth rate of aragonite may become higher than that of calcite, and become the dominant mineral of the precipitate. Figure 5.4 illustrates the growth tendency of calcite and aragonite at different saturation indexes and temperatures.

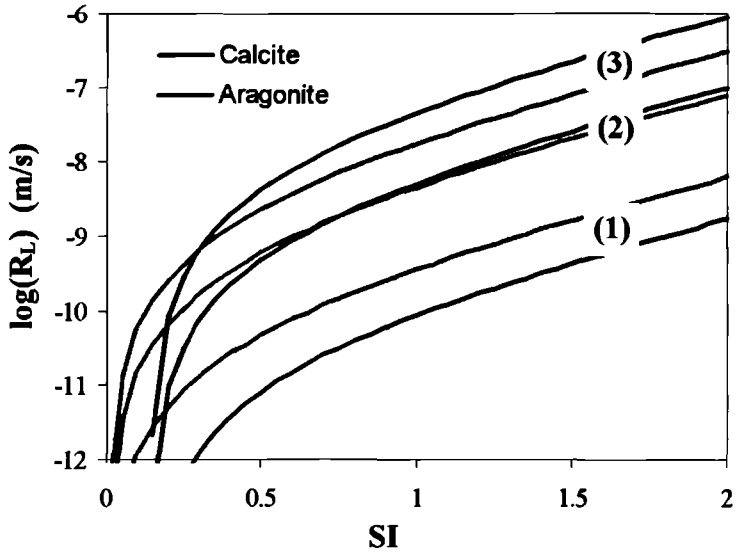

Figure 5.4 The illustration of calcite and aragonite growth rates at different temperatures. Each group (two lines) has the same temperature: (1) 25°, (2) 70°C, and (3) 100°C, respectively. The saturation indexes of calcite were used for x axis values.

It can be expected that when the growth rate of aragonite is comparable with the growth rate of calcite, aragonite will be formed from a $CaCO_3$ supersaturated solution, although aragonite is not most thermodynamic stable $CaCO_3$ mineral. If the aragonite growth rate is much higher than that of calcite, aragonite will be the dominant mineral of the precipitate. However this can only occur when the calcite supersaturation is higher than a certain value, i.e. $SI_{(calcite)} > pK_{sp(calcite)} - pK_{sp(aragonite)}$, where $K_{sp(calcite)}$ and $K_{sp(aragonite)}$ are the solubility products of calcite and aragonite, respectively, in other words, when $SI_{(calcite)} < pK_{sp(calcite)} - pK_{sp(aragonite)}$, only calcite can be formed because aragonite is undersaturated.

5.3 Spontaneous nucleation

5.3.1 The critical saturation index of $CaCO_3$ nucleation

The critical saturation index of $CaCO_3$ nucleation is a function of solid surface energy and temperature and can be calculated from equation 2.48. It can also be determined experimentally by measuring induction times. The induction times of calcium carbonate nucleation at different solution pHs and temperatures are given in Table 5.1. The critical saturation index (SI_{crit}) determined by experiment as well as calculated from equation 2.48 ($SI_{crit(c)}$) are also given in Table 5.1.

Table 5.1 The calcite nucleation time at different solution pH and temperatures.

No	SI	pH	PPT (mmol/kg)	Temperature (°C)	Induction time (hours)	SI_{crit}	SI_{crit} (C)
1	1.28	8.05	1.18	25	0.22		
2	1.13	7.78	1.92	25	0.33		
3	1.11	7.79	1.75	25	>24	1.12	1.02
4	0.96	7.77	1.41	50	0.56		
5	0.85	7.01	3.00	50	> 24	< 0.92	0.88
6	0.94	6.92	3.66	70	0.27		
7	0.77	6.74	3.22	70	0.38		
8	0.72	7.92	1.30	70	2.00	0.71	0.85
9	0.95	6.50	5.50	25	0.95		
10	0.79	6.49	3.79	25	1.67		
11	0.76	6.48	3.77	25	2.33	0.75	1.02

As we can see, the critical saturation indexes decrease with increasing temperature. The measured critical saturation indexes are very close to the calculated values from equation 2.48 at the temperatures of 25 and 50°C, but are lower than the calculated values at 70°C. The reasons could be: first, some nuclei are followed by heterogeneous nucleation; second, the solid surface energy is temperature dependent (Mullin, 1994), and is low at a high temperature. According to equation 2.48, a lower critical supersaturation will be obtained at a lower solid surface energy.

Normally critical saturation indexes at higher temperatures are more difficult to determine. If we know the critical saturation at a low temperature (e.g. 25°C), the SI_{crit} at different temperatures can be estimated by equation 2.49. For example, supposing the

SI_{crit} at temperature 25°C is 1.0, the SI_{crit} at 50°C and 70°C can be calculated by equation 2.49 to give

$$SI_{crit50^\circ C} = 1.1 \times \left(\frac{297}{323}\right)^{3/2} = 0.97$$

$$SI_{crit70^\circ C} = 1.1 \times \left(\frac{297}{343}\right)^{3/2} = 0.89$$

It is also interesting to note that the calcite critical saturation is also influenced by the solution pH. Lower critical saturation indexes were obtained at lower pHs, and the induction time around the critical saturation index was not as sharp as that in the solutions with higher pH. This suggests that heterogeneous nucleation may also be contributing to the amount of nuclei formed in the low pH solutions. Most oilfield waters have a very low pH (< 5), so that the influence of low pH on the estimation of critical saturation index has to be considered when we predict where scaling will start.

5.3.2 The effect of presence of gas phase on $CaCO_3$ nucleation

In our nucleation experiments, we found that calcium carbonate nucleation was influenced by the presence of a gas phase. When dissolved gas was released from the calcite supersaturated solutions, the induction times of $CaCO_3$ nucleation were much shorter than those without gas bubbles. Some results from these experiments are given in Table 5.2:

Table 5.2 The effect of gas bubbles on the induction time of calcite nucleation.

No	SI	Temperature (°C)	Induction Period (min)	Gas Bubbles
1	0.940	70	7	with
2	0.940	70	16	without
3	1.053	50	46	with
4	1.053	50	163	without

When a calcite supersaturated solution flowed through a glass micromodel, we found that the calcite saturation index required for spontaneous nucleation was lower than the critical saturation index when there were gas bubbles released from the liquid phase. The calcium carbonate nuclei were observed downstream of the gas bubbles (Figure 5.5), whereas no nucleation occurred under the same conditions when there were no gas bubbles present. This suggests that a gas-liquid interface can stimulate $CaCO_3$ spontaneous nucleation.

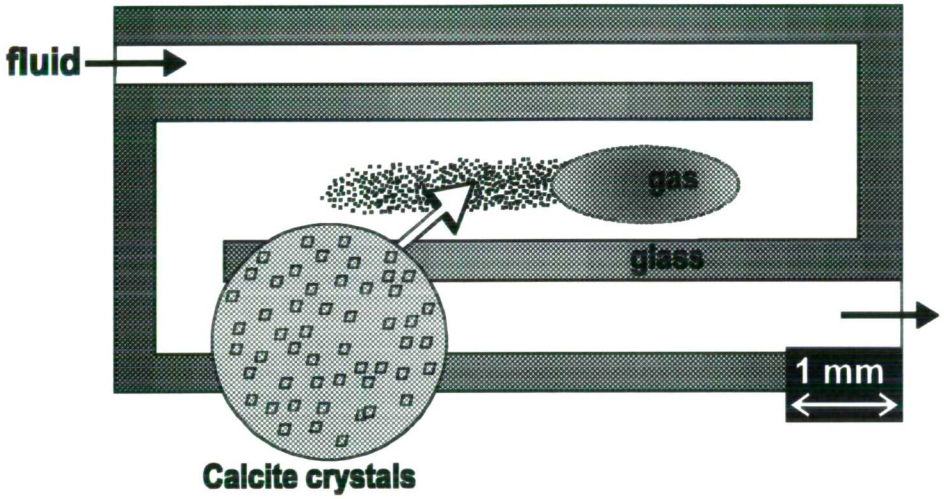

Figure 5.5 Spontaneous nucleation (rhombohedral calcite) occurred after gas bubbles were formed at 70°C when the calcite supersaturation was below the critical value.

The reasons why $CaCO_3$ nucleation is enhanced by degassing could be (i) the local $CaCO_3$ saturation near the gas phase is higher because of water evaporation; (ii) if the released gas is CO_2, the solution pH would be increased locally, (iii) the tiny gas bubbles help $CaCO_3$ nucleation. Water evaporation could happen in an open water system. The concentration of the precipitating ions becomes gradually higher. A solution pH change during degassing is a function of CO_2 partial pressure (pCO_2) and solution chemical composition, especially the solution alkalinity. The pH in an open water system can be calculated by combining equations 2.4, 2.8 to 2.10 and 2.12,

$$pCO_2 K_H = C_T Alk \frac{\alpha_0}{\alpha_1 + 2\alpha_2} \tag{5.1}$$

Because α_t is a function of pH, we can calculate the corresponding pCO_2 from the water composition using equation 5.1 from each given pH. Figure 5.6 shows how solution pH changes as a function of CO_2 partial pressure at two different alkalinities.

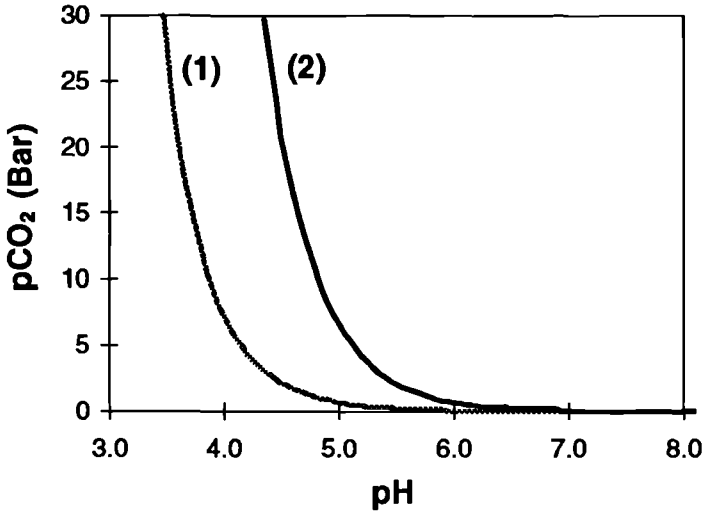

Figure 5.6 A solution pH changes as a function of CO_2 partial pressure at 25°C, (1) Alk = 0.001eq/kg, (2) Alk = 0.01eq/kg.

From Figure 5.6 we can see that the higher the solution alkalinity, the higher the solution pH at a given solution composition and pCO_2. We can also find that the pCO_2 has a strong influence on a solution pH at a low pCO_2 (< 1 bar). When the pCO_2 is above 2 bar, the solution pH changes with pCO_2 are very small. For example, if pCO_2 decreases from 10^{-2} to 10^{-3} bar, the solution pH will increase by 1.0 pH unit, whereas, if the pCO_2 decreases from 10 to 5 bar the pH will only increase by 0.28 pH unit. From Langelier's saturation index (equation 4.18), we can estimate the solution saturation index change (ΔSI) from the solution pH change (ΔpH): $\Delta SI \approx \Delta pH$.

A gas phase influence for other scaling solution has been noted from heat exchangers by Gill and Nancollas (1980). They found that the calcium sulphate (gypsum) scale is preferentially deposited at the edges of the air bubbles which appeared on the metallic surfaces. A solution pH change does not affect the saturation index of $CaSO_4$ significantly so that Gill and Nancollas believe that the surface-temperature gradient in

the presence of gas bubbles was the main cause. However in our experiments, the system pressure and temperature are constant during the injection of supersaturated solutions, and there was no temperature gradient inside the micromodel. The solution pH chosen for our experiments was high (around 8) and close to the equilibrium pH corresponding to the atmospheric pCO_2 (constant), so that the solution pH should not be affected significantly by the degassing. Therefore we believe that the role of the gas bubbles in starting scaling is that they act as nucleation catalysts. It is well known that the dehydration of hydrated lattice ions (Ca^{2+} and Mg^{2+}) can be the rate controlling step for crystal growth and nucleation (Mullin, 1994). The newly formed small gas bubbles probably act as heterogeneous nuclei because the Gibbs free energy of these small gas bubbles is high (Adamson, 1990) which can lower the energy barrier for forming a new phase. This may be the main reason why most oilfield $CaCO_3$ scale occurs after the a gas bubble point, where gas phase starts to separate from the liquid phase.

The lower critical saturation indexes at lower pHs (< 6.5) obtained in our experiments can also be explained by the influence of gas bubbles, because the low solution pH in these experiments was obtained by bubbling in CO_2. Although the water systems were closed during the precipitation, the possibility of CO_2 gas escaping from the solution is very high because its in-situ CO_2 partial pressure is much higher (about 0.8 bar) than those in a solution with a high pH (>8). The gas bubbles stimulate the calcite nucleation, as the result, spontaneous nucleation occurs at a low saturation index.

5.4 Summary

When there is more than one form of $CaCO_3$ mineral thermodynamically possible to precipitate, the resulting precipitate is not necessarily the one that is thermodynamically most likely (high SI), but the one that has the fastest growth rate. As the activation energy for forming aragonite is higher than calcite, the aragonite growth rate at a high temperature (≥ 70°C) may be higher than that of calcite so it may appear from spontaneous nucleation. According to our experimental results, calcite is the dominant scale mineral when the temperature is below 70°C, or saturation indexes are below the critical values when the temperature is above 70°C. If the temperature is above 70°C and

the SI is above the critical value, aragonite is the dominant scale mineral from spontaneous nucleation.

At temperatures below 50°C a minimum saturation (the critical saturation) has to be achieved to start a $CaCO_3$ spontaneous nucleation and then chemical scaling, whereas at temperatures above 70°C, the scaling will start by heterogeneous nucleation so long as the solution is supersaturated with calcite. Spontaneous nucleation of $CaCO_3$ can also be stimulated by forming gas bubbles in the water system. This is the main reason why most oilfield $CaCO_3$ scale is found where dissolved gas has started to leave the liquid phase. We suggest that this is mainly due to the dehydration of hydrated lattice ions at the gas-liquid interface been less energy demanding than from the bulk solution.

CHAPTER 6

THE KINETICS OF CALCITE GROWTH

6.1 Introduction

Thermodynamic models of carbonate precipitation or scaling give estimates of the tendency to precipitate and the maximum amount of deposition that can occur. Kinetic models determine the rate of precipitation from which the profile of the precipitation on the tubing surface can be estimated. To a petroleum engineer it is very important to know this scale profile (the rate and place of precipitation) because it will make a significant difference to production and well stimulation techniques if the precipitate is deposited in a small region or spreads out over a large area or even is delayed until the water is produced at the surface.

Many rate laws for crystal growth have been reviewed in Chapter 2. However most of these models were developed using the chemistry of surface waters under ambient conditions, e.g. seawater rather than reservoir conditions. For surface waters, the pH is usually high (above 8) and the carbonate ion concentration is lower, whereas oilfield formation waters can have ionic strengths as high as 6 eq/kg (Warren and Smalley, 1994), and the pH can be much lower (< 5), because the oilfield reservoir fluids (oil and water) contain dissolved CO_2. For a solution with a low pH and high alkalinity and ionic strength, the solution buffer capacity can be very high. As the result, more $CaCO_3$ can be precipitated from such solutions at the same level of supersaturation. Table 6.1 demonstrates the mass of precipitation calculated using Solmineq88 for a range of supersaturated solutions with similar saturation indexes and different solution pH values, ionic strengths and alkalinity. The calculations were based on a closed water system at one atmosphere and 25°C.

From Table 6.1 we can see that the solutions with low pH (< 6) will deposit more scale than those with high pH (pH > 7) even though they have the same supersaturation level. On the other hand, a high ionic strength does not appear to cause too much of an increase in the amount of calcite precipitate.

Table 6.1 The comparison of the amount of precipitation at different ionic strengths, alkalinity and pH values.

No	pH_i	Ionic strength (eq/kg)	Alk_T (meq/kg)	$[Ca^{2+}]$ (mmol/kg)	SI	PPT (mmol/kg)
1	7.80	0.02	7.2	3.6	1.05	0.93
2	7.80	1.00	13.0	6.5	1.00	1.34
3	7.80	1.00	2.2	45.7	1.01	0.28
4	7.80	1.00	92.0	1.2	1.01	1.01
5	6.00	1.00	53.0	106	1.00	29.0

The aim of this chapter is to develop a kinetic model to describe calcite growth rates. Factors which control the calcite growth rate and the mechanisms of calcite growth, such as solution pH and the carbonate alkalinity, have been examined. The growth rates have been determined by the pH free drift method developed in Chapter 4. These rate data have been interpreted by the rate equations introduced in Chapter 2 to find out which model can be used to describe the calcite growth under different solution compositions. The influences of the crystal size, ionic strength, the solution transport rate and temperature on the calcite growth rate have also been examined by visual observation for steady state solution conditions in glass micromodels.

6.2 Calcite growth rate determined from a pH-free-drift method

A series of calcite precipitation experiments have been conducted using a pH-free-drift method in solutions with different alkalinities and pH values. The rate laws introduced in Chapter 2 were then examined using our own rate data. The advantage of using a pH-free-drift method is that the calcite growth rate between the initial to the equilibrium states can be obtained in a single experimental run for a given condition. The interval between two pH readings can be as small as 0.001 pH unit. Therefore it is very convenient to examine the available rate laws over a wide range of water pH values and chemical compositions, especially for measuring high growth rates which are very difficult to determine by sampling and Ca^{2+} analysis.

6.2.1 Interpretation of calcite growth rate data

The calcite growth rates from the solutions with the stoichiometric ratio of Ca^{2+} and HCO_3 ($C_{Ca^{2+}}/C_{HCO_3} = 0.5$), medium pH (7.75), 25°C and the supersaturation from the initial value to the equilibrium states have been determined. The experimental data are listed in Table 6.2, including the measured solution pH changes as a function of time, the concentrations of Ca^{2+} and CO_3^{2-} ions as well as the saturation indexes and calcite growth rates calculated from the measured solution pH using equations 4.1 - 4.14. This group of rate data has been used to examine which rate law gives the best interpretation of calcite growth rate as a function of saturation state. Figure 6.1 shows the measured solution pH and the converted Ca^{2+} concentration changes as a function of time.

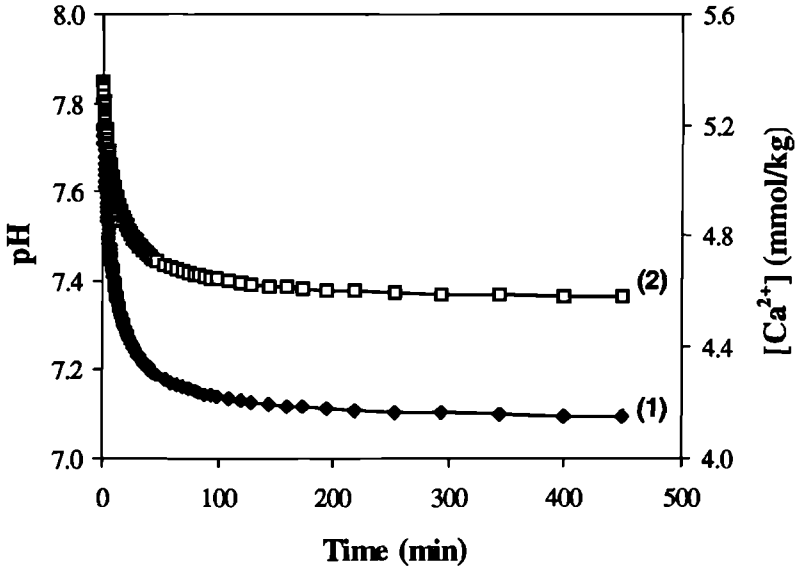

Figure 6.1 The measured pH values as a function of time (curve 1) were converted into the Ca^{2+} concentrations as a function of time (curve 2).

Figure 6.2 shows the results of rate data in Table 6.2 interpreted by the rate equations 2.65 and 2.66. We can see that equation 2.65 gives a good fit to the rate data in Table 6.2 and that the reaction orders are very close to the given value ($n = 2$) from the original rate laws (the BFC rate law and the Davies and Jones rate equation), but that the reaction order from fitting equation 2.66 is 1.66 which is much higher than the value from the original equation of 1 (Nancollas and Reddy's rate model).

Table 6.2 The results of calcite growth rate measurements from the pH-free-drift method

Time (min)	pH	α_1	α_2	$[CO_3^{2-}]_T$ (mmol/kg)	$[Ca^{2+}]_T$ (mmol/kg)	SI	PPT_t (mmol/kg)	Rate (mmol/m^{2}h.kg)
0.00	7.751	0.9481	0.0355	0.0761	5.353	0.796	0.001	0.696
0.25	7.741	0.9485	0.0347	0.0743	5.342	0.785	0.012	0 863
0.50	7.726	0.9491	0.0336	0.0717	5.324	0.768	0.031	1.056
0.75	7.710	0.9496	0.0324	0.0691	5.306	0.750	0.050	1.107
1.00	7.693	0.9501	0.0311	0.0663	5.287	0.731	0.071	1.059
1.25	7.678	0.9505	0.0301	0.0640	5.270	0.714	0.089	0.948
1.50	7.664	0.9508	0.0291	0.0619	5.255	0.698	0.105	0.906
1.75	7.650	0.9510	0.0282	0.0599	5.240	0.683	0.122	0.865
2.00	7.637	0.9512	0.0274	0.0581	5.225	0.668	0.137	0.858
2.25	7.623	0.9514	0.0265	0.0562	5.210	0.652	0.153	0.852
2.50	7.610	0.9515	0.0258	0.0544	5.196	0.637	0.168	0.784
2.75	7.598	0 9516	0.0251	0.0529	5.183	0.624	0.182	0.598
3.10	7.587	0.9516	0.0244	0.0515	5.172	0.611	0.195	0.714
3.25	7.575	0.9516	0.0238	0.0501	5.159	0.598	0.208	0.681
3.60	7.565	0.9515	0.0232	0.0489	5.148	0.587	0.220	0.648
3.75	7.554	0.9515	0.0226	0.0476	5.136	0.574	0.232	0.677
4.10	7.543	0.9514	0.0221	0.0463	5.125	0.562	0.245	0.559
4.30	7.534	0.9513	0.0216	0.0454	5.115	0.551	0.255	0.553
4.60	7.525	0.9512	0.0212	0.0444	5.106	0.541	0.265	0.552
4.80	7.516	0.9510	0.0207	0.0434	5.096	0.531	0.275	0.552
5.1	7.507	0.9509	0.0203	0.0425	5.086	0.521	0.286	0.490
5.3	7.500	0.9507	0.0200	0.0418	5.079	0.513	0.294	0.460
5.6	7.492	0.9506	0.0196	0.0410	5.070	0.503	0.303	0.460
5.8	7.485	0.9504	0.0193	0.0403	5.063	0.495	0.311	0 430
6.1	7.478	0.9502	0.0190	0.0396	5.055	0.487	0.319	0.358
6.4	7.471	0.9500	0.0187	0.0389	5.048	0.479	0.327	0.431
6.6	7.464	0.9498	0.0184	0.0383	5.040	0.471	0.335	0 400
6.9	7.458	0.9497	0.0181	0.0377	5.034	0.464	0.342	0.370
7.1	7.452	0.9495	0.0179	0.0372	5.027	0.458	0.348	0.371
7.4	7.446	0.9493	0.0176	0.0366	5.021	0.451	0.355	0.371
7.6	7.440	0.9491	0.0174	0.0361	5.014	0.444	0.362	0.341
7.9	7.435	0.9489	0.0172	0.0357	5.009	0.438	0.368	0.310
8.1	7.430	0.9487	0.0170	0.0352	5.003	0.432	0.374	0.311
8.4	7.425	0.9485	0.0168	0.0348	4.998	0.426	0.380	0.311
8.6	7.420	0.9483	0.0166	0.0344	4.992	0.421	0.386	0.312
8.9	7.415	0.9481	0.0164	0.0340	4.987	0.415	0.391	0 260
9.2	7.410	0.9479	0.0162	0.0336	4.981	0.409	0.397	0.282
9.4	7.406	0.9477	0.0160	0.0332	4.977	0.404	0.402	0.251
9.7	7.402	0.9475	0.0159	0.0329	4.972	0.400	0.407	0.283
9.9	7.397	0.9473	0.0157	0.0325	4.967	0.394	0.413	0.283
10.2	7.393	0.9471	0.0156	0.0322	4.962	0.389	0.417	0.252
10.4	7.389	0.9469	0.0154	0.0319	4.958	0.385	0.422	0.221
10.9	7.381	0.9465	0.0151	0.0313	4.949	0.375	0.431	0.285
11.2	7.377	0.9463	0.0150	0.0309	4.944	0.371	0.436	0.222
11.4	7.374	0.9462	0.0149	0.0307	4.941	0.367	0.440	0.223
11.7	7.370	0.9460	0.0147	0.0304	4.936	0.362	0.445	0.223
11.9	7.367	0.9458	0.0146	0.0302	4.933	0.359	0.448	0.192
12.2	7.364	0.9456	0.0145	0.0300	4.929	0.355	0.452	0.187
12.5	7.360	0.9454	0.0144	0.0297	4.925	0.351	0.457	0.224
13.0	7.353	0.9450	0.0142	0.0292	4.917	0.342	0.465	0.225
13.2	7.350	0.9448	0.0141	0 0290	4.913	0.339	0.469	0.258
13.5	7.345	0.9445	0.0139	0.0286	4.908	0.333	0.475	0.202
14.0	7.340	0.9442	0.0137	0.0282	4.902	0.327	0.481	0.179

Time (min)	pH	α_1	α_2	$[CO_3^{2-}]_T$ (mmol/kg)	$[Ca^{2+}]_T$ (mmol/kg)	SI	PPT_t (mmol/kg)	Rate (mmol/m^{2}h.kg)
14.5	7.334	0.9439	0.0135	0.0278	4.895	0.320	0.488	0.196
15.0	7.328	0.9435	0.0133	0.0274	4.888	0.313	0.496	0.164
15.5	7.324	0.9432	0.0132	0.0271	4.883	0.308	0.501	0.148
16.0	7.319	0.9429	0.0131	0.0268	4.877	0.302	0.507	0.165
16.5	7.314	0.9425	0.0129	0.0265	4.871	0.297	0.513	0.149
17.0	7.310	0.9423	0.0128	0.0262	4.867	0.292	0.518	0.133
17.5	7.306	0.9420	0.0127	0.0260	4.862	0.287	0.523	0.150
18.0	7.301	0.9416	0.0125	0.0256	4.856	0.281	0.529	0.136
18.6	7.297	0.9413	0.0124	0.0254	4.851	0.276	0.535	0.106
19.1	7.294	0.9411	0.0123	0.0252	4.847	0.273	0.538	0.117
19.6	7.290	0.9408	0.0122	0.0249	4.843	0.268	0.543	0.118
20.6	7.283	0.9403	0.0120	0.0245	4.834	0.260	0.552	0.118
21.6	7.276	0.9397	0.0118	0.0241	4.825	0.251	0.561	0 136
22.1	7.272	0.9394	0.0117	0.0239	4.821	0.246	0.567	0.105
22.9	7.268	0.9391	0.0116	0.0236	4.816	0.242	0.572	0.103
23.6	7.263	0.9387	0.0114	0.0233	4.809	0.236	0.578	0.092
24.4	7.260	0.9384	0.0113	0.0231	4.806	0.232	0.582	0.086
25.2	7.255	0.9380	0.0112	0.0229	4.799	0.226	0.589	0.092
26.7	7.249	0.9375	0.0111	0.0225	4.792	0.219	0.597	0.065
28.2	7.242	0.9369	0.0109	0.0221	4.783	0.210	0.606	0.082
29.0	7.239	0.9366	0.0108	0.0220	4.779	0.207	0.610	0.094
29.7	7.234	0.9361	0.0107	0.0217	4.773	0.201	0.617	0.068
31.8	7.227	0.9355	0.0105	0.0213	4.764	0.192	0.626	0.080
32.8	7.223	0.9351	0.0104	0.0211	4.759	0.187	0.632	0.062
34.1	7.219	0.9347	0.0103	0.0209	4.753	0.183	0.637	0.050
35.3	7.216	0.9344	0.0102	0.0207	4.750	0.179	0.641	0.050
36.6	7.212	0.9340	0.0101	0.0205	4.744	0.174	0.647	0.055
37.9	7.208	0.9336	0.0100	0.0203	4.739	0.169	0.652	0.051
39.1	7.205	0.9333	0.0099	0.0201	4.735	0.165	0.656	0.045
40.7	7.201	0.9329	0.0098	0.0199	4.730	0.161	0.662	0.047
42.2	7.197	0.9325	0.0098	0.0197	4.724	0.156	0.667	0.042
44.2	7.193	0.9321	0.0097	0.0195	4.719	0.151	0.673	0.040
46.3	7.188	0.9316	0.0095	0.0193	4.712	0.145	0.680	0.028
54.0	7.178	0.9305	0.0093	0.0188	4.699	0.132	0.694	0.025
59.0	7.171	0.9297	0.0092	0.0185	4.689	0.124	0.704	0.022
64.0	7.166	0.9292	0.0090	0.0182	4.682	0.118	0.712	0.019
69.0	7.161	0.9286	0.0089	0.0180	4.676	0.111	0.719	0.021
74.0	7.155	0.9279	0.0088	0.0177	4.667	0.104	0.728	0.017
84.0	7.148	0.9271	0.0087	0.0174	4.657	0.095	0.738	0.015
89.0	7.144	0.9266	0.0086	0.0172	4.652	0.090	0.744	0.012
99.0	7.139	0.9260	0.0085	0.0170	4.645	0.084	0.751	0.012
109.0	7.133	0.9253	0.0084	0.0168	4.636	0.077	0.760	0.009
119.1	7.130	0.9249	0.0083	0.0166	4.632	0.073	0.765	0.007
129.1	7.126	0.9244	0.0082	0.0165	4.626	0.068	0.771	0.006
144.1	7.122	0.9239	0.0081	0.0163	4.620	0.063	0.777	0.005
159.1	7.118	0.9234	0.0081	0.0161	4.614	0.058	0.783	0.005
174.1	7.115	0.9230	0.0080	0.0160	4.610	0.054	0.787	0.004
194.1	7.111	0.9225	0.0079	0.0158	4.604	0.049	0.794	0.003
219 1	7.108	0.9221	0.0079	0.0157	4.600	0.045	0.798	0.002
254.2	7.104	0.9216	0.0078	0.0156	4.594	0.040	0.804	0.002
294.2	7.101	0.9212	0.0077	0.0154	4.589	0.036	0.809	0.001
344.2	7.098	0.9208	0.0077	0.0153	4.585	0.032	0.814	0.001
399.3	7.096	0.9205	0.0076	0.0152	4.582	0.030	0.817	0.001
449.3	7.094	0.9202	0.0076	0.0152	4 579	0 027	0 820	0.000

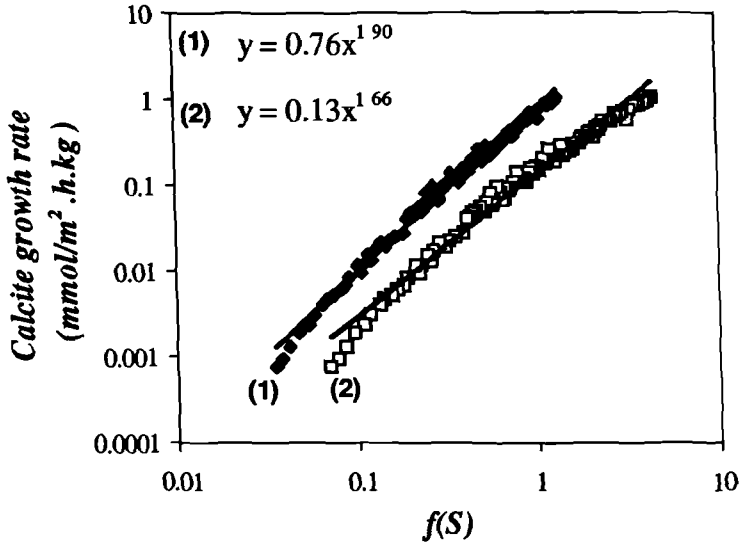

Figure 6.2 Calcite growth rate data interpreted by kinetic models, $pH_i = 7.75$. (1) $f(S) = (S^{0.5}-1)$, fit equation 2.65; (2) $f(S) = (S^5-1)$, fit equation 2.66.

To compare the validation of these rate equations over a wide range of solution pH values, another group of rate data obtained from a solution with a low pH solution ($pH_i = 6.23$) has been interpreted in the same way as the rate data in Table 6.2 and plotted in Figure 6.3.

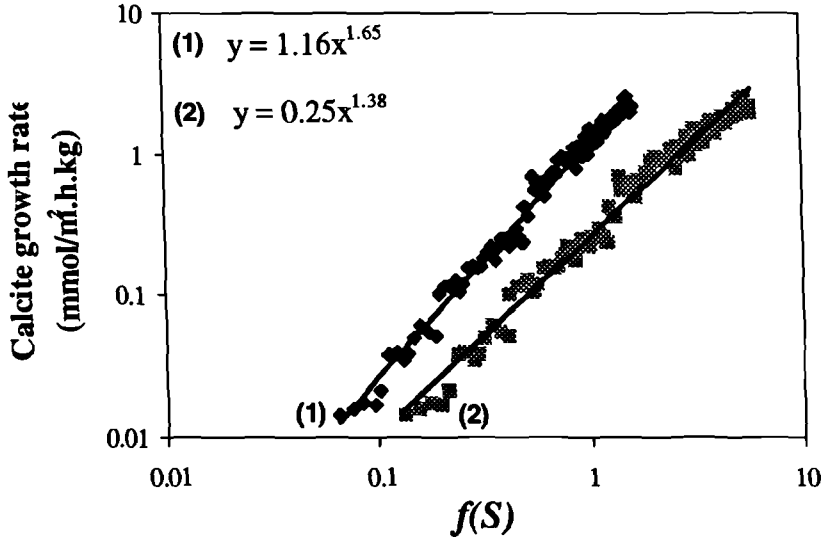

Figure 6.3 Calcite growth rate data interpreted by kinetic models $pH_i = 6.23$. (1) $f(S) = (S^{0.5}-1)$, fit equation 2.65; (2) $f(S) = (S^5-1)$, fit equation 2.66.

From the results in Figure 6.3 we can see that the reaction order from fitting rate equation 2.66 is closer to 1 at a lower pH, but this is mainly caused by the increase in the total crystal

surface area during crystal growth because of spontaneous nucleation. This will be discussed further in 6.2.2. Therefore, in our work the rate equation 2.65 has been mainly used to interpret the rate data from our experiments.

6.2.2 pH effect

The effects of solution pH on the calcite growth rate were examined by conducting a series of calcite growth experiments in solutions with different initial pH values. Other factors, such as ionic strength, supersaturation ratios and the composition ratios of calcium and alkalinity were approximately constant. Because the amount of precipitation from the solution with a low pH is higher than from the solution with a high pH, a higher seed concentration (0.78g/kg) was used for the solutions with lower pH (lower than 7) in order to keep the difference between the initial and final calcite crystal surface area small. Table 6.3 gives the solution compositions and the rate equation parameters obtained from these solutions.

Table 6.3 $CaCO_3$ growth rate[1] on the calcite seed[2] at different pH

No	pH_i[3]	pH_{ec}[3]	pCO_2	Alk_T	$[Ca^{2+}]$	SI	PPT	k_p	n
			(bar×10^3)	(meq/kg)	(mmol/kg)		(mmol/kg)	$R_m = k_p(S^{0.5} - 1)^n$	
1	8.63	7.70	0.10-0.73	1.89	7.81	0.894	0.32	0.626	1.91
2	8.08	7.24	0.78-4.5	3.14	12.4	0.890	0.32	0.527	2.24
3	7.72	6.89	2.7-15.7	4.35	21.1	0.922	0.48	0.334	2.42
4	7.47	6.67	6.9-33.1	6.23	26.1	0.923	0.82	0.306	2.19
5	6.60	5.99	134-283	17.5	71.3	0.891	4.09	0.520	1.69
6	6.23	5.69	469-761	28.1	111.7	0.874	7.46	1.16	1.65
7	6.13	5.68	592-871	28.4	113.4	0.739	7.42	1.65	1.41

(1) The unit of the precipitation rate: mmol/m^2h.kg (milimole of precipitation per square metre of seed surface area, per hour and per one kg solution).

(2) pH_i, and pH_{ec} represent solution initial pH and the calculated equilibrium pHs, respectively.

(3) The CO_2 partial pressures corresponding to the initial and equilibrium pH calculated from Solmineq88.

Figure 6.4 shows the calcite growth rates as a function of the relative saturation ($S^{0.5}$-1) at different solution pH values (Nos 1, 3 and 7 in Table 6.3). From Table 6.3 we can find

that when the solution pH is below 7.5, the calcite growth rates sharply increase with decreasing pH; when the pH is above 7.5, the calcite growth rates increase with increasing pH. The reason why the calcite growth rates are different at different pH values could be due to there being different reaction mechanisms at different solution pH values.

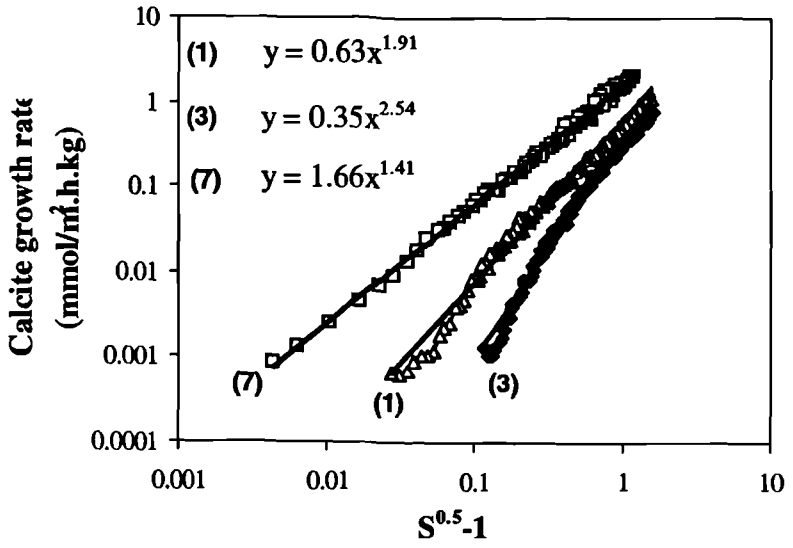

Figure 6.4 The comparison of the calcite growth rate at different pH (experiments Nos 1, 3 and 7 in Table 6.3).

Figure 6.5 shows how the distribution of HCO_3^- and CO_3^{2-} changes with solution pH. As we can see, when the solution pH is below about 7.5, most of the carbonate species exists in the form of HCO_3^- (> 99%). However, when the solution pH is above 7.5, the concentration of CO_3^{2-} sharply increases with increasing pH and the concentration of the bicarbonate starts to decrease. There may be two reactions:

$$Ca^{2+} + 2HCO_3^- = CaCO_3 + H_2CO_3 \quad (6.1)$$

$$Ca^{2+} + CO_3^{2} = CaCO_3 \quad (6.2)$$

occurring simultaneously on the calcite surface during calcite precipitation. The reaction rate will be dominated by the faster reaction. From Figure 6.5 we can expect that calcite

precipitation is dominated by the reaction 6.1 at low pH (< 7) and by the reaction 6.2 at high pH (> 8). Because the reaction 6.2 involves releasing a water molecule and a CO_2 gas molecule on the calcite surface, the reaction rate can be expected to be much slower for reaction 6.2 than the reaction 6.1. This may be the reason why the calcite precipitation rates increase with increasing pH.

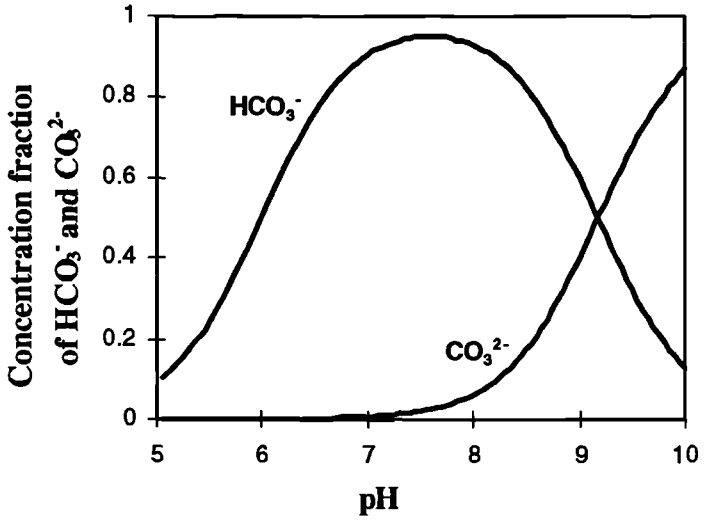

Figure 6.5 The concentration fractions of HCO_3^- and CO_3^{2-} at different pH values (IS = 1mol/kg).

When the pH is much lower (< 6), the reaction rate again becomes high. This may be caused by other reasons. A study by Dove and Hochella (1993) showed that surface nucleation occurred at lower saturation states (S =1.5 - 2.5) at the early stage of growth on calcite surfaces from solutions with low pH (pH < 6). On the other hand the calcite growth experiments by Gratz and Hillner (1993) suggested that no surface nucleation was observed on the calcite surface. The technique used by both workers was similar; the former used scanning force microscopy and the latter used atomic force microscopy. A difference is that Dove and Hochella used solution pH values lower than 6 and Gratz et al. used solution pH values around 8 to 10 (Gratz et al., 1993). Because spontaneous nucleation gradually increases the number of calcite seeds, which in turn increases the surface area, the measured growth rates would be higher than the true value. If surface nucleation continues after precipitation starts then the crystal surface area will increase as a function of time, so that a lower reaction order and higher rate constant obtained from a low pH solution can be the

consequence of the additional increase in calcite surface area. As we discussed in Chapter 5, the presence of a gas-liquid interface may encourage calcite nucleation. A low solution pH is normally maintained by bubbling CO_2 gas into the solutions. Maybe the gas bubbles stimulates surface nucleation in the lower pH solutions.

6.2.3 Alkalinity effect

The stoichiometric ratio of Ca^{2+} and HCO_3^- is 1 to 2 and can be represented by the reaction of equation 6.1. If we want to increase the concentration of HCO_3^- and keep the supersaturation constant, the Ca^{2+} concentration must be reduced, i.e. the ratio of $C_{Ca^{2+}}/C_{HCO_3}$ becomes lower. In order to examine kinetic models over a wide range of solution compositions, calcite growth rates have been determined at different ratios of $C_{Ca^{2+}}/C_{HCO_3^-}$ (Table 6.4). Because alkalinity can be directly analysed from an acidmetric titration, it is more convenient to use alkalinity than the concentration of HCO_3^- ion. The values of alkalinity and HCO_3^- concentration are very close at the solution pH values chosen in the experiments in Table 6.4.

Table 6.4 Calcite growth rate on the seed at different alkalinity

No	pH_i	pH_e	Alk_T (meq/kg)	$[Ca^{2+}]$ (mmol/kg)	SI	PPT (mmol/kg)	k_p $R_m = k_p(S^{0.5} - 1)^n$	n
8	7.74	6.94	2.03	41.9	0.868	0.21	0.320	1.69
9	7.61	6.89	3.55	25.1	0.805	0.35	0.308	2.29
10	7.72	6.93	4.08	19.8	0.875	0.41	0.389	2.05
11	7.80	7.06	5.17	10.8	0.816	0.45	0.399	2.12
12	7.80	7.08	7.6	7.64	0.803	0.63	0.480	2.02
13	7.68	7.06	10.9	5.40	0.733	0.82	0.742	1.86
14*	7.75	7.07	10.6	5.52	0.795	0.85	0.764	1.87
15	7.85	7.27	12.6	3.26	0.738	0.81	0.955	1.98
16	7.86	7.31	20.1	2.55	0.846	1.20	0.896	1.79
17	7.78	7.54	47.6	1.21	0.844	0.95	0.450	2.69

* calcite seed concentration was 0.78g/kg, for others, the seed concentration of 0.30g/kg was used.

The influence of calcite seed concentration on growth rate was examined by conducting two parallel rate measurements with the same solution composition and different seed concentration (No 13 and 14). The results indicate that the influence of concentration does not appear to be significant at the seed concentrations used in this study. House and Tutton (1982) also examined the influence of seed concentration and found that if the seed concentration is too low, the surface area contribution from a calcite heterogeneous nucleation can be significant and a lower rate constant will be obtained from such rate measurements using calcite seeds.

From Table 6.4 we can see that the calcite growth rate increased with increasing solution alkalinity. When the calcium ion concentration decreased to a very low level (2mmol/kg), the rate constant started to decrease with increasing alkalinity and the apparent reaction order goes up sharply. A high reaction order implies that the growth rates sharply reduce with decreasing supersaturation. When the ratios of $C_{Ca^{2+}}/C_{HCO_3}$ are away from the stoichiometric ratio ($C_{Ca^{2+}}/C_{HCO_3}$ >>0.5 or << 0.5), the concentration of either Ca^{2+} or HCO_3^- can be very low. As the concentration reduction of Ca^{2+} and HCO_3^- is based on the stoichiometric ratio during the precipitation, the ratios of $C_{Ca^{2+}}/C_{HCO_3}$ will be much further away from the stoichiometric ratio when the reaction is close to equilibrium. Under the same mass transport condition, the difference of the mass concentration in the bulk solution and near the crystal surface can be much higher for the ions with very low bulk concentrations than those with high bulk concentrations. In other words the supply of the ions with a low bulk concentration is much slower than for the ions with a high bulk concentration. The calcite growth rate will be limited by those ions with low concentration.

There are two processes occurring during crystal growth: mass transport (including diffusion and convection) and surface reaction. To determine which mechanism controls the precipitation, a transport rate including convection and diffusion via a control index (q_D) can be introduced. q_D is the ratio of the measured crystal growth rate (R_L) to the growth rate calculated by a diffusion-controlled growth rate equation (R_D) (Nielsen and Toft, 1984).

$$q_D = R_L / R_D \tag{6.3}$$

When $q_D \leq 0.1$ the crystal growth is surface reaction controlled. If $q_D \geq 0.9$, diffusion dominates the growth process, but between $0.9 > q_D > 0.1$ both surface reaction and diffusion participate in the growth process as a combined mechanism. The diffusion controlled reaction rate can be calculated by:

$$R_D = DV_m(C_x - C_{eq})/r \ , \tag{6.4}$$

where D is the diffusion coefficient, (D for different ions is very similar and the difference is small and can be neglected), V_m is the molar volume and r is the crystal particle radius. C_x is the lower of $C_{Ca^{2+}}$ and $2C_{HCO_3^-}$. From equation (6.4) we can see that the maximum reaction rate will be achieved when $C_{Ca^{2+}} = 2C_{HCO_3}$.

If we assume that the calcite crystal growth is solely diffusion controlled, that the diffusion coefficient of $D = 10^{-9}\ m^2/s$ and the average crystal size is 3 μm, then the theoretical diffusion controlled calcite crystal growth rate for experiment No. 14 in Table 6.4 will be: $R_D = 1.5 \times 10^{-8}\ m/s$, the growth rate obtained form the experiment is $R_L = 2.1 \times 10^{-10}\ m/s$, and thus $q_D = 0.02$, i.e. the reaction is surface controlled under these condition. However, for experiment No.8, the total amount of precipitation was only 0.21mmol/kg, and from equations 6.3 and 6.4 we get $R_D = 7.5 \times 10^{-9}\ m/s$, $q_D = 0.10$, so that the calcite crystal growth becomes a combined controlled process under these conditions.

Our results from the mass deposit experiments suggest that when the ratios of $C_{Ca^{2+}} / C_{HCO_3}$ are not far away from the stoichiometric ratio (for example, from 0.25 to 4) and the solution pH is greater than 7, the effects of mass transport and surface nucleation on the calcite growth rate are small. The reaction order (n) should be close to 2 which is the reaction order given by rate equation 2.65. If we increase the transport rate for the solutions with the ratios of $C_{Ca^{2+}} / C_{HCO_3}$ further away from the

stoichiometric ratio, the calcite growth rate should increase until it is close to the growth rate from the solutions with the stoichiometric ratio of Ca^{2+} and HCO_3^-. However the influence of mass transport rate cannot be determined simply by changing the stirring rate in a reaction vessel. This is because according to Nielsen (1984) if the crystal size is smaller than about 5 μm, the crystals will sediment relatively slowly so that when the solution is stirred the crystals will be carried with it. In addition, there are other factors which can affect the accuracy of the rate constants by using a mass deposit method, including the surface area of calcite seeds and pH electrode drift during long time measurements, especially at high temperatures (≥ 50°C). This is why many studies suggested that the crystallisation parameters cannot be determined with an accuracy better than about a factor 2 (Garside, 1977 and Koutsoukos et al., 1980). A flowing system with stationary calcite seeds in a glass micromodel can however provide an ideal method (discussed later) for studying the influences of the flow velocity on the crystal growth kinetics, so that by measuring crystal layer growth rates, a more accurate rate constant especially at higher temperatures can be obtained.

6.3 Calcite growth rate determined by visual observation method

6.3.1 The effect of water injection rate and flow velocity

Calcite growth rates were determined from our visual observation method at the fixed ratios of $C_{Ca^{2+}}/C_{HCO_3}$ of 1/2 but at different temperatures and ionic strengths as described in detail later. We found that in a simple water solution (containing only Ca^{2+} and carbonate species and *NaCl*), the crystals retained the original rhombohedral morphology of the calcite seeds. If the growth rate of all the crystal surfaces is a linear function of time, the crystal growth rate can be determined by measuring the crystal size as a function of time. Figure 6.6 shows the results of the crystal size change as function of time measured from the same supersaturated solution but at different water injection rates. As we can see, when the injection rates were above 0.94ml/h, the calcite crystal size increased as a linear function of time, which suggests that the calcite growth rate is not affected by the crystal size, and that the mass supply rate of ions was faster than the amount of ions needed for growth. The calcite growth rates at different solution injection rates can be determined from the slope of the straight lines. However as we can see that

when the injection rate was low (0.47 ml/h), the calcite crystal growth rate decreased with increasing crystal size (the slope of the curve decreases with time).

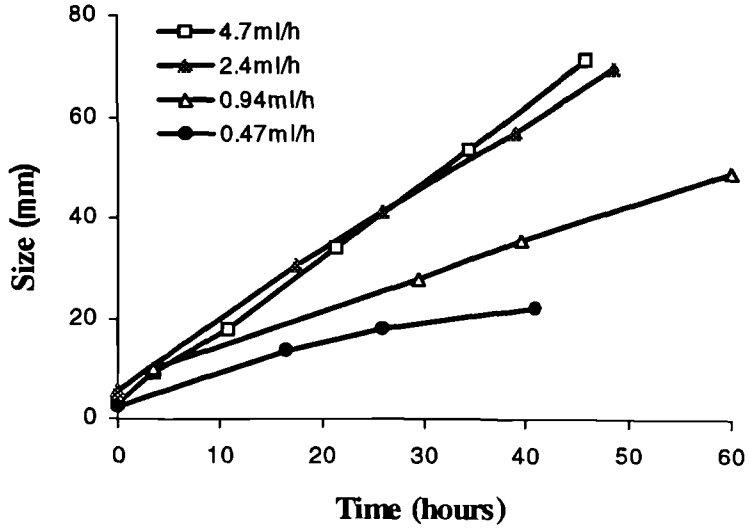

Figure 6.6 The crystal sizes increase as a function of time at different injection rates.

There may be three reasons which cause the calcite growth rates to decrease with decreasing water injection rate: i) the crystal growth rate is a function of crystal size, ii) the supersaturation of calcite decline when the crystals become larger because there is insufficient mass supply inside the micromodel, iii) the calcite crystal growth rate is a function of water flow velocity, i.e. the crystal growth rate is influenced by a mass transport rate. The percentage of ions consumed (A_c %) during calcite growth compared to the original total potential precipitation can be calculated from,

$$A_c(\%) = \frac{C_{in} - C_{out}}{C_{in} - C_{eq}} \times 100 = \frac{N(a+2rt)^3 \rho}{MV_{inj}(PPT)} \times 100 \qquad (6.5)$$

where C_{in} and C_{out} represent the concentration of lattice ions at the entrance and outlet of the micromodel, C_{eq} is the equilibrium concentration, N is the number of crystal placed inside the micromodel, a is the seed size in μm, r is the calcite growth rate (m/s), t is the time in seconds, ρ is the density of the crystal (2710 kg/m^3), M is the molecular weight (0.1kg/mol for calcite) and V_{inj} is the solution injection rate. According to equation 6.5, if

the injection rate is low, the solution supersaturation will decrease significantly as the crystals become larger. Figure 6.7 demonstrates the crystal size change and the amount of ions consumed as a function of time at the given conditions.

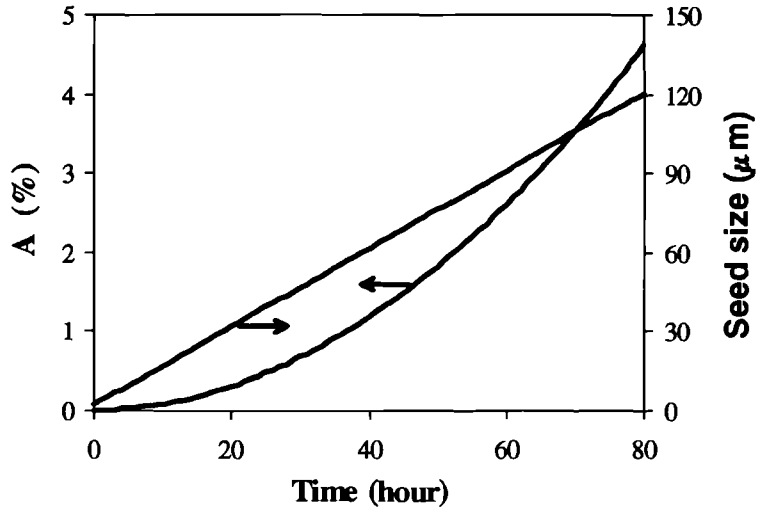

Figure 6.7 The crystal size and the amount of ions consumed during the crystal growth, V_{inj} = 4.7ml/h, N = 100, PPT = 0.54mmol/kg, a = 5μm and r = 2.06×10^{-10} m/s.

Our experimental conditions for crystal size measurement have been designed such that the Ca^{2+} and CO_3^{2-} ions consumed for growing calcite are less than 2% of the maximum amount of the precipitation. Therefore a steady state can be maintained inside the micromodel.

It is interesting to note that when the mass supply is above a minimum of 0.94 ml/h, the crystal growth rates still increase with the injection rate (actually the water flow velocity) which suggests that the calcite growth is affected by the mass transport rate as we suggested in section 6.2.3, when we found that the crystal growth rate is influenced by the alkalinity. When the injection rate is above 2.4 ml/h, the calcite growth rate does not appear to increase with increasing injection rate significantly. The calcite growth rate at 25°C from the experiments with the solution injection rate of 4.7ml/h is 2.06×10^{-10} m/s. The rate constant can then be calculated from the growth rate and the solution saturation ratio by using the rate equation obtained from section 6.2 to give 9.6×10^{-11} m/s. The

rate constants obtained from the experiments at different injection rates were determined in the same way and are plotted in Figure 6.8.

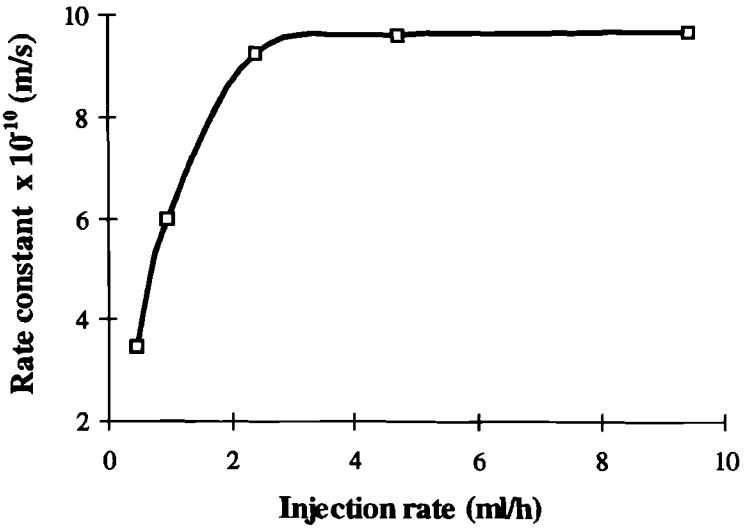

Figure 6.8 The effect of the solution injecting rate on the calcite growth rate inside a micromodel at 25°C, N_c < 500.

As the measured growth rates did not increase with increasing water injection rate when the injection rates were above 4.7ml/h at 25°C, this injection rate is considered to be the critical injection rate at 25°C. For all the experiments conducted for the determination of rate constants the injection rate was 4.7 ml/h at 25°C. It is obvious that the critical injection rate increases with increasing temperature because the crystal growth rate is higher at a higher temperature. The rate constants obtained from different temperatures and ionic strengths have been determined in the same way and are listed in Table 6.5.

Table 6.5 Calcite growth rate constant at different temperature and ionic strength

No	T (°C)	pH_{25}	$[Ca^{2+}]$ (mmol/kg)	$[HCO_3^-]$ (mmol/kg)	[NaCl] (mol/kg)	SI	R_L ($m/s \times 10^{10}$)	k_p (size) ($m/s \times 10^{10}$)	k_p (mass) ($mmol/m^2.h.kg$)
1	25	7.80	5.400	10.70	2.0	0.866	3.10	1.06	0.253
2	25	8.10	3.543	6.940	1.0	0.783	2.06	0.96	0.231
3	25	8.05	2.505	5.055	0.09	0.754	1.47	0.769	0.184
4	50	7.99	2.505	5.055	0.09	0.714	6.04	3.65	0.808
5	70	7.92	2.505	5.055	0.09	0.712	15.8	9.64	2.30
6	50	8.09	3.543	6.940	1.0	0.491	14.3	25.2	6.01
7	70	8.09	3.543	6.940	1.0	0.362	33.1	58.1	13.9

In order to compare the rate constants obtained from the mass deposit experiments, the rate constants have been converted from R_L in m/s to R_m in mmol/m^2.h.kg by using equation 4.17. They are listed in the last column of Table 6.5.

6.3.2 Ionic strength effect

From the experiments at different ionic strengths of 0.1, 1 and 2 eq/kg (Nos 1 to 3) in Table 6.5 we can find that the calcite growth rates increase as the solution ionic strength increase. The rate constants at different ionic strengths are plotted in Figure 6.9. The results show that the calcite growth rates can be described as a function of the square root of solution ionic strength.

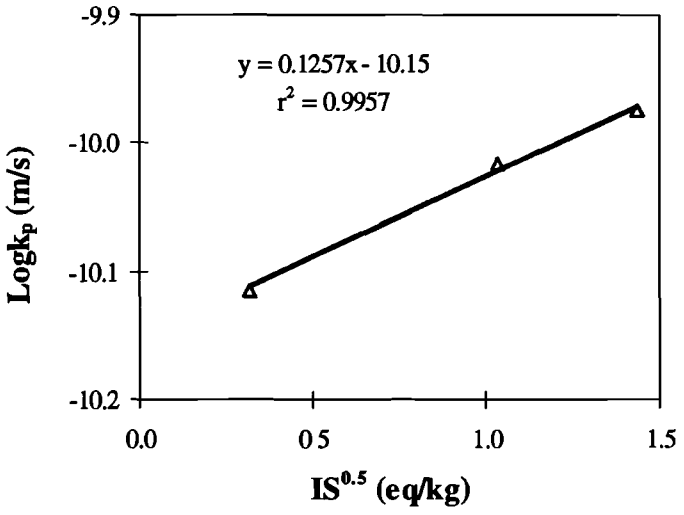

Figure 6.9 Calcite growth rate constants changes as a function of the square root of ionic strength (25°C).

From the results in Figure 6.9, the calcite growth rate constant as a function of ionic strength can be represented by:

$$Logk_p = 0.1257(IS)^{0.5} - 10.15 \qquad (6.6)$$

A general theory of ionic strength effects on rates of reaction in aqueous solution, called the primary kinetic salt effect (Bronsted, 1928), is based on the assumption that the reaction rates are proportional to the number of ions in the activated state, i.e. the

molality, not the activity, of the activated ion pair. Thus a reaction rate will vary by the activity of the activated ion pair, which in turn is a function of ionic strength. This theory suggests that the rate constant is a function of the square root of ionic strength. Our experimental results can be supported by this theory.

Another effect of ionic strength on crystal growth rate is that there may be an analogy to the flocculation of colloids by salts. It is well known that increased electrolyte concentrations decrease the double layer thickness and result in stronger interparticle attraction. Ionic strength catalysis of calcite growth is probably due to decreased surface energy barriers, so that reactants can more easily traverse the double layer. If the controlling step of calcite growth is the dehydration of Ca^{2+}, the growth rate can be expected to increase with increasing ionic strength because a higher ionic strength reduces the tendency of ion hydration.

6.3.3 Temperature effect

The calcite growth rates measured at the temperatures of 25°, 50° and 70°C show that there is a strong influence of temperature. The plot of the rate constants at an ionic strength of *0.1 eq/kg* (Nos 3 to 5 in Table 6.5) against *1/T* gives a straight line (Figure 6.10).

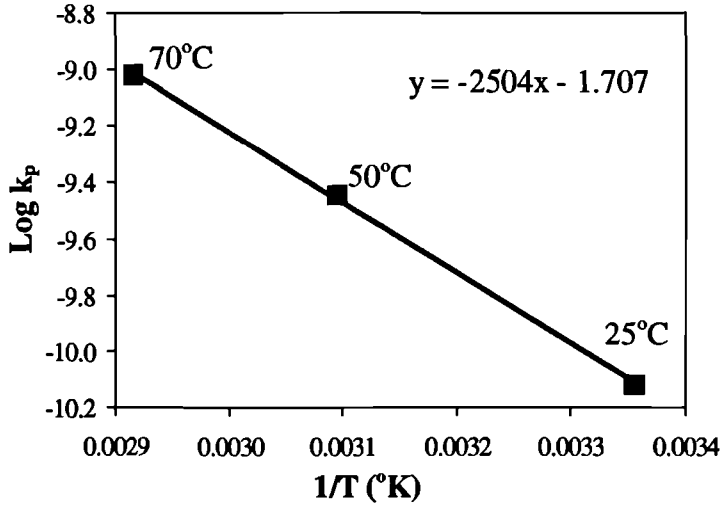

Figure 6.10 The plot of the rate constants at an ionic strength of *0.1 mol/kg* against temperature (*1/T*).

An activation energy of 46.8±2.3 kJ/mol is obtained which is in good agreement with the values of 46.1 kJ/mol given by Nancollas and Reddy (1971), 43.1±3.8 kJ/mol by Wiechers et al. (1975) and 48.1 kJ/mol by Inskeep and Bloom (1985).

From the straight line in Figure 6.10, the calcite growth rate constant at an ionic strength 0.1eq/kg but at different temperatures can be calculated from:

$$Log\ k_p = -2504/T - 1.708\ (m/s) \tag{6.7}$$

However when we used the rate data from the solutions with a high ionic strength (Nos 2, 6 and 7 in Table 6.5), a much higher activation energy was obtained (87 kJ/mol). As we know for the same chemical reaction the lower the E_{act}, the faster the reaction. We have found that the calcite growth rate is higher at a high ionic strength, thus the E_{act} obtained from high ionic strength solutions should be lower than those from low ionic strength solutions. Such a large difference of activation energy from the solutions with high ionic strength could be due to error in the calculations of the saturation indexes by Solmineq88. If we compare the saturation indexes for two groups of calculations, one with low ionic strengths (Nos 3 to 5 of Table 6.5) and the other with high ionic strengths (No 2, 6 and 7 in Table 6.4), we can find that the saturation indexes of the low ionic strength solutions at higher temperatures (≥ 50°C) are very close to those at 25°C, whereas the saturation indexes of the high ionic strength solutions are much lower at high temperatures. Therefore we believe that the activation energy obtained from the solutions with high ionic strength is not correct. The reasons will be discussed in section 6.4.

6.3.4 Transport effect

As we suggested in 6.2.3, a low growth rate from a low alkalinity solution is mainly due to the mass transport factor. If this suggestion is correct, the calcite growth rate should increase with increasing transport rate until the growth rate is close to that for systems with the same saturation index at the stoichiometric ratio of $C_{Ca^{2+}} / C_{HCO_3}$. We have conducted experiments to examine the effect of mass transport rate on the calcite growth rate

by measuring the calcite crystal size in the channels with different sizes, so that different solution flow velocities can be achieved in a micromodel at a constant injection rate. The solution injection rate used in these experiments was 4.7ml/h. The calcite growth rate at non-stoichiometric ratios from these crystal size measurements is given in Table 6.6.

The results show that the calcite growth rate increases with fluid flow velocity at non-stoichiometric ratios. The calcite growth rate constant obtained from the highest flow velocity (No 1) is still lower than the rate constant obtained from solutions with the same ionic strength but with stoichiometric ratios of $C_{Ca^{2+}}/C_{HCO_3}$ (9.6×10^{11} m/s, No 2 in Table 6.5). It can be expected that in this case if we increase the water flowing velocity, the calcite growth rate will continuously increase until the flow velocity reaches its critical value.

Table 6.6 The effect of flow velocity on calcite growth rate*

No	Channel width (mm)	Flow velocity (m/min)	Growth rate (m/s×10^{10})	Rate constant (m/s×10^{11})
1	0.3	1.8	3.70	7.43
2	1.2	0.6	2.67	5.36
3	2.0	0.3	2.10	4.21

Solution compositions: [Ca^{2+}] = 0.0237 mol/kg, [Alk] = 0.00366 eq/kg, pH = 7.83, T=25°C, IS = 1 eq/kg, SI = 1.02, solution injection rate = 4.7 ml/h.

6.4 The determination of ion pair or ion pair constants

In a carbonic acid - water system, the distribution of carbonic acid species governs the solution pH. Formation of ion pairs has a strong influence on solution pH. If a solution pH is unknown and has to be calculated from the water composition, e.g. oilfield formation water under downhole conditions, the reliability of the thermodynamic data will be very important for the calculations of the distribution of carbonate species and their ion pairs. The accurate calculation of a solution pH can then be possible. However, the reported carbonate ion pair constants show unbelievable wide dispersion, in some cases a difference of an order of magnitude. Table 6.7 lists some of carbonate ion pair constants.

The reasons for such a wide dispersion of data are because first, many reported ion pairing equilibrium constants were determined from the pH observations in high ionic strength solutions without taking account of residual diffusion potential effects; second, the ion pair constants require knowledge of the values for single ion activity coefficients. The activity coefficients however cannot be determined absolutely, and can only be estimated from theory. Therefore, it is important to note that for particular test solutions using the ion pairing theory and reported thermodynamic data or ion pairing equilibrium constants, the activity coefficients must be determined using the same approach as used in the determination of the ion pairing equilibrium constants.

Table 6.7 Experimentally determined thermodynamic values for pK for ion-pairs or ion pairs in carbonate water system at 25°C and 1 atm total pressure.

ion pair	pK value of ion pair
$NaCO_3^-$	0.65 [7], 1.0[1], 1.27 [2]
$NaHCO_3^o$	-0.25 [3], -0.55 [7]
$CaCO_3^o$	3.00[1], 3.10[5], 3.16 [7], 3.20[3], 3.22 [6], 4.48[4]
$CaHCO_3^-$	0.59 [7], 0.80 [1], 1.25 [4]

(1) Kotrlý and Stanislav (1985); (2) Garrels et al (1960); (3) Garrels and Thompson (1962); (4) Nakayama (1968); (5) Lafon (1971); (6) Larson et al (1976); (7) Loewenthal and Marais (1984).

It is also important to note that there have been many reports that ion pair constants are ionic strength dependent (Beck and Nagypal, 1990; Kotrlý and Stanislav, 1985). However, only the ion pair constants from dilute solutions are used in many commercial geochemistry packages for saturation index calculations. There is no comprehensive theory to estimate the dependence of the ion pair constants on ionic strengths. For these ion pairs we are interested in the increased ion pair constants with increasing ionic strength up to 1.0 eq/kg. This means that the ion pairs are less stable in the solutions with high ionic strengths. We have used the ion pair constants for two carbonate ion pairs obtained from solutions with increased ionic strength (pKs = 3.00 for ion pair $CaCO_3^o$ and 1.00 for $NaCO_3^-$, Kotrlý and Stanislav, 1985). The ion pair constants at temperatures above 25°C were determined by measuring the solution pH changes with temperature. In a closed water system, the total carbonic acid in the system remains constant

as the temperature is raised, but the pH will change because the dissociation constants of water, carbonic acid and their ion pairs change with temperature. Thus, a new distribution of carbonate species will be established and alter the solution pH. The ion pair constants at elevated temperatures can be calculated from the solution pH at 25°C and at the examined temperature as well as the ion pair constant at 25°C. The ion pair constants for $CaCO_3$ and $NaCO_3^-$ at 50° and 70°C were estimated in this way and are given in Table 6.8.

Table 6.8 Ion pair constant from the Solmineq88 data base and from the measurements at ionic strengths of 1.0 eq/kg

Temperature (°C)	$pKCaCO_3^\circ$		$pKNaCO_3^-$	
	reported	determined	reported	determined
25	3.22	3.00*	1.27	1.00*
50	3.51	3.19	1.81	1.24
70	3.79	3.40	2.24	1.47

* obtained from literature for the solutions with ionic strength > 0.1eq/l (Kotrý and Stanislav, 1986)

The logarithm of the ion pair constants listed in Table 6.8 are plotted as a function of temperature (Figure 6.11).

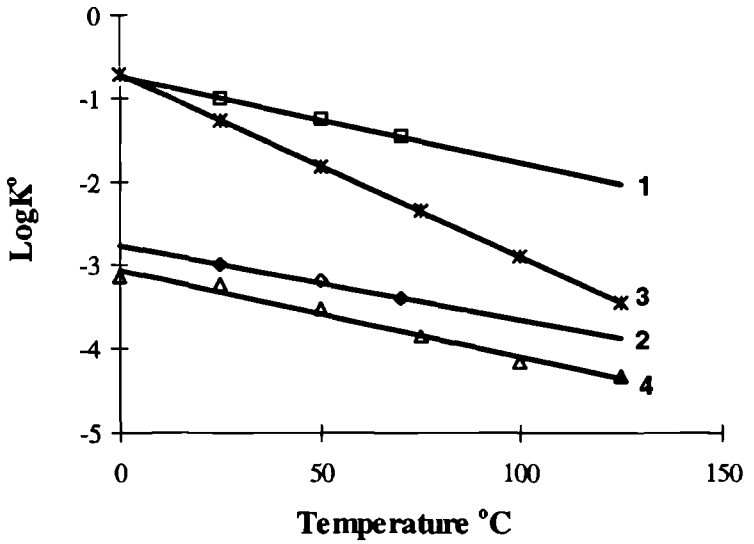

Figure 6.11 The measured and reported ion pair constants as a function of temperatures, measured ion pair constants: 1 $NaCO_3^-$, 2 $CaCO_3^\circ$, reported ion pair constants: 3 $NaCO_3^-$, 4 $CaCO_3^\circ$.

From Figure 6.11 we note that the slopes of the straight lines 1 and 2 from our measurements are smaller than those of lines 3 and 4 from the literature (Solmineq88 data base). This result indicates that the temperature deviation for these two ion pairs is smaller than that obtained from the literature.

When the estimated ion pair constants at the elevated temperatures were used to re-calculate the solution initial pH at the elevated temperatures for Nos. 2, 6 and 7 from 1 eq/kg ionic strength solutions in Table 6.5, the calculated initial pH values are in good agreement with the measured values (Table 6.9).

Table 6.9 The calculated solution pH, SI and K_p at elevated temperatures by using estimated ion pair constants of this study.

No	*T (°C)*	pH_{25}	$pH_{t(c1)}$	$pH_{t(c2)}$	$pH_{(m)}$	SI_1	SI_2	k_{p1}	k_{p2}
2	25	8.10	-	-	-	0.783	0.789	0.96	0.92
6	50	8.09	7.58	7.81	7.83	0.491	0.756	25.2	7.42
7	70	8.09	7.26	7.65	7.70	0.362	0.817	58.1	13.6
						Ea (kJ/kg)		87.0	47.4

The subscript *c* and *m* represent the calculated and measured values, subscript *1* and *2* refer to the calculated results by using reported and measured ion pair constants, respectively.

When the corrected initial solution pH values were used to calculate the saturation index of the solutions with high ionic strength (1.0 eq/kg), a similar tendency of rate constant change as a function of temperature has been obtained as for the low ionic strength solutions (≤ 0.1 eq/kg). The calculated activation energies obtained from the high ionic strength solutions is now 47.4 kJ/kg, which is much closer to the activation energy obtained from solutions with an ionic strength of 0.1 eq/kg.

6.5 The influence of the surface area of calcite crystal seed

The layer growth rate constants in m/s can be converted to the mass deposit rate constants in mmol/m^2.h.kg by equation 4.18. They are also listed in the last column of Table 6.5. If we compare the rate constants of No. 2 in Table 6.5 with No.14 in Table 6.4, we find that the rate constants from the mass deposit experiment are lower than

those from the visual observation experiments by a factor of 3. There are three main factors which may be the causes of this difference:

1. the uncertainty of the calcite seed surface area determined by BET,
2. non-equilibrium crystal surface structure and
3. small crystal size.

The surface area of the calcite seeds used in this study was measured by the BET method using a Coulter Omnisorp 100, a volumetric adsorption instrument, and nitrogen gas as adsorbate at liquid nitrogen temperatures, with an accuracy of better than ±30%. However there is no direct connection between the surface area measured by the BET method and by crystal geometric shape. If the surface area of 5.88m^2/g of calcite seeds is used to back-calculate the average size of the calcite seed, we obtained the average size of 0.38 μm which is much smaller than that observed microscopically (1-5 μm). If the measured surface area is higher than the actual value, a lower growth rate will be obtained.

Even if the initial surface area of the calcite seeds is correct, the calcite seeds may not be well-formed when they are produced, for example under the conditions of high temperature and high supersaturation or broken by mechanical force. Thus these seeds may contain a high density of kink sites which will cause a high initial growth rate (Marlin, 1994). However the original kink site density of these seeds will not stay for long. A new equilibrium structure will be achieved between the supersaturation solution and the crystal surface. This can be illustrated in Figure 6.12. Figure 6.12a shows a flat seed surface with a lower kink density. Figure 6.12 demonstrates a new seed surface containing a high kink site density. As we can see, for the crystal seeds with the surface properties like the one shown in Figure 6.12b, a higher growth rate will be obtained.

It has been well known that the growth rates of small crystals are slower than larger crystals if the crystal growth is controlled by surface reaction, because the surface energy of the small crystal are higher than the larger ones (Söhnel and Garside, 1992).

Therefore if the calcite seeds used for the determination of calcite growth are very small (< 1μm), a lower growth rate can be obtained.

6.13a 6.13b

Figure 6.12, Schematic representation of a flat crystal surface with a lower growth rate (6.12a) and a new seed surface with a higher kink site density and initial growth rate (6.12b). The white squares represent newly grown parts of the lattices.

From above discussion we can see that there are two factors which cause the mass growth rate to be reduced and one to increase it. The overall influence will be the combination of these three factors. However it is obvious that the crystal growth rate determined by measuring a single crystal size change is not affected significantly by these three factors, because the thickness of the growth layers to reach a stable surface (e.g. from the shape in 6.13b to the shape in 6.13a) is very small compared to the final size of the crystal. On the other hand the influence of all these three factors on the absolute rate can be significantly high for a crystal growth rate determined by the mass deposit method. However the determination of the crystal growth rate could be relatively constant for the experiments with the same seed concentration and similar saturation indexes, so that the data obtained from the mass deposit rate can still be used to compare the relative growth rate for waters with different compositions.

Therefore, the mass deposit method is suitable for the relative comparison of the calcite growth rates at different solution compositions because this method is more efficient for the determination of the crystal growth rates over a wide range of supersaturation levels in a single experimental run. A reliable growth rate model then can be developed based on this wide range of measurements. On the other hand, the visual observation method

will allow us to obtain an absolute growth rate more accurately and in turn to obtain more reliable rate constants.

6.6 Conclusions

The calcite growth rate data from pH- free-drift experiments can be interpreted by the Davies and Jones rate equation. A function for calculation of rate constants at temperatures up to 70°C and ionic strengths up to 2 eq/kg for a simple water system has been developed from visual observation experiments conducted in a glass micromodel. From the observation of calcite growth rates at different transport rates we have found that the calcite growth rate is influenced by the solution transport rate. Calcite growth rates show a dependency on solution alkalinity and pH which is believed to represent transport influence and surface nucleation.

CHAPTER 7

SCALE INHIBITORS

7.1 Introduction

Many compounds and ions inhibit calcite growth rate, such as phosphonate, organic acids, Mg^{2+} and Fe^{2+} and some of them have been used as carbonate scale inhibitors (Akin and Lagerwerff 1965a, 1965b; Cicerone et al, 1992; Dromgoole and Walter, 1990a, 1990b; Morse, 1974b, 1978; Mucci and Morse, 1983; Morse and Mackenzie, 1990; Paquette and Reeder, 1995 and Reeder and Grams, 1987). These inhibitors can be divided into three groups according to their function. The first group are those which can be adsorbed onto the crystal surfaces, particularly at the active sites of the crystal surfaces (such as kinks) or along the growth steps, and disrupt the further growth of the crystals. These inhibitors are typically organic derivatives of phosphoric acids, and can be active at concentrations as low as 0.1 μmol/kg. Some of them can even stop crystal growth irreversibly. Most industrial scale inhibitors belong to this group. The second group consists of those ions which can be incorporated into the crystal lattice of the scale, thereby influencing the morphology of the scaling crystal and change the crystal growth rate. These inhibitors are active at concentrations above 0.1 to 10 mmol/kg, such as Mg^{2+}, Sr^{2+}, Mn^{2+}, Fe^{2+} and SO_4^{2-}. Because some of these ions exist in most natural waters at a relatively high level, their influence on the kinetics of calcite precipitation can be significant, and must be taken into consideration when predicting $CaCO_3$ scaling tendencies. The third group consists of those ions and chemicals which can form stable complexes with lattice cations and reduce the crystal growth rate by reducing the concentration of free lattice ions in the solution. The examples of the third group of compounds are EDTA and short chain (C_2-C_4) carboxylic acids. They are active at concentrations comparable to the concentration of the substances being precipitated.

The objective of this chapter is to study the kinetics of calcite growth influenced by the presence of these three types of inhibitors and to identify their functions. The mechanistic change caused by the incorporation of foreign ions into calcite crystals, especially Mg^{2+}

has been examined in order to understand why such Mg^{2+} incorporation can reduce the calcite growth rate and influence the calcite crystal morphology. The molecular structure and the functional groups of common scale inhibitors are also discussed in order to help us choose scale inhibitors and optimise scale treatment in the oilfield. A kinetic model to describe the calcite growth rate at different solution compositions with Mg^{2+} present and different temperature has been developed.

7.2 The influence of inhibitors on the kinetics of calcite growth rate

Many studies have shown that the calcite growth rate can be reduced by the presence of Mg^{2+} and other divalent metal ions, such as Ba^{2+}, Sr^{2+}, Mn^{2+} and Fe^{2+} (Akin and Lagerwerff, 1965b, Dromgoole and Walter, 1990; House and Howson, 1988; Morse and Mackenzie, 1990; Mucci and Morse, 1983; Paquette and Reeder, 1995 and Reeder and Grams, 1987). The possible reason is because these cations can also be incorporated into the calcite crystal lattices at Ca^{2+} ion sites (Morse and Mackenzie, 1990 and Paquette and Reeder, 1995). There is a rate reduction which is often approximately proportional to the concentration ratio of the foreign cations with Ca^{2+} ions (Morse and Mackenzie, 1990). However, the fundamental controls on foreign ion incorporation during calcite growth remain poorly understood. There is no strong evidence to explain why the reported values of the amount of Mg^{2+} incorporated into the calcite as a function of solution chemical compositions varies from one study to another. For example, the values from the experiments using seawater ($Mg^{2+}/Ca^{2+} = 5$) have ranged from 2 to 18% (Back et al., 1992; Doerner and Hoskins, 1925; Folk, 1974; Garrels and Wollost, 1978; Griffioen and Appelo, 1993; Hartley and Mucci, 1996; Katz, 1993; Morse and Machenzie, 1990; Mucci and Morse, 1983 and Mucci and Zhong, 1989), depending on the experimental methods and conditions. Normally the amount of Mg^{2+} incorporated into the calcite in laboratory experiments is lower than that in natural calcite by a factor of up to 3 at similar solution compositions. Some workers believe that the amount of Mg^{2+} incorporated is influenced by the water composition and precipitation rate as well as temperature (Morse and Mackenzie, 1990 and Plummer and Mackenzie, 1974). These factors make prediction of the calcite growth rate in oilfield formation water from currently available thermodynamic and kinetic data complicated. Therefore, some calcite growth experiments have been conducted to study:

- what causes such variations in the determination of the amount of Mg^{2+} ion incorporation;
- what is the relationship between the calcite growth rate and the amount of Mg^{2+} ions incorporated;
- whether the kinetic model obtained for simple systems can be used for solutions containing inhibitors.

Both a mass deposit method and a size observation method have been used to examine the influences of other ions on the calcite growth rate, and what kinetic model can be used to describe this influence. The study of Mg^{2+} incorporation can help us understand the influence of other foreign ions on calcite growth.

7.2.1 Calcite growth influenced by the incorporation of Mg^{2+} ions

Calcite growth rates from solutions with different ratios of magnesium and calcium ($[Mg^{2+}]/[Ca^{2+}]$) were determined by the pH free drift method (Chapter 4). The ratios of $[Mg^{2+}]/[Ca^{2+}]$ in the solutions ranged from 0.1 to 5 whereas the solution pH and supersaturation ratios were kept approximately constant. Table 7.1 gives the solution compositions and the calcite growth rate constants determined from the interpretation of rate data by rate equation 2.65.

Table 7.1 The effect of Mg^{2+} on calcite growth rates at 25°C and different calcite seed concentrations

No	pH_t	$[Mg^{2+}]$ (mmol/kg)	Alk_T (meq/kg)	$[Ca^{2+}]$ (mmol/kg)	SI	k_p	n	r^2	calcite seed (g/kg)
						$R_m = k_p(S^{0.5} - 1)^n$			
14	7.75	0	10.6	5.52	0.795	0.764	1.86	0.992	0.738
18	7.81	1.0	10.9	5.31	0.847	0.519	3.03	0.980	0.295
19	7.79	2.8	11.6	5.61	0.875	0.611	3.00	0.968	0.738
20	7.81	5.5	11.1	5.57	0.851	0.133	4.29	0.951	0.295
21	7.87	5.1	11.4	5.6	0.936	0.262	3.24	0.979	0.738
22	7.74	25.1	11.3	5.59	0.758	0.010	6.52	0.990	0.295
23	7.82	27.3	11.5	5.76	0.825	0.008	6.07	0.990	0.738
24	7.11	49	5.44	109	0.924	0.281	2.92	0.970	0.738

The calcite growth rate was also determined for a formation water sample (No. 24 in Table 7.1) from the Glamis Field (Wright et al., 1994). The composition of the water sample is listed in Table 7.2. This water sample was filtered through a 0.45μm filter to remove any suspended particles and trace oil. A weighed amount of $NaHCO_3$ was added to this water sample to achieve a calcite supersaturation similar to other solutions in Table 7.1.

Table 7.2 The water composition of experiment No 24

Ions	Ba^{2+}	Sr^{2+}	Ca^{2+}	Mg^{2+}	K^{+}	Na^{+}	Cl^{-}	SO_4^{2-}	HCO_3^{-}
mg/l	653	1360	4272	729	417	28783	51265	19	324

As we can see from Table 7.1, the presence of any Mg^{2+} reduces the calcite growth rate, and causes the reaction order n to increase, and the rate constant k_p to decrease. The rate reduction is proportional to the ratios of $[Mg^{2+}]/[Ca^{2+}]$ in the solutions rather than the absolute Mg^{2+} concentration. For example, the formation water (No 24) has a high Mg^{2+} concentration, but the $[Mg^{2+}]/[Ca^{2+}]$ ratio is about *0.5* so that the measured calcite growth rate is comparable with experiment No1B, which has a similar ratio of $[Mg^{2+}]/[Ca^{2+}]$. It seems that the rate data obtained from the experimental solutions containing Mg^{2+} cannot be interpreted by rate equation 2.65 very well (low r^2). In order to compare the tendency of calcite growth rate reduction by Mg^{2+}, three groups of rate data from experiments at different ratios of $[Mg^{2+}]/[Ca^{2+}]$ and calcite seed concentrations (Nos. 14, 20 and 21) have been plotted in Figure 7.1. We can see from Figure 7.1 that the initial precipitation rates are very close for all three water systems. The curves start to bend as the supersaturation drops, i.e. the apparent reaction order n increases with decreasing supersaturation. The reaction orders given in Table 7.1 are the averaged values. However, when the ratios of $[Mg^{2+}]/[Ca^{2+}]$ reached a high level (≥ 5), the data interpretation becomes better again ($r^2 > 0.99$).

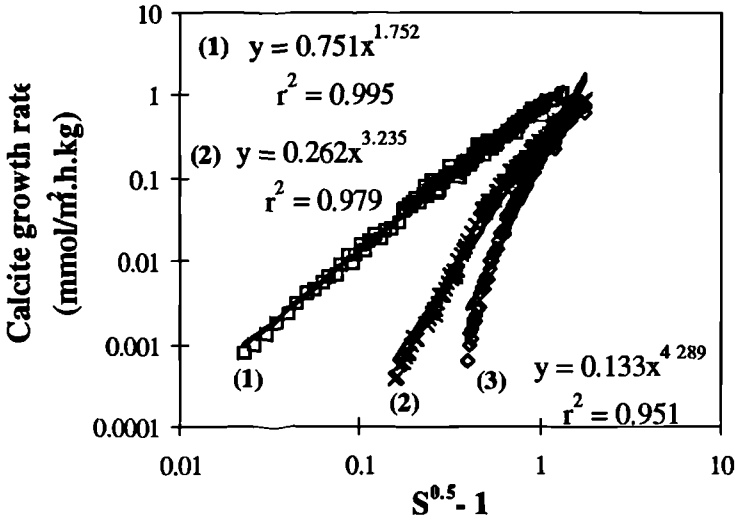

Figure 7.1 The measured calcite growth rate data are plotted as a function of relative saturation *($S^{0.5}$-1)*. Curve (1), calcite growth rate in a supersaturated solution without *Mg^{2+}*; curves (2) and (3), the solution *$[Mg^{2+}]/[Ca^{2+}]$ = 1* and seed concentrations were *0.78g/kg* and *0.30 g/kg*, respectively.

It is also interesting to note that the calcite growth rates are affected by calcite seed concentrations when a solution contains Mg^{2+}. The rate reduction was higher at a lower calcite seed concentration (curve 3 of Figure 7.1), whereas there was no significant influence of seed concentrations in the simple water systems without Mg^{2+} (comparing experiment Nos. 13 and 14 in Table 6.1). These results suggest that the calcite growth rate decreases with increasing calcite crystal size when there is Mg^{2+} present in a solution. In other words, the influence of Mg^{2+} on calcite growth is proportional to the ratio of Mg^{2+} concentration in a solution to the total calcite seed surface area. This will be discussed in the next section (7.2.2).

7.2.2 The influence of Mg^{2+} ions on calcite crystal morphology

To understand why the calcite growth rate is affected by the presence of Mg^{2+} and calcite seed concentration, we microscopically observed the process of calcite growth inside a glass micromodel. We found that when Mg^{2+} was present in the solution, not only did the calcite growth rates decrease with increasing ratios of $[Mg^{2+}]/[Ca^{2+}]$, but also the crystal shape changed (Figure 7.2). The original calcite rhombohedral crystal structure was gradually replaced by new surfaces developed from the edges (crystal No.2

of Figure 7.2) or the corners (crystal No.3 of Figure 7.2) of the original flat calcite surfaces.

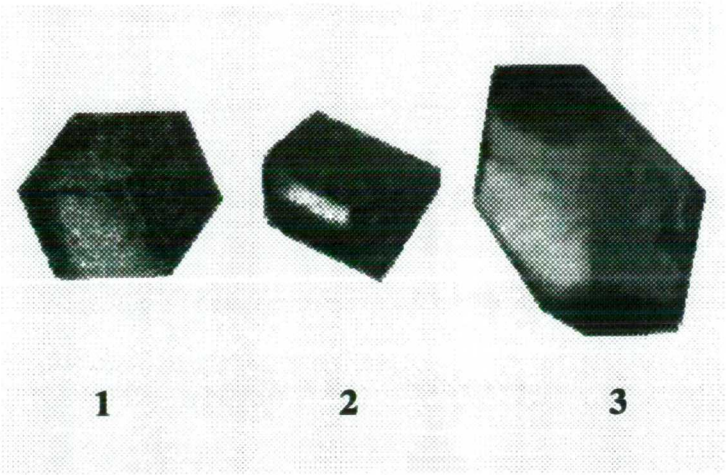

Figure 7.2 Calcite crystals obtained from (1) a supersaturated solution without Mg^{2+}; (2) $[Mg^{2+}]/[Ca^{2+}] = 0.5$, 25°C, (3) $[Mg^{2+}]/[Ca^{2+}] = 0.5$, 40°C.

To understand how Mg^{2+} ions change calcite crystal morphology we can look at the crystal structure at the molecular scale. Calcite ($CaCO_3$) is an ionic crystal with positively charged Ca^{2+} ions and negatively charged CO_3^{2-} ions bonded by ionic bonds. Both calcite and magnesite crystals have rhombohedral morphology, but the lattice size of calcite is larger than that of magnesite. This may be because of the size difference between Ca^{2+} (0.99Å) and Mg^{2+} (0.65Å) (Evans, 1966). The rhombohedral unit cell edge length of the lattices are 6.37 Å and 5.68 Å for calcite and magnesite, respectively (Deer et al., 1992). When Mg^{2+} ions are present in a $CaCO_3$ supersaturated solution, they may also be incorporated into the calcite crystal structure at Ca^{2+} sites (Mucci and Morse, 1983; Paquette and Reeder, 1995; Reeder and Grams, 1987 and Titiloye et al., 1991). It can be expected that the calcite crystal with incorporated Mg^{2+} ions is not as closely packed as would be for the pure calcite or pure magnesite crystals, so the surface energy could be higher for the calcite crystals with Mg^{2+} incorporation and growth rate could be slower. Our experimental results in Table 7.2 show that the reduction of the calcite growth rate by the presence of Mg^{2+} is proportional to the ratio of $[Mg^{2+}]/[Ca^{2+}]$ in the solutions. Mucci and Morse (1983) also found in their experiments that the higher the $[Mg^{2+}]/[Ca^{2+}]$ ratio in the solution, the more Mg^{2+} is incorporated into the calcite

crystals. Therefore, the rate reduction is proportional to the amount of Mg^{2+} incorporated into the calcite crystal surface.

In Chapter 6 we have shown that when the calcite seed concentration is above 0.3g/kg, the calcite growth rate determined from the pH free drift method is not influenced by the calcite seed concentration. The experimental results from Reddy and Gaillard (1981) also showed that when the calcite seed concentration was about 0.3 g/kg, calcite growth rate was not influenced by the solid/solution ratio. The solutions they used were also inhibitor free. The curve No 2 in Figure 7.1 indicates that the calcite growth rate constants decrease with increasing crystal size because the lower the seed concentration the larger the final crystal size from a free drift experiment with the same supersaturated solution. If the calcite growth rate is proportional to the amount of Mg^{2+} incorporated onto the crystal surfaces, the average Mg^{2+} density on the crystal surfaces increases as the crystal growth continues. To understand how the density of the incorporation of Mg^{2+} increases with increasing calcite crystal size, we adopted a simple crystal model (Hartman, 1973) to describe the surface structure. In this model, the surfaces of a crystal was classified into three groups, *F* (flat), *S* (stepped) and *K* (kinked) surfaces depending on whether they are parallel to at least two of the most dense rows of atoms, one most dense row of atoms, or are not parallel to any at all, respectively (Figure 7.3).

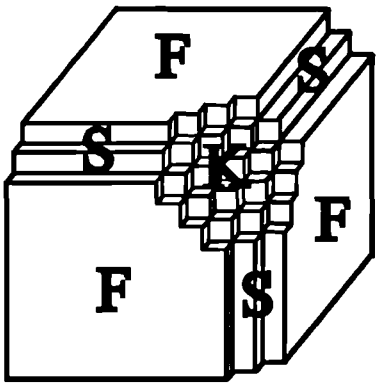

Figure 7.3 A schematic representation of a crystal illustrating F (flat), S (stepped) and K (kinked) surfaces depending on whether they are parallel to two and one most dense rows of atoms, or are not parallel to any of the most dense rows of atoms at all, respectively.

The *K* and *S* surfaces can be considered as full of kinks and steps, respectively. It is obvious that the highest growth rate will be achieved at the *K* surface, then the *S* surface. The lowest growth face is the F face. Therefore, the *S* and *K* faces are normally absent from equilibrium crystal morphologies (Hartman, 1973).

Our experimental results show that only the F faces were observed from the crystals obtained from the simple solutions without Mg^{2+}, whereas other faces, such as the *S* and *K* faces, started to appear when Mg^{2+} was present in the solution. As we can see from Figure 7.2, the crystal No 2 is the result of the *S* surface being developed and the *F* surface gradually diminishing, whereas the crystal shape such as crystal No 3 in Figure 7.2 may be the consequence of the *F* surface being replaced by the *K* surface. What can cause the growth rate to slow down on those surfaces with a high density of kink sites? One possibility is that the Mg^{2+} density on the *S* and *K* surfaces is higher than that on the *F* surface. As a high Mg^{2+} density gives a lower growth rate, the relative growth rate on the *F* face can be higher than those on the other two faces and starts to disappear. The experimental results from Reeder and Grams (1987) and Paquette and Reeder (1995) can support our suggestion. They studied the relationship between crystal surface structure and foreign cations incorporated into calcite and determined the Mg^{2+} density on the *F* and *S* faces of magnesium calcite by the EPMA (electron probe microanalysis) and the SXRFMA (synchrotron X-ray fluorescence microanalysis). They found that the Mg^{2+} density on the *S* faces is higher than on the *F* faces by a factor of 3-4.

Because in our calcite growth experiments and most experiments in other studies, calcite seeds have been used, there is no Mg^{2+} initially on the surface of the calcite seeds. Once the calcite seeds contact a $CaCO_3$ supersaturated solution with Mg^{2+} present, Mg^{2+} ions start to be incorporated into the calcite surfaces. As more Mg^{2+} ions are incorporated onto the S and K faces than onto the F faces, the growth rate of the S or K faces will slow down and start to cause a change in the crystal structure. However we must remember that the crystal structure is gradually changing from the F face dominant to the S or K faces dominant structure. The average Mg^{2+} density on the total calcite surface area increases gradually until the entire structure has changed and the equilibrium crystal shape has been formed. This is what we found in our mass deposit experiments. The rate

reductions by Mg^{2+} were low at the beginning of the experiments and higher at the later stages (as seen in Figure 7.1). Figure 7.4 shows a schematic of the crystal shapes at the beginning, middle and final stages of Mg^{2+} incorporation.

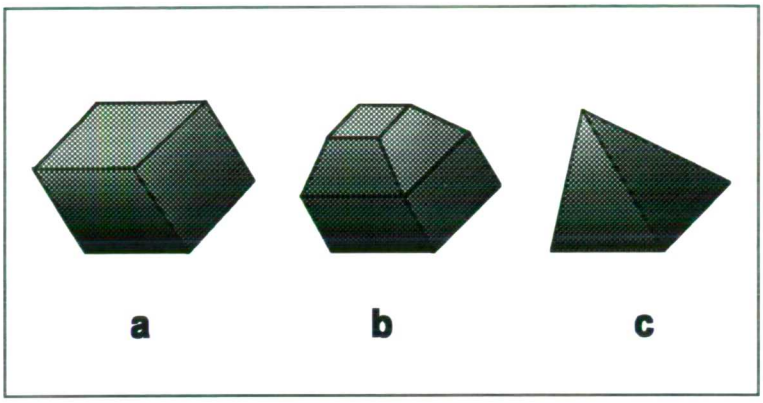

Figure 7.4 The crystal shapes at the beginning (a), middle (b) and final (c) stages of Mg^{2+} incorporation into a rhombohedron calcite (a).

From the above discussion we can understand why a lower seed concentration can cause a higher reduction of the calcite growth rate constant. This is because at a constant solution composition and constant environmental conditions, the percentage of the F surface replaced by the S or K surfaces increases with increasing crystal size. The lower the seed concentration, the larger the crystal will be when the solution reaches its equilibrium state. Because the total mass precipitation is fixed for the same $CaCO_3$ supersaturated water system, the crystal shape change at a low seed concentration will be faster than that at higher seed concentrations. As a consequence, the crystal growth rate reduction due to the crystal shape change will be higher at a low seed concentration than that at a higher seed concentration. A higher reaction order n will appear in the rate equation from the solutions with lower seed concentrations as shown in Figure 7.1.

From the observations of the crystal size change we found that the crystal shape change caused by the incorporation of Mg^{2+} can be a slow process, especially at a low $[Mg^{2+}]/[Ca^{2+}]$ ratio and high seed concentration. As we can see from Figure 7.2 the crystal No. 2 has not reached its equilibrium shape at a large edge size (50-70μm). It is very rare that a crystal can grow to this large size during any normal calcite mass deposit experiment reported in literature. For example, according to the precipitation

experiments conducted by Mucci and Morse (1983), the amount of overgrowth precipitation was less than 10% of the initial seed weight, so that any surface area variations can be neglected. The overall calcite growth rate on a pure calcite crystal seed at a constant supersaturation and ratio of $[Mg^{2+}]/[Ca^{2+}]$ will not remain constant until the crystals reach their equilibrium shape, so that only then can a real steady state be achieved. The calcite growth rate and reaction order determined under steady state will then truly represent the influence of Mg^{2+} on the calcite growth kinetics that can be used to model the calcite precipitation process under natural conditions.

From these findings, we can understand why the Mg^{2+} partition in naturally occurring marine calcite cements is much higher (as high as 23 mol% $MgCO_3$) than that obtained under controlled laboratory conditions from natural or artificial seawater on pure calcite seeds at 25°C (about 8% mol% $MgCO_3$). The incorporation of Mg^{2+} into calcite crystal surface changes the surface structure so that the morphology of the calcite crystals changes. The average Mg^{2+} partition increases during the morphology transfer. When the growth rates are measured at the different stages of the morphology change, different growth rates will be obtained. The natural conditions allow the reactions between the natural waters and natural calcite surfaces to occur over a geological time period so that equilibrium crystal structure can be achieved, i.e. the amount of incorporated ions on the crystal surface has reached the maximum value for the given water compositions and conditions. We believe that once the crystal surface becomes equilibrium (most natural calcite surface should be), the crystal growth rate will become stable and the amount of Mg^{2+} incorporated determined at this stage will be uniform. However, the calcite growth rate constant in the presence of Mg^{2+} (or other inhibitors) cannot be determined by the pH-free-drift method even if the crystals have reached the equilibrium structure (or shape) because the total surface area of the crystal will have changed and the shape of the newly formed crystal structure depends on the water composition and experimental conditions. Therefore the rate constant cannot be obtained with uncertain surface area. But, it can be determined more accurately using a steady state method similar to our visual observation method. The influence of Mg^{2+} on the calcite growth is one of the most important factors in the kinetic of calcite growth. The result can also help us to

understand how other inhibitor ions and scale inhibitor work and hence to optimise scale inhibitors for oilfield use.

7.2.3 The kinetic model of calcite growth with the influence of Mg^{2+}

As we have shown in chapter 6, the calcite growth rate can be described by rate equation 2.65 and the reaction order n is close to 2 for water systems without Mg^{2+} present. We have demonstrated in 7.2.2 that the higher reaction orders obtained from the pH-free drift experiments with Mg^{2+} is mainly due to the growth rate gradually decreasing. A much lower reaction order should be expected when the calcite seeds have an equilibrium crystal structure. The calcite growth rate, therefore, should be stable at a given condition. Therefore, in our kinetic model of calcite growth we assume that the presence of Mg^{2+} only decreases the rate constant but the reaction order remains constant and $n = 2$. However because it is more difficult to estimate the surface area change during calcite crystal growth with Mg^{2+} incorporation, the rate constant cannot be obtained by a pH-free-drift method with good accuracy. Therefore the calcite growth rate constants at different ratios of $[Mg^{2+}]/[Ca^{2+}]$ were determined by measuring the crystal size increase inside a glass micromodel at a given water composition, temperature and solution flow velocity. The results are given in Table 7.3. It can be seen that the calcite growth rates are reduced by the presence of Mg^{2+}, but the differences in the reduction in the growth rates at the ratios of $[Mg^{2+}]/[Ca^{2+}]$ of 0.1 and 0.5 appear very small. Mucci and Morse (1983) also found that in solutions with $[Mg^{2+}]/[Ca^{2+}]$ ratios lower than 1, the incorporation of Mg^{2+} was small (< 3 mole%) and had little effect on the calcite solubility product (K_{sp}) and the growth kinetics. As most oilfield formation waters contain much less Mg^{2+} than Ca^{2+} (Warren and Smalley, 1994), the $[Mg^{2+}]/[Ca^{2+}]$ ratios range of our experiments will cover most oilfield formation waters. The average rate constant at the ratios of $[Mg^{2+}]/[Ca^{2+}]$ below 0.5 at 25°C is about 60% of the rates without Mg^{2+} ion present (Table 7.3). If $[Mg^{2+}]/[Ca^{2+}]$ >1, the calcite growth rate started to reduce sharply. Much longer times will be needed to obtain the calcite growth rate by measuring the crystal size from the solutions with $[Mg^{2+}]/[Ca^{2+}]$ ratios much higher (> 1). Nevertheless, if we compare the rate constants in Table 7.3 with those in Table 7.1, we find that a similar rate reduction tendency at low

$[Mg^{2+}]/[Ca^{2+}]$ ratios is obtained from the pH-free-drift experiments and from which a similar rate reduction tendency at high $[Mg^{2+}]/[Ca^{2+}]$ ratios can be estimated.

Table 7.3 The calcite growth rate at different ratios of $[Mg^{2+}]/[Ca^{2+}]$ at 25°C*

No	pH	$[Ca^{2+}]$ (mmol/kg)	$[HCO_3^-]$ (mmol/kg)	$[Mg^{2+}]/[Ca^{2+}]$	SI	R_L ($m/s \times 10^{10}$)	k_p ($m/s \times 10^{10}$)
2G	8.05	2.505	5.055	0	0.754	1.47	0.768
5A	8.01	2.505	5.055	0.1	0.705	0.777	0.496
5B	8.05	2.505	5.055	0.5	0.735	0.803	0.453
5C	8.05	2.604	5.027	1.0	0.761	0.456	0.232

* ionic strength was 0.1 eq/kg

The growth rates in the presence of Mg^{2+} shown in Table 7.3 were obtained by the measurements of crystal edge length changes as a function of time. However, as the crystal shape changes the crystal growth rate cannot be determined directly from the measurement of the edge length increase rate. The crystal shape change, however, will not affect the layer growth rate significantly as long as the rate is determined from the surfaces with an equilibrium structure or shape. If the growth rate is for the prediction of calcium carbonate scale, the layer growth rate on the equilibrium shaped surfaces is more convenient to use. The growth rate of the equilibrium shaped surfaces can be calculated by the crystal geometry shape. Figure 7.5 shows a 2D diagram of a crystal with an initial rhombohedral shape changing to a trapezium shape.

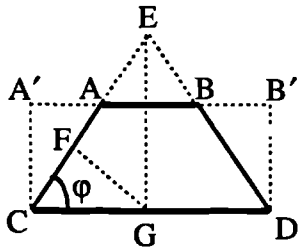

Figure 7.5 A 2-D model to illustrate how to determine a crystal growth rate when a crystal shape changes from a rhombohedral to a trapezium.

The lines *AC* and *BD*, *A'C* and *B'D* represent the equilibrium surfaces of a crystal before and after the crystal shape change due to Mg^{2+} influences. The growth rate of the surface *A'C* can be directly determined from the increase of the crystal length *CG* as a function of time *(CG = 0.5 CD)*. The layer growth rate of the surface in *AC* equals the length *FG*. If we measure the length of *CD* and the angle φ, the layer growth rate on the surface *AC* can be obtained and is equal to $0.5CD \times sin\varphi$. It is clear that the smaller the angle β, the lower the surface *AC* layer growth rate will be. There may be a relationship between the angle φ and the amount of Mg^{2+} incorporated into the surface.

The calcite growth rates at $[Mg^{2+}]/[Ca^{2+}]$ ratios below 0.5 can be estimated as *52%* ($\varphi=60^{o}$) of the growth rate without Mg^{2+} present. The effect of temperature on the calcite growth rate constant can be evaluated by equation 6.6 which was obtained from solutions with 0.1eq/kg ionic strength. To estimate any ionic strength effect, the rate constant as a function of ionic strength obtained at $25^{o}C$ (equation 6.7) can be used if we assume that at other temperatures the rate constant changes as ionic strength in the same way as the tendency at 25°C. The rate constant at different temperatures and ionic strengths with the presence of Mg^{2+} up to $[Mg^{2+}]/[Ca^{2+}]$ ratios of 0.5 can be obtained from:

$$k_{p(T.IS)} = 0.52 k_{p(T)} \frac{k_{p(IS)}}{k_{p(IS=0.1)}} \quad , \tag{7.1}$$

where $k_{p(T)}$ and $k_{p(IS)}$ are the rate constant at different temperatures (equation 6.6) and ionic strengths (equation 6.7). From equation 7.1 we have:

$$\log k_{p(T.IS)} = \log 0.52 + \log k_{p(T)} + \log k_{p(IS)} - \log k_{p(IS=0.1)} \quad . \tag{7.2}$$

From equation 6.6 we can obtain the rate constant at 25°C and IS = 0.1eq/kg as:

$$\log k_{p(IS=0.1)} = 0.0397 - 10.15 \quad .$$

Therefore, the rate constants at different temperatures, ionic strengths and at $[Mg^{2+}]/[Ca^{2+}]$ ratios below 0.5 is then given by equations 7.2, 6.6 and 6.7,

$$logk_{p(T.IS)} = 0.1257(IS)^{0.5} - 2504/T - 2.03 . \quad (7.3)$$

7.2.4 Prediction of the influences of other ions on the calcite growth rate

There have been many reports that other ions with similar size and electric charge as Ca^{2+} or CO_3^{2-}, such as Mn^{2+}, Ba^{2+}, Sr^{2+}, Fe^{2+} and SO_4^{2-}, have an influence on calcite growth (Dromgoole and Walter, 1990; Mucci and Morse, 1983; Morse and Mackenzie, 1990; Reeder and Grams, 1987 and Staudt et al, 1994). The theory for Mg^{2+} influencing calcite growth can be applied to the inhibiting effect of these cations. For example Mn^{2+} *(0.80Å)* and Fe^{2+} *(0.80Å)* are also smaller than Ca^{2+} ions (Evans, 1966), and may also be incorporated into the calcite crystals to reduce the calcite growth rate. It is very interesting to note that the density of Mn^{2+} and Fe^{2+} on the S faces was also higher than on the F faces. Therefore we can expect a similar morphology change due to the presence of Mn^{2+} and Fe^{2+} in a solution. On the other hand, cations larger than Ca^{2+}, such as Sr^{2+} (1.13 Å) or Ba^{2+} (1.15 Å) (Evans, 1966), can also be incorporated into calcite structure and which also affect the calcite growth kinetics (Reeder and Grams, 1987, Staudt et al., 1994 and Paquette and Reeder, 1995). However, the density of these larger ions on the S faces is lower than on the F faces. The study by Staudt et al., (1994) suggested that the geometric sizes of the kink sites are slightly smaller on the S faces than on the F faces, so we can understand why the ions smaller than Ca^{2+} are always enriched on the S faces whereas the larger ions are enriched on the F faces.

By the same principle of cation incorporation in calcite structure, the anions with similar electric charge and size as CO_3^{2-}, such as SO_4^{2-}, PO_4^{3-} and SeO_4^{2-}, may also be able to be incorporated into the calcite structure at the CO_3^{2-} sites and influence the calcite growth (House, 1987 and Staudt et al., 1994). They may also change the shape of the crystal because of the ionic size difference (House, 1989).

The knowledge of the influence of such foreign ions on crystal growth kinetics can help us to find new ways to solve calcium carbonate scale problems. For example, new scale

inhibitors can be formulated using chemicals with functional groups which can be incorporated into the calcite crystal, such as SO_4^{2-}, PO_4^{3-} and SeO_4^{2-}, and especially the chemicals with a high molecular weight and/or multiple functional groups, because a chemical with a high molecular weight has relatively low solubility and high adsorption potential (Breen et al., 1990). Multiple functional groups will increase the strength of the attachment on the crystal surface. It is already well known that many high efficiency scale inhibitors are made from polyphosphate (with $-PO_4^{3-}$ functional groups). We suggest that some alkyl sulphanates, which are also common surfactants in our daily life may be good scale inhibitors, because these chemicals contain functional groups with $-SO_3^-$. It has also been found that SO_4^{2-} ions show a strong inhibiting effect on the calcite growth rate (Staudt et al., 1994). If SO_4^{2-} ions are connected by a long chain hydrocarbon (such as R^+-SO_3^-), their efficiency in reducing calcite scaling should be much higher than simple SO_4^{2-} ions.

In most oilfield formation waters, the calcite scaling rate may be estimated accurately if the most important items, such as temperature, Mg^{2+} and ionic strength are considered. For example we can use the kinetic data obtained from simple water systems to estimate the calcite growth rate for a formation water with compositions similar to that listed in Table 7.2 and only consider the influences of alkalinity (section 6.2.3) and Mg^{2+} (section 7.2.1). As the ratio of $[Mg^{2+}]/[Ca^{2+}]$ in the solution No.24 is close to that of No.19 in Table 7.1 ($[Mg^{2+}]/[Ca^{2+}]$ = 0.5) and the alkalinity is close to No.8 in Table 6.4 ($[Ca^{2+}]/Alk$ ratio = 20), the reaction order for water sample of No.24 close to 3 can be expected. As the pH-free-drift method was used for the rate measurement in experimental No.24, the rate constant should be further reduced from the rate constant of No.19 by 56% due to the low alkalinity. The estimated rate constant for No.24 will be 0.269 (mmol/h.m^2) which is very close to the value obtained from our experiment. This comparison suggests that, at the concentration range of this oilfield formation water sample, the influence of natural inhibitors, such as organic acids, Ba^{2+}, Sr^{2+}, and SO_4^{2}, PO_4^{3}, on calcite growth rate is not significant. However the influence of Fe^{2+} Mn^{2+} ions may not be reflected in this case because of dissolved oxygen in the sample, which will be discussed later in section 7.4.

7.3 The inhibitors for preventing $CaCO_3$ scaling

The most widely used method to solve scaling problems today is to inject (i.e. squeeze) scale inhibitors into the formation to prevent (or slow down) the crystal nucleation and growth of the scale (Browning and Fogler, 1993; Lejon and Vikane, 1996; Powell et al, 1995 and Sweeney and Cooper, 1993). In a typical squeeze treatment, a slug of scale inhibitor, along with a brine overflush, is injected into a reservoir where it is shut-in for about twenty-four hours. During the shut-in period, the inhibitor is kept in the formation by: (1) being adsorbed onto the rock surface of the formation; and (2) being precipitated by available cations in the reservoir system. After the shut-in period, production is resumed and the inhibitor is slowly released back into the produced fluid where it is able to prevent scale forming on the tubing and other equipment surfaces. The lifetime of each treatment ranges from three to six months if the inhibitors act by an adsorption mechanism, but may last for as long as two years if the inhibitors act in a precipitation mechanism (Oddo et al., 1993 and Tomson et al., 1990).

The scale inhibitors are usually classified into three groups according to their chemical composition: phosphonates, phosphoric acid esters and polymers such as polyacrylic acid (Crowe et al, 1994 and Momozaki et al, 1992). The functional group groups of an inhibitor molecule are the parts which react with other chemicals. The functional group of the phosphonate inhibitors and phosphoric acid esters is $-PO_3^{2-}$ and the functional group of polyacrylic acid inhibitors is $-CO_2^-$. The mechanisms of these inhibiting chemicals on carbonate scale growth is probably due to the functional groups of the inhibitors being absorbed onto the calcite surface or incorporated into the calcite lattices at the CO_3^{2-} sites.

There are three main factors which can affect the efficiency of any inhibitor's activity:

- solution pH,
- the number of functional groups in the molecule,
- the molecular weight of the inhibitor molecule.

Because the active parts of an inhibitor are the anion form of the functional groups, it is obvious that a high pH (e.g.7) is more favourable for it to be active (Sorbie and Jiang et al., 1993; Sorbie and Yuan et al., 1993 and Sweeney and Cooper, 1993). If the solution pH is below the acid dissociation constant (pK_a) of these inhibitors by one pH unit, 90% of the functional group exists in the form of its acids (i.e. H_nPhn where Ph^{n-} is the functional group of the inhibitor molecule, subscript n is the number of hydrogen ions), and the efficiency of inhibition scaling will be very low, this is why many scale inhibitors do not work very well at a low pH (e.g. < 4.5). When a functional group has multiple levels of association, such as phosphonate, the dissociation of each proton requires a different pH. Therefore, phosphonate chemicals can be used over a wide range of solution pHs.

Multiple functional groups provide multiple contact points with solid surfaces, and as a result the strength and efficiency of adsorption onto the crystal surfaces are high. An inhibitor with a high molecular weight gives a high adsorption potential on a solid surface, however if the molecular weight is too high, its solubility is so small that its adsorption onto the formation rock can be irreversible and/or the required lowest efficient concentration cannot be achieved (Breen et al., 1990 and Tomson et al., 1990). If the inhibitor works by the adsorption mechanism during the squeeze treatment, this irreversible adsorption will influence its efficiency. To optimise the molecular weight and the numbers of functional groups of a scale inhibitor, both the processes of inhibition of the scale and the squeeze treatment have to be considered.

Phosphonate inhibitors are one of the most commonly used inhibitors in the field today. It has been found that the advantages of phosphonate inhibitors include:

- inhibit scale at low concentrations;
- stable over a wide range of temperatures and pH values. Hence they will be able to inhibit scale in many reservoirs at different conditions;
- can inhibit many different types of scale, making them flexible to use;

- the concentration of phosphonates in the produced fluid can be readily determined by oxidation and calorimetric techniques, hence it is easy to determined when a formation needs to be squeezed.

The molecular structures of two phosphonate inhibitors are shown in Figure 7.6.

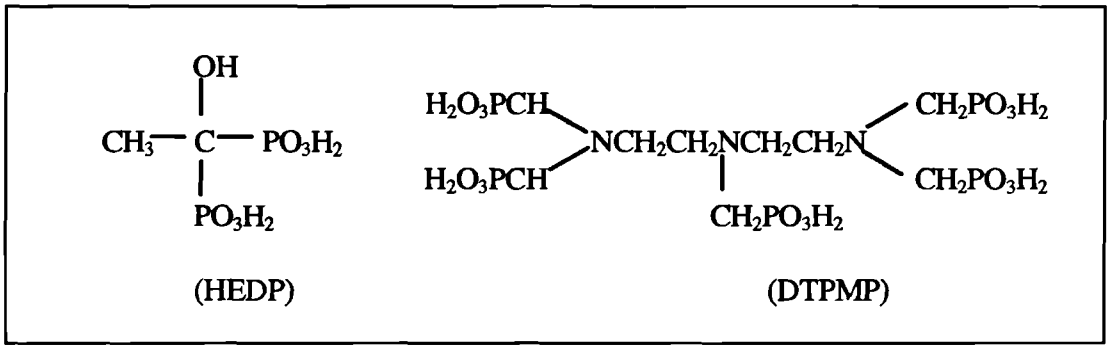

Figure 7.6 Molecular structures of common Phosphonates, HEDP, 1-Hydroxyethylidene-1,1-diphosphonic acid and DTPMP, Diethylenetriaminepenta (methylenephosphonic acid).

Both HEDP and DTPMP inhibitors work by precipitation mechanisms, i.e. they can form a precipitate with divalent metal ions in formation waters, mainly Ca^{2+}, and will be slowly released during oil and water production. The required concentration of inhibitor for efficient inhibition at 25°C is about 10^{-7}mol/kg. The solubility of their calcium salts decreases with increasing temperature. The inhibitor with a high molecular weight (DTPMP) is recommended for use at low temperature (e.g. < 100°C), otherwise, low molecular chemicals can give higher efficiency for the formations with high temperatures.

7.4 The influence of organic acids and oxygen on the calcite growth rate

The influence of short chain carboxylic acids on the calcite growth rate has also been examined by the pH-free-drift method. The carboxylic acids used in the experiments were a mixture of 50% (mole) acetic acid, 25% propionic acid and 25% butyric acid. Furthermore, it is very unlikely that any dissolved oxygen is present in oilfield formation waters, but the solutions prepared in a laboratory usually contain some oxygen unless very special treatments are involved. Therefore it is necessary to know whether dissolved oxygen affects the calcite growth rate. Thus some of our calcite growth experiments

were conducted using solutions with and without oxygen. Dissolved oxygen in the solution was removed by bubbling nitrogen gas into the solution. The results are listed in Table 7.4.

Table 7.4 The influence of organic acids and oxygen on calcite growth rate

No	pH_t	Other ions (mmol/kg)	Alk_C[2] (meq/kg)	$[Ca^{2+}]$ (mmol/kg)	SI	k_p $R_m = k_p(S^{0.5} - 1)^n$	n
1	7.86	$[A^-]$[1] = 5.0	11.2	5.59	0.863	0.654	1.94
2	7.80	no oxygen	11.6	5.82	0.900	0.678	1.86
3	7.75		10.6	5.52	0.795	0.764	1.86

(1) the concentration of the mixed organic acids (50% acetic acid, 25% propionic acid and 25% butyric acid)

(2) Alk_C is carbonate alkalinity.

As we can see from Table 7.4 the short chain carboxylic acids and dissolved oxygen do not appear to affect the calcite growth rate significantly. Normally the presence of oxygen in aquatic solutions is influenced by the chemical reactions involved in oxidation and reduction. Therefore oxygen should not affect the reaction of calcite precipitation. However, if a solution contains iron (Fe^{2+}) or Mn^{2+} at concentrations above 5 and 10ppm, respectively, the calcite growth rate can be reduced by as much as a factor of 10 (Dromgoole and Walter, 1990, Katz et al, 1993) In an anoxic environment, Fe^{2+} and Mn^{2+} may reach such concentrations, especially at low pH (<5), however under an oxygenated environment, the concentrations of Fe^{2+} and Mn^{2+} are normally so low (<1ppm) that their influence on the calcite growth rate can be neglected. Oilfield reservoirs are normally anoxic environments so that if the formation water contains more than 5 ppm Fe^{2+}, the calcite scaling rate can be expected to be much lower than the calculated values using a model that does not consider the inhabiting effect of Fe^{2+}.

There are many reports about the influence of organic acids on calcite growth rate (Amjad, 1988, Compton et. al., 1989; Barwise et al., 1990; Giannimaras and Koutsoukos, 1988; Inskeep and Bloom, 1986; Kharaka et al., 1986; Lebron and Suarez, 1996; MacGowan et al., 1990 and Zullig and Morse, 1988). Most of the organic acids

which show such influences on calcite growth rate are those with larger molecular weight (e.g. C_{12+}) and one or more functional groups of *-COOH*. For example, Amjad (1988) found that the addition of benzenepolycarboxylic acid has a striking inhibitory effect upon the rate of crystal growth of calcium carbonate. These results showed that at a concentration 4.88 $x10^{-6}$ mol/l of benzenepolycarboxylic acids, the rate of $CaCO_3$ growth was reduced by a factor of 10. Compton et al. (1989) studied the effect of maleic and fumaric acids on the dissolution of calcite in aqueous solution. They noticed that although these carboxylic acids have the same molecular formula of $(CH_2)_2(COOH)_2$, only maleic acid has an influence on calcite dissolution. This is because of the molecular structure difference where the functional groups (*-COOH*) of maleic acid are on the same side of the hydrocarbon chain so giving a better attachment at the scale crystal surfaces. The mechanism of these organic acids acting as inhibitors is that they can adsorb onto the calcite surface at the active sites, such as kink sites, and slow down or even stop lattice ions being incorporated into the active sites. Furthermore, these larger molecules can prevent lattice ions forming on the crystal surface and so prevent large crystal being formed. However, most of the organic acids found in oilfield formation waters are short chain carboxylic acids (C_1 - C_4) with only one functional group and with acetic acid dominating (Barth, 1987, 1991). These carboxylic acid anions can act as complexes to reduce the concentration of Ca^{2+} ions when the acid concentration is comparable with the concentration of Ca^{2+} ions, so that the saturation index of $CaCO_3$ can be reduced. Table 7.5 gives calcite saturation indexes of supersaturated solutions with different amounts of added acetic acid.

Table 7.5 The calcite supersaturation influenced by the presence of acetic acid

No	$[HAc]_T$ (mol/kg)	SI	PPT (mol/kg)
1	0	0.686	0.0131
2	0.003	0.660	0.0126
3	0.03	0.641	0.0127
4	0.3	0.338	0.0083

($[Ca^{2+}]$ = 0.03mol/kg, $[HCO_3]$ = 0.06mol/kg, $[NaCl]$ = 0.1mol/kg and pH = 6.0 at 25 C).

As we can see when the concentration of acetic acid is 10 times higher than the concentration of Ca^{2+} ions, the influence of acetic acid on the saturation indexes by the formation of complexes with Ca^{2+} ions becomes significant (No 4 in Table 7.5)

Compared with phosphonate, it appears that carboxylate is a weak functional group. Because its electric charge is one, its adsorption potential on the crystal surface will be lower than for phosphonate. Increasing the number of functional groups may help increase the adsorption potential. That is why butyric acid ($CH_3CH_2CH_2COOH$) at a concentration of 10^{-3}mol/kg does not show any inhibiting effect whereas maleic acid does at concentrations as low as 10^{-6} mol/kg (Compton et al., 1989). Maleic acid ($(CH_2COOH)_2$) has two functional groups, and both of them are on the same side of the carbon hydrogen chain which can provide a more efficient static contact with the solid surface.

7.5 Conclusions

The most important effect of Mg^{2+} on the calcite growth is that Mg^{2+} can be incorporated into the calcite structure and reduce the calcite growth rate. However the Mg^{2+} distribution on the calcite surfaces is not uniform. There is a higher Mg^{2+} density on the S faces than on the F faces of the calcite crystals, which causes the calcite structure to change. Therefore, when pure calcite seeds are used for conducting experiments to examine the influence of Mg^{2+} on calcite growth, the crystal structure will gradually change from a regular rhombohedral to other morphologies, such as the ones shown in Figure 7.2 crystals Nos. 2 and 3. During the crystal shape change, the Mg^{2+} density on the crystal surface is not uniform. This is probably the main cause of the variations in the determination of the amount of Mg^{2+} ion incorporation from laboratory experiments. Because the calcite growth rate is proportional to the amount of Mg^{2+} incorporated into the crystal surface, the growth rate determined by using pure calcite seeds cannot be stable during the initial stages of growth. For the same reason, the calcite growth rate in the presence of Mg^{2+} or other inhibitors cannot be accurately determined by the pH-free-drift method, but a steady state method similar to the visual observation method described earlier could be more reliable.

The mechanism of scale inhibitors slow down scaling rate is that their function growth(s) can absorb or incorporated into the scale crystal structure to change the surface energy of the crystals. The results from the study of inhibitor ions can help us to optimise more efficient scaling inhibitors. Our study also shows that short chain carboxylic acids (C_2 - C_4) and oxygen do not affect calcite growth rate significantly.

CHAPTER 8

APPLICATIONS IN PREDICTION OF FIELD CALCIUM CARBONATE PRECIPITATION

8.1 Introduction

The kinetic model developed in this study allows us to predict the $CaCO_3$ scale deposition profile from the bottomhole to the surface. However the kinetic model requires the temperature and pressure profile as well as CO_2 partial pressure profile from the wellbore to the well-head or surface facility. The thermodynamic saturation index along the tubing has to be calculated correctly, including the brine pH, the concentrations of the major CO_2 species and Ca^{2+} ions change during the precipitation (Vetter, 1980, 1987). In addition, the critical saturation index for spontaneous precipitation has also to be known. The aim of this chapter is to apply our kinetic model to predict oilfield $CaCO_3$ scaling for an oilfield production system. In addition, mathematical models for the calculations of the $CaCO_3$ scale profile along an oilfield production well are given. Finally the kinetic model developed in Chapters 6 and 7 is tested for two field $CaCO_3$ precipitation cases.

8.2 Prediction of $CaCO_3$ scaling under the oilfield downhole conditions

The calcium carbonate scaling rate under downhole oilfield conditions can be predicted using the kinetic model developed in this study. At least four important aspects have to be considered for any prediction:

1. where the scaling will start,
2. what is the mineralogy of the scale,
3. the physical properties, and
4. the scaling rate along the water path.

8.2.1 Where the scaling will start

It is obvious that calcium carbonate scaling will start from where the nucleation begins and crystals adhere onto the surface. When the reservoir rock contains limestone ($CaCO_3$) or has calcium carbonate cement, the formation water is normally saturated with $CaCO_3$ under formation conditions and no precipitation will occur. As the water flows upwards inside a production well, the pressure and temperature fall, but no significant calcium carbonate precipitation will occur either before any degassing occurs because the solubility of calcium carbonate increases with a lowering of temperature and the influence of pressure on the solubility is very small when there is no gas phase present (i.e. when the pressure is above the bubble point).

When the pressure falls to below the bubble point, a gas phase starts to appear, so that some of the dissolved CO_2 will escape from both water and oil to the gas phase. This will cause the water pH to rise and the supersaturation of calcium carbonate to increase. However from the kinetic point of view, a certain level of supersaturation must be exceeded to start spontaneous nucleation. In this study, the saturation index corresponding to the supersaturation level above which spontaneous precipitation occurs is defined as the critical saturation index. Thus only when both the thermodynamic and the kinetic conditions have been satisfied, can scale formation occur. According to our experimental results in Chapter 5, a critical saturation index for starting a spontaneous $CaCO_3$ precipitation under 70°C can be estimated from equation 2.46. When the temperature is above 70°C, the critical saturation index can be considered as zero, i.e. the $CaCO_3$ precipitation will start as long as the brine is supersaturated.

The determination of the critical supersaturation level for an oilfield flowing-water system is a difficult task, since many factors can influence the value, including temperature, pH, ionic strength, particle numbers in the water, natural inhibitor ions (e.g. Mg^{2+}) and gas bubbles being released from the solution (Nancollas and Reddy, 1974). Nevertheless most of these factors cause the critical saturation to be *lower* than the values obtained from clean calcium carbonate supersaturated solutions from laboratory experiments. To form scale, the nuclei have to adhere to the surfaces (e.g. tubing surfaces). This is relatively easy if the surfaces are wetted by water, such as on iron and

steel surfaces (Guun, 1980), but it is more difficult for scale to adhere to non-wetting surfaces, e.g. plastic surfaces. Therefore the possible position for starting $CaCO_3$ nucleation on metal tubing surfaces should be where the total pressure is below the bubble point and the supersaturation is between 0 and the critical supersaturation value determined from laboratory experiments. The exact value of the in-situ critical saturation index can be determined from a small scale laboratory simulator using the formation water under oilfield downhole conditions. If the temperature is 70°C or above, heterogeneous nucleation will be dominant when water is supersaturated with calcite and the scaling should therefore also start there.

8.2.2 Mineralogy of the $CaCO_3$ scale

According to our experimental results, aragonite normally forms at temperatures above 70°C and when the supersaturation is above the critical supersaturation values for calcite homogeneous nucleation. In general, when the aragonite growth rate is comparable to the calcite growth rate, aragonite can be seen from $CaCO_3$ nucleation. However when the temperature is above 70°C, heterogeneous nucleation will start as long as the solution is supersaturated with calcite. The mineralogy of the nuclei will be only calcite because when the calcite becomes supersaturated the aragonite will still be undersaturated. Calcite nucleation will be followed by crystal growth immediately after the nucleation, so that the concentration of scaling ions will be reduced and a high saturation for aragonite (i.e. above the critical value) is then unlikely. Therefore the dominant $CaCO_3$ scale will be calcite. As Mg^{2+} ions are present in all oilfield formation waters and reduce the growth rate of calcite and not aragonite, the critical saturation index and temperature to obtain aragonite will be lower for solutions containing Mg^{2+} than those without Mg^{2+}.

8.2.3 The calculation of the physical properties along the well

When oilfield formation fluids (water, oil and/or gas) are produced from the reservoir to the surface, the temperature and pressure will decrease. As the calcite growth rate is strongly influenced by temperature and the saturation index of calcite is a function of pCO_2, which is a function of total pressure, the correct temperature and pressure are essential to obtain a correct estimate of $CaCO_3$ precipitation and scaling rate under downhole conditions, i.e. we have to know:

$$T = f_T(x), \tag{8.1}$$

$$p = f_P(x) \tag{8.2}$$

where f_T and f_p are the functions for calculating the temperatures and pressures at the different positions up the tubing, and x refers to the position inside the tubing where the brine composition, temperature and pressure are being calculated. From functions 8.1 and 8.2, the CO_2 partial pressure can be obtained from,

$$pCO_2 = f_g X_{CO2} p_{total} \tag{8.3}$$

Both f_g and X_{CO2} are functions of pressure and temperature. The CO_2 in the gas phase comes from both water and oil, but as the solubility of CO_2 gas in oil is higher than in water (Oddo and Tomson, 1994), the CO2 partial pressure X_{CO2} will be also influenced by WOR (the ratio of water and oil) and the gas liquid ratio under downhole conditions. According to Oddo and Tomson (1994), f_g and X_{CO2} under oilfield downhole conditions can be calculated by

$$f_g = \exp\left(p(2.84\times10^{-4} - \frac{0.255}{T+460})\right) \tag{8.4}$$

$$X^x_{CO_2} = X^o_{CO_2} \Big/ \left(1.0 + \frac{pf_g(5.0BWPD + 10.0BOPD)\times10^{-5}}{MMscf(T+460)}\right) \tag{8.5}$$

where T = temperature (°F), p = pressure (psi), $X^x_{CO_2}$ and $X^o_{CO_2}$ are the mole fractions of CO_2 at the position x and at the surface at standard conditions, BWPD and BOPD are water and oil production rate (barrels per day), and MMscf is the total gas production rate (million standard cubic feet per day). Once the pCO_2 as a function of tubing position is obtained, the solution pH along the tubing can be then calculated from pCO_2 and alkalinity at the position x using equations 2.3 to 2.12.

8.2.4 The scaling rate along the water flowing path.

The overall $CaCO_3$ scaling rate along the tubing surface should be the total amount of precipitate divided by the total time, including the time for the nucleation and growth. The homogeneous nucleation time depends on the supersaturation level, but the rate of heterogeneous nucleation time depends on the amount of suspended particles in the water. Nevertheless, because the time for nucleation is much shorter, it can usually be neglected. The water flowing velocity inside a tubing is normally much higher than the critical value obtained from our study (about 2.8 m/min). For example, in the test case used later in this Chapter, the flowing velocity was about 65 m/min (1600 m^3/d in a 6 in tubing). Therefore the rate constant equation obtained from the flowing velocity above the critical value can be used directly. The influence of other inhibitor ions, such as Ba^{2+}, Sr^{2+}, Fe^{2+} and SO_4^{2-} has not been considered in this work, and can usually be neglected in most oilfield carbonate scaling cases because their inhibiting effect on calcite growth is similar to Mg^{2+}, and depends on their concentration ratio to Ca^{2+} or CO_3^{2-}, but the concentrations of these ions are very low compared with Ca^{2+} and/or total carbonate. Therefore the scaling rate for oilfield formation waters can be determined from the rate law and rate constant equation developed for calcite in this study with reasonable confidence.

The calculations of scaling rates at different positions in a tubing require the correct saturation indexes of calcite at any position along the tubing. Under downhole conditions there is CO_2 exchange between the gas phase and liquid phases when the pressure is below the bubble point, which means that the total carbonic acid in the water phase will not be constant, and will be influenced by the pCO_2 of the gas phase. The solution saturation index during the $CaCO_3$ precipitation cannot be calculated from the equations given in Chapter 4 because these equations are for a one-phase closed water system. For such a gas-water system, each mole of $CaCO_3$ precipitation from the water phase will result in one mole of Ca^{2+} reduction and two moles of alkalinity reduction, i.e.,

$$(C_{Ca^{2+}})_x = (C_{Ca^{2+}})_x - (PPT)_x \tag{8.6}$$

where subscript x is the values at the x position and $(PPT)_x$ is the total amount of $CaCO_3$ precipitated at the position x. If there is no organic acids present in the water, total carbonic acid, C_{T1}, at the x position can be calculated from:

$$(C_{T1})_x = \frac{(Alk_C)_t - 2(PPT)_x}{(a_1)_x + 2(a_2)_x} \tag{8.7}$$

Once the pCO_2 as a function of tubing position is obtained, the solution pH along the tubing (an open system) can be then calculated from pCO_2 and alkalinity at the position x by combining equations 8.7, 2.10 and 2.11,

$$Alk_T = \frac{K_1 K_H pCO_2}{C_{H^+}} + 2\frac{K_1 K_2 K_H pCO_2}{(C_{H^+})^2} + K_w / C_{H^+} - C_{H^+} \tag{8.8}$$

and solving the function 8.8. The concentration of free carbonate ion can be obtained from:

$$(C_{CO_3^{2-}})_x = (C_{T1})_x (\alpha_2)_x \tag{8.9}$$

The total amount of $CaCO_3$ precipitate on the tube, $(PPT)_x$, can be calculated from:

$$(PPT)_x = \frac{2\pi r_T \rho x (R_L)_x}{MQ} \tag{8.10}$$

where, r_T is the radius of the tubing (metre), ρ is the density of the scale (kg/m^3), M is the molecular weight of the scale component (kg/mol), Q is the water production rate (kg/s), $(R_L)_x$ is the calcite growth rate at the position x. It is obvious that $(PPT)_x$ cannot be calculated if $(R_L)_x$ is unknown. However if we split the well length into a number of small intervals in which the growth rate change is very small, the growth rate in the previous interval (i.e. $(R_L)_{x-1}$) can be used. The saturation index at any position in the tubing can then be calculated using equations 8.6 - 8.11,

$$SI = log\left(\frac{(C_{Ca^{2+}})_x(C_{CO_3^{2}})_x}{K'_{sp}}\right) \tag{8.11}$$

However, when the temperature is above 50°C and the ionic strength is high (e.g. > 1 mol/kg), corrections are needed to account for the ion pair constants. These have been discussed in detail in Chapter 7. As long as the saturation index as a function of the position can be obtained, the scaling rate can be calculated from the kinetic model developed in this study.

8.3 Field data comparison and applications

To validate the rate constants of calcite growth obtained in this study, a field scale case reported by Schmidt and Bentsen (1992) of Statoil has been used to examine our kinetic model. An oilwell stated to be in the Norwegian sector of the North Sea has been found to precipitate calcium carbonate scale (91.6% $CaCO_3$) in a 6 inch tubing such that 2.5 cm was precipitated just downstream of the choke in one year of production. This corresponds to a growth rate of 7.9×10^{-10} m/s. Table 8.1 lists the compositions of the oilfield formation water and some of the oilwell production parameters.

Table 8.1 The compositions of a oilfield formation water after Schmidt and Bentsen (1992).

Ions	mg/l
Ba^{2+}	41
Sr^{2+}	100
Ca^{2+}	720
Mg^{2+}	70
Cl^-	350
SO_4^{2-}	13
HCO_3	650
$HAc^{(1)}$	540

other parameters	
water cut	2 - 8 %
water production rate	130 m^3/day
temperature	85°C
bubble point pressure	68 bar
CO_2 mole fraction	0.0058
pH[2]	6.43
ionic strength[2]	0.405 eq/kg
saturation index[2]	0.582

[1] the total organic acids
[2] calculated using Solmineq88.

Many field scale cases show that most carbonate scaling starts after the liquid bubble point pressure has been reached, since the dissolved gases then start to come out of the liquid phases (oil and water) and the water pH starts to increase. Compared with the calcite saturation increase due to the temperature and pressure decrease along the tubing, the increase in calcite saturation due to the solution pH increase can be significant. In addition to this saturation increase, a gas phase can also help the nucleation and so start the scaling. Therefore we assume that the $CaCO_3$ scale starts at the liquid bubble point (68 Bar for the Norwegian field case) where the maximum supersaturation also occurs. For this field scaling case, a heterogeneous nucleation will occur as long as the brine is supersaturated with calcite because the temperature is above 70°C. The pCO_2 at the bubble point can be calculated from equation 8.3 which is about 0.31 bar. then the brine pH and saturation index can be calculated by Solmineq 88 and also listed in Table 8.1. For all the thermodynamic calculations, we also assumed that, the temperature from bubble point upwards is constant (average 80°C was used). The $CaCO_3$ scaling rate of this formation water estimated by our rate equation 7.1 is 9.05×10^{-10} m/s which is very close to the actual measured field scaling rate of 7.9×10^{-10} m/s. As the precipitation continues, $CaCO_3$ comes out of solution, the solution supersaturation decreases and the scaling rate will then reduce. Figure 8.1 shows the calculated brine pH and pCO_2 (equations 8.3, 8.4 and 8.5) at different positions inside the tubing.

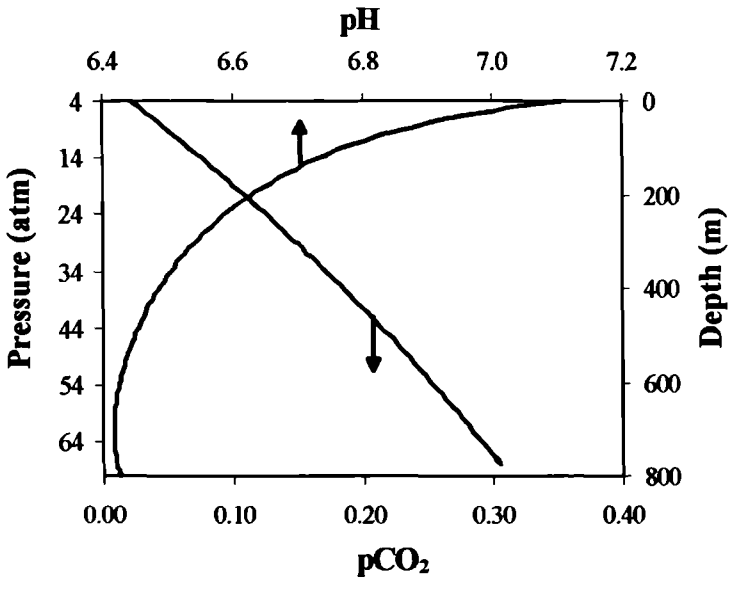

Figure 8.1 The pH and pCO_2 at different positions inside the tubing.

Figure 8.2 presents the calculated concentrations of Ca^{2+} (equation 8 6) and CO_3^{2-} (equation 8 9) as well as total carbonate C_{TI} (equation 8.7) in the brine at different positions inside the tubing. As we can see, when the brine is close to the surface the pH increases sharply. As the result of pH increase, the concentration of CO_3^{2-} also increases although the total carbonate C_{TI} decreases when the brine is close to the wellhead.

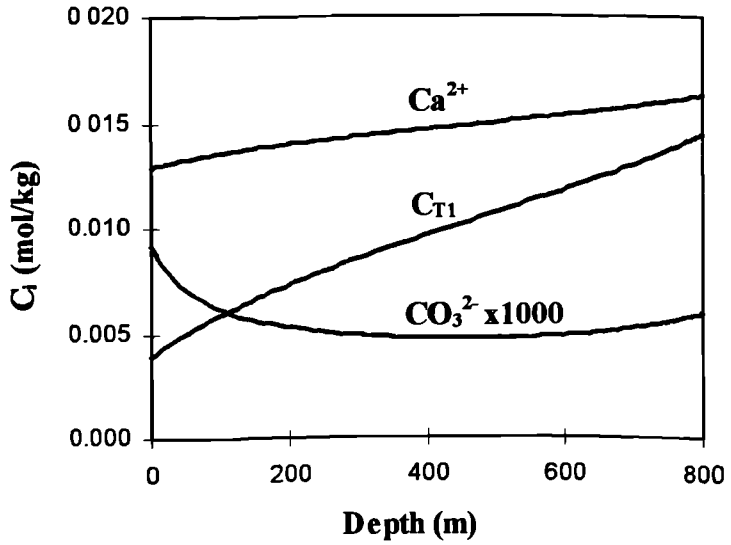

Figure 8.2 The concentrations of Ca^{2+} and CO_3^{2-} as well as the total carbonate C_{TI} in the brine at different positions inside the tubing.

Figure 8.3 shows the $CaCO_3$ scale deposit profile on the 6 inch tubing surface calculated by our kinetic model. The supersaturation index at different positions has been calculated from equations 8.6 - 8.11, and is plotted in Figure 8.3.

As we can see from Figure 8.3, the highest scaling rate predicted to be at where the degassing occurs and close to the wellhead. From this field case prediction we can note that although there are many other factors which can affect the precipitation of the $CaCO_3$ scaling rate onto the oilwell tubing surface, such as multi-phase flow (oil, gas and water), tubing surface properties, pressure, flowing velocity and the kinetics of CO_2 degassing and nucleation under oilfield downhole conditions, the scaling rate can be predicted with good accuracy by our calcite scaling kinetic model if the influences of temperature, Mg^{2+} and ionic strength are considered.

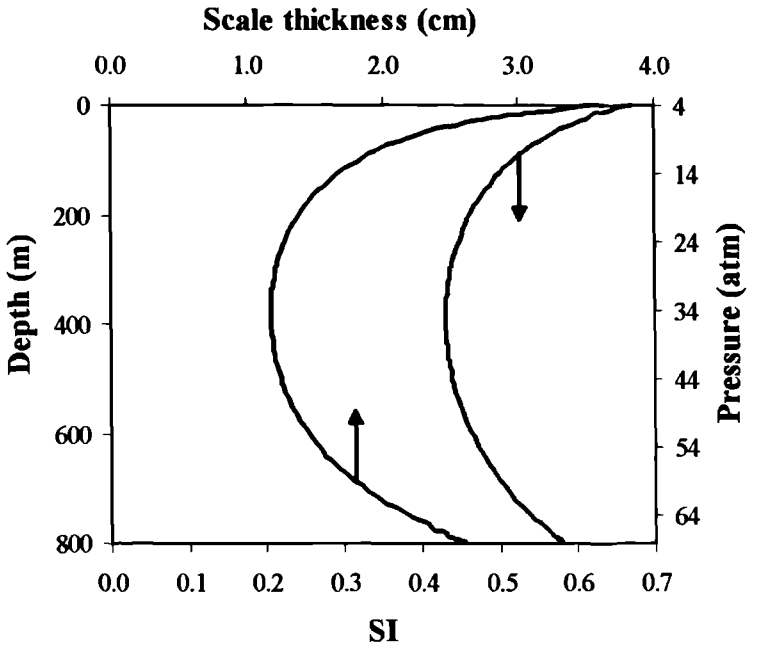

Figure 8.3 The $CaCO_3$ scale profile inside the tubing of a Statoil North Sea oilwell predicted by our kinetic model.

Two methods can be used to reduce the $CaCO_3$ scaling rate:

1. Injecting scale inhibitor to the position where the scaling started.

   For example concentric tubing (a capillary tube inside coiled tubing) has been used in many oilfields to inject scale inhibitor downhole (Brown et al., 1991 and Lovekin, 1990). It is shown that this technique is quite reliable and convenient in the treatment of $CaCO_3$ scaling. If the position where scale will start can be predicted accurately, more efficient treatments can be achieved.

2. Increasing wellhead pressure.

   From Figure 8.1 we can see that when the total pressure is below 30atm, the solution pH increases with decreasing pressure rapidly. Therefore we can expect that if we increase the pressure at the wellhead to above 30atm, the scaling rate can be significantly reduced. Figures 8.4 shows the scale disposition profile at a increased wellhead pressure.

As the result of increase wellhead pressure by 32 atmosphere, the scale will start from 400m and the total amount of precipitation will be reduced from 3.41mmol/kg (if the scaling profile likes shown in Figure 8.3) to 1.67mmol/kg. But the thickness of the scale at the bubble point will be almost the same (assumed that there is no temperature change). The limitation of controlling $CaCO_3$ scaling by increasing wellhead pressure is that the production rate will be affected.

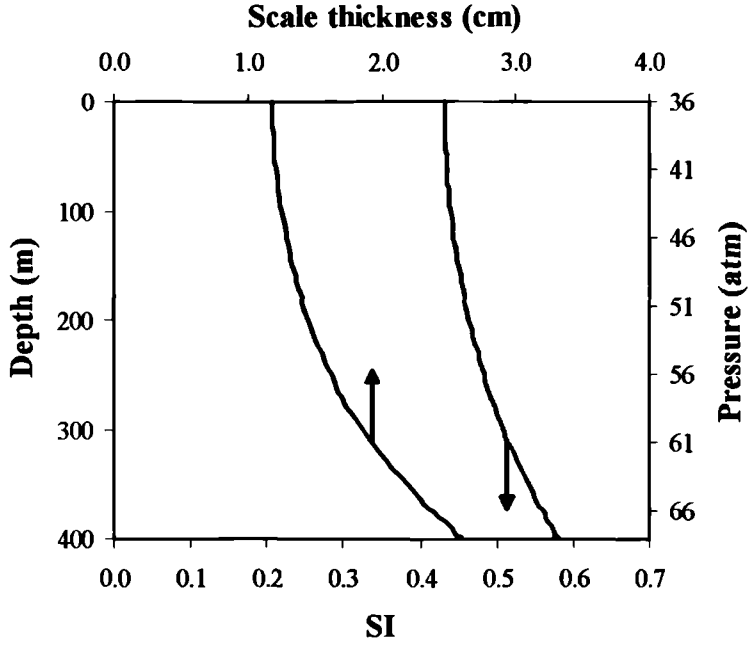

Figure 8.4 The $CaCO_3$ scale profile inside the tubing if we increase the wellhead pressure to 36 atm.

8.4 Summary

In this chapter, the kinetic model of $CaCO_3$ nucleation and precipitation has been used to predict where and how much $CaCO_3$ scale will be deposited in a production well. The mathematical models for the calculation of oilfield scaling profile inside tubing have been given. A field $CaCO_3$ precipitation cases has been used to test our kinetic model and good agreement with the field measurements has been achieved from these calculations.

CHAPTER 9

CONCLUSIONS AND SUGGESTIONS

In this chapter, the contributions from this study towards calcium carbonate scaling have been summarised, final conclusions have been drawn and some suggestions for further studies are presented.

9.1 Summaries of the most important results from this study

The most important contributions from this study can be summarised:

1. An analytical method to analyse both carbonate species and organic acids has been developed using acid titration by an automatic titrator and some mathematical data treatment (section 8.1.1).
2. Experimental methods developed during this study have demonstrated the thermodynamic and kinetics of $CaCO_3$ precipitation (8.1.2).
3. The critical saturation as well as the morphologies of $CaCO_3$ nucleation at different temperatures has been determined (8.1.3).
4. A kinetic model for the prediction of calcite precipitation and scaling from a water system with similar compositions as oilfield formation waters have been developed (8.1.4).
5. The understanding of the influences of Mg^{2+} ion incorporation and flowing velocity on calcite growth rate has been improved (8.1.5).

9.1.1 How to determine alkalinity when a solution contains organic acids

The determination of concentrations of carbonate species by acid titration in a water system containing organic acids has been always a problem. The conventional acid titration method using organic indicators fails because of the overlapping of the titration end points for bicarbonate and organic acid anions. In Chapter 3, a method has been developed to analysis carbonate species and organic acid anions from acid titration using an automatic titrator and simple calculations. Over a wide range of alkalinity, organic acid concentration and ionic strength, the $H_2CO_3^*$ EP (for the determination of

bicarbonate) can be identified directly by a titrator, and where: (a) the total alkalinity is from 0.006 to 0.02 mol/l; (b) the fractions of acetate in total weak acids (total carbonic acids pluses total organic acids) are from 0.3 to 0.7; (c) the solution ionic strength is less than 1.0 mol/l.

We have found that the titration end point pH is a function of the amount of the total organic acids in the solution, so that when the concentration of carbonate and organic acids is outside the direct measurement range and the $H_2CO_3^*$ EP cannot be identified during the titration, the concentration of total organic acids can be calculated from the titration end point pH (equation 3.14):

$$C_{T2} = \frac{(C_{H^+(e2)})^2}{K_a} + C_{H^+(e2)}$$

and the concentration of organic acid anion can be then calculated from equation 3.16:

$$C_{Ac} = \frac{C_{T2}}{1+10^{-pH_i}/10^{-pK_a}}$$

The alkalinity contributed from carbonate can be obtained from equation 3.17:

$$Alk_c = Alk_T - C_{Ac^-}$$

and the bicarbonate and acetate concentration of a solution can be calculated from the titration end point pH, the total alkalinity and solution ionic strength using the equations developed from this study with an error of less than ±5%.

9.1.2 The experimental technique for the study of the kinetics of calcite growth

Two experimental methods have been developed in Chapter 4 for the study of the kinetics of calcite growth: the pH-free-drift method and the visual observation method. These two methods emphasises different aspects of calcite growth. The pH-free-drift method can provide data for the kinetic model over a wide range of saturation states in a

closed water system. The calcite growth rate is determined by monitoring solution pH changes from the initial state to the equilibrium state in just single run. Therefore the calcite precipitation rate as a function of saturation can be determined with much better reproducibility than that from many single rate measurements at different saturation states. The visual observation method is suitable for the determination of a rate constant for $CaCO_3$ growth under steady state conditions and avoids the uncertainty from the determination of the seed surface area and the crystal surface property changes during the crystal growth. Therefore our two experimental methods can provide data at the different aspects of calcite precipitation, in order to obtain a more reliable kinetic model for the prediction of scaling tendency for the oilfield formation waters.

9.1.3 Spontaneous nucleation and the morphologies

In Chapter 5 we have demonstrated that when more than one form of $CaCO_3$ mineral is thermodynamically possible to be precipitated, the precipitate is not the one that is thermodynamically the most likely (high SI), but the one that has the fastest growth rate. At low temperatures (below 70°C) and low saturation index, the calcite growth rate is higher than aragonite. However as the temperature goes up, the increase in aragonite growth rate is larger than for the calcite growth rate because the activation energy for aragonite is higher than for calcite. When the temperature and saturation are above the critical value of spontaneous nucleation (70°C and calcite SI = 0.71 under our experimental condition) the aragonite growth rate becomes higher than that for calcite, and is the most probable scale mineral from the spontaneous nucleation. However calcite is the dominant scale mineral when the temperature is below 70°C, or the saturation index is below the critical value when the temperature is above 70°C.

Our study also demonstrated that at temperatures below 70°C, a minimum supersaturation (the critical saturation) has to be achieved to start $CaCO_3$ a spontaneous nucleation and then scaling, whereas at temperature above 70°C, the scaling will start by a heterogeneous nucleation as long as the solution is supersaturated with calcite.

Furthermore, if there are gas bubbles formed within a $CaCO_3$ supersaturated solutions, spontaneous nucleation can be stimulated and occur at a much lower supersaturation

than that from solutions without any gas bubble. This is the main reason why most oilfield $CaCO_3$ scale is found after dissolved gas has started to be evolved from the liquid phase. We suggest that the nucleation is due to gas bubbles which can lower the energy barrier required for calcium carbonate spontaneous nucleation.

9.1.4 Kinetic model for calcite growth

The calcite growth rates at different solution compositions, including alkalinity, pH, Mg^{2+} and ionic strength have been examined in Chapters 6 and 7. The experimental results show that the calcite growth rate is mainly controlled by the calcite supersaturation, ionic strength, the mole ratio of $[Mg^{2+}]/[Ca^{2+}]$ and temperature. The experimental results suggest that the calcite growth rate is also influenced by the mass transport rate, especially at low alkalinity and high pH (> 8). As the mass transport rate is proportional to the mass concentration, the concentration of one or both scaling ions can be very low at lower alkalinity (Alk << $[Ca^{2+}]$) and high pH (pH > 8). This is why the calcite growth rate changes with alkalinity and pH. In addition surface nucleation also contributed to the high calcite growth rate at low pH (< 7). The calcite growth rate constants were determined at flowing velocities above the critical value from which the rate constant does not increase with increasing flowing velocity. The influence of other inhibitor ions in formation water is usually very small compared to the influence of Mg^{2+} and can be neglected. A rate law for describing calcite growth rate has been developed for the rate data obtained from our pH-free-drift experiments over a wide range of saturation indexes.

$$R_L = k_p (S^{0.5} - 1)^2$$

An equation for calculating the rate constants at temperatures up to 70°C and ionic strengths up to 2 eq/kg has been developed, and the influence of Mg^{2+} at the mole ratio of $[Mg^{2+}]/[Ca^{2+}]$ less than 0.5 has been considered. The equation is (equation 7.3),

$$\log k_p = 0.1257(IS)^{0.5} - 2504/T - 2.03$$

This kinetic model has been tested for a oilfield $CaCO_3$ scaling case. The predicted precipitation rate is in good agreement with the measured scaling rate.

9.1.5 The influence of Mg^{2+} incorporation on calcite morphology and growth rate

The influence of Mg^{2+} on the calcite growth is that Mg^{2+} can be incorporated into the calcite crystal lattices at the Ca^{2+} sites and reduce the calcite growth rate as the result of change surface energy. However the Mg^{2+} distribution on the calcite seed is not uniform on each of the different faces. A higher Mg^{2+} density occurs on the S (step) faces than on the F (flat) faces of the calcite crystals. As the calcite growth rate reduction by the incorporation of Mg^{2+} is proportional to the Mg^{2+} density on the calcite surfaces, the S faces are gradually developed and the F faces eventually diminished. Therefore, when pure calcite seeds are used to examine the influences of Mg^{2+} on the calcite growth, the crystal structure will gradually change from a regular rhombohedral to other morphologies such as the ones shown in Figure 7.2 crystals Nos. 2 and 3. During the crystal shape change the Mg^{2+} density on the crystal surface is not uniform. When the growth rates are measured at the different stages of the morphology change, different growth rates will be obtained. This is the main reason why the amount of Mg^{2+} ion incorporation determined by different workers varies. We believe that once the crystal surface becomes equilibrated (most natural calcite surface should be), the crystal growth rate will become stable and the amount of Mg^{2+} incorporated determined at this stage will be uniform.

Nevertheless, the calcite growth rate constant in the presence of Mg^{2+} (or other inhibitors) cannot be determined by the pH-free-drift method even if the crystals have reached the equilibrium structure (or shape), because the total surface area of the crystal will have changed. The rate constant will be unreliable if obtained from seeds of surface area of uncertain. However, the rate constant can be determined more accurately using a steady state method similar to our visual observation method. The influence of Mg^{2+} on the calcite growth is a most important aspect of the kinetics of calcite growth. This data can also help us to understand how other inhibitor ions and scale inhibitors work and ultimately will help us to optimise scale inhibitors for oilfield use.

9.2 Conclusions

The following conclusions can be drawn from this study:

1. Both carbonate species and organic acids within the same solution can be simply analysed from an acid titration by an automatic titrator, although some calculations for total alkalinity and the titration end point pH are sometimes needed to obtained the individual concentrations of bicarbonate and organic acids.
2. The experimental design for the study of the kinetics of calcite precipitation by the pH-free-drift method developed in this study is especially suitable for the determination of the reaction rate law over a wide range of solution compositions. The visual observation method makes it possible to determine rate constants at different temperatures and water flow velocities.
3. Spontaneous nucleation of $CaCO_3$ is assisted by the presence of gas-liquid interfaces. This is one of the main reasons why most oilfield $CaCO_3$ scaling occurs after the pressure drops to below the bubble point and the dissolved gas starts leaving the liquid phase. The gas bubbles generated from a calcite supersaturated solution may lower the energy barrier required for the spontaneous nucleation of calcium carbonate.
4. A kinetic model for the prediction of scaling of calcite has been developed from this study. The calcium carbonate scaling rate at different temperatures and ionic strengths at oilfield $[Mg^{2+}]/[Ca^{2+}]$ ratios can be described by the Davies and Jones rate equation. The calcite precipitation rates calculated from our kinetic model: $\log k_p = 0.1257(IS)^{0.5} - 2504/T - 2.03$, appear to be in very good agreement with the reported data from field calcite precipitation cases.
5. Calcite growth rate follows a combined mechanism of both transport and surface reaction controlled, since the calcite growth rate is significantly influenced by the mass transport rate. The results that the calcite growth rates depend on a solution alkalinity and pH is mainly caused by the system transport rate difference.
6. The Mg^{2+} ions affect the calcite growth in two ways: reducing calcite growth rate and changing the morphology of calcite growth. The distribution of Mg^{2+} ions on the calcite surfaces is not stable at the initial stage of calcite growth when calcite seeds are used. If the initial growth rate determined from monitoring the bulk solution

property changes is used to examine the influence of Mg^{2+} ions on the calcite growth, unstable rate data will be obtained and will depend on the experimental conditions.

7. The mineralogy of calcium carbonate scale is calcite dominant when oilfield downhole temperature is below 70°C. At the temperature above 70°C, aragonite is possible if the saturation index is high (e.g. $SI > SI_{crit}$).

9.3 Suggestions for Further Work

The kinetics of calcium carbonate precipitation is very important for determining not only where scaling will start, but also the mineralogy of the precipitation and how fast the scale will be built-up under oilfield downhole conditions. The results from this study were obtained from low pressure (1 atm) and low temperature (≤ 70°C). It will be more reliable if we can test the kinetic model at higher temperatures and pressures (similar to oilfield downhole condition). Reliable calculations for a water thermodynamic state are essential for reliable kinetic predictions. The thermodynamic calculations for a high temperature water system become unreliable because of limited thermodynamic data at high temperatures. It is necessary to expand the data base, especially for the complex constants of carbonate species.

9.3.1 The test of a kinetic model at higher temperatures and pressures

Temperature is the most sensitive parameter in the prediction of the calcite growth rate. According to equation 4.16, the calcite growth rate increases with temperature exponentially. Therefore a small laboratory simulation test at high temperatures and pressures will give us more confidence on how to deal with field scaling cases. The influence of Mg^{2+} on the calcite growth rate at high temperatures has been assumed to have the same tendency as at low temperatures. Some reports have shown that the amount of Mg^{2+} incorporated into the calcite crystal structure increases with increasing temperature. Because the reduction of calcite growth rate is proportional to the amount of Mg^{2+} incorporated into the calcite surface, the calcite growth rate is reduced by the presence of Mg^{2+} at high temperatures and will be higher than at low temperatures at the same water composition.

9.3.2 Expand the thermodynamic data at high temperatures

The solution pH is the key parameter for the thermodynamic calculations of a carbonate water system. It is difficult to directly measure the downhole water pH. The calculation of water pH requires the correct thermodynamic data for a high temperature water system, but most data needed for the carbonate water system are currently not available for high temperatures. Although the Pitzer equation does not require the complex constants, the activity coefficients of all species influenced by complexing have been included in the Pitzer interaction parameters. The complex constants are essential for determination of the Pitzer interaction parameters. Therefore to improve the reliability of the thermodynamic calculation for a carbonic-acid and water system, more high temperature thermodynamic data are needed.

9.3.3 Applications

This study has concentrated on the fundamental understanding of the thermodynamics and kinetics of $CaCO_3$ nucleation and crystal growth, especially the function of Mg^{2+} on calcite growth kinetics. This study can be the guide for the further studies of the kinetics of calcite growth at elevated temperatures. Nevertheless the results from this study will give a useful direction for the prediction of carbonate scaling and solving downhole carbonate scaling problem more efficiently, e.g. optimise the treatment of scale inhibiting. On a wider front, it will be also helpful for the study of the geochemistry of sedimentary carbonates, such as how to simulate the process of coprecipitation of Mg^{2+} with calcite under the natural marine conditions.

References

Adamson, A.W., (1990) Physical chemistry of surfaces, Fifth edition, John Wiley & Sons, Inc.

Akin G.W. and Lagerwerff J.V., (1965a) Calcium carbonate equilibria in aqueous solutions open to the air. I. The solubility of calcite in relation to ionic strength. *Geochimica et Cosmochimica Acta*, **29**, p. 343-352.

Akin G.W. and Lagerwerff J.V., (1965b) Calcium carbonate equilibria in aqueous solutions open to the air. II. Enhanced solubility of $CaCO_3$ in the presence of Mg^{2+} and SO_4^{2-}. *Geochimica et Cosmochimica Acta*, **29**, p. 353-360.

Amjad Z., (1987) Kinetic study of the seeded growth of calcium carbonate in the presence of benzenepolycarboxylic acids. *Langmuir*, **3**, p. 224-228.

Anonymous, (1997) FT North Sea Letter, Financial Time, July 23.

Appelo C.A.J. and Postma D., (1993) Geochemistry, Groundwater and Pollution, A.A Balkema / Rotterdam / Brookfield.

Arakaki T. and Mucci A., (1995) A continuous and mechanistic representation of calcite reaction-controlled kinetics in dilute solutions at 25°C and 1 atm total pressure. *Aquatic Geochemistry* **1**, p. 105-130.

Arnold E., et al., (1992) Standard Methods for the Examination of Water and Wastewater, Washington, D.C., American Public Health Association, p.467-468.

Barth T., (1987) Quantitative Determination of Volatile Carboxylic Acids in Formation Waters by Isotachophoresis. *Analytical Chemistry*, **59**, p. 2232-2237.

Barth T., (1991), Organic acids and inorganic ions in waters from petroleum reservoirs, Norwegian continental shelf: a multivariate statistical analysis and comparison with American reservoir formation waters. *Applied Geochemistry*, **6**, p. 1-15.

Barth T., (1992) Interactions between organic acid anions in formation waters and reservoir mineral phases. *Org. Geochem*, **19**, p. 455-482.

Barwise A.J., Compton R.G. and Unwin P.R., (1990) The effect of carboxylic acids on the dissolution of calcite in aqueous solution. *J. Chem. Soc. Faraday Trans*, **86**(1), p.137-144.

Bates R. G. (1964) Determination of pH - Theory and Practice, John Wiley & Sons, Inc. p. 123-124.

Beck J.W., Berndt M.E. and Seyfried W.E., (1992) Application of isotopic doping techniques to evaluation of reaction kinetics and fluid/mineral distribution coefficients: An experimental study of calcite at elevated temperatures and pressures. *Chemical Geology*, **97** p. 125 - 144.

Bennema P., (1967) Analysis of crystal growth models for slightly supersaturated solutions. *J. of Crystal Growth*, **1**, p. 278-286.

Berner R.A. and Morse J.W., (1974) Dissolution kinetics of calcium carbonate in seawater: IV. Theory of calcite dissolution. *Amer. J. Sci.*, **274**, p. 108-134.

Bischoff J.L. and Fyee W.S., (1968) Catalysis, inhibition, and the calcite-aragonite problem. 1. the aragonite-calcite transformation. *Amer. J. Sci.*, **266**, p. 65-79.

Breen P.J., Diel B.N. and Downs H.H., (1990) Correlation of scale inhibitor structure with adsorption thermodynamics and performance in inhibition of barium sulfate in low-pH environments. SPE, 20688, SPE Annual Technical Conference and Exhibition. Sep.

Brown A.D., Merrett S.J. and Putnam J.S., (1991), Coil-tubing milling/underreaming of barium sulphate scale and scale control in the forties field. SPE 23106, Offshore Eur 91, Sep.

Browning F.H. and Fogler H.S., (1993), Precipitation and dissolution of calcium phosphonates form the enhancement of squeeze lifetimes. SPE 25164, International Symposium on Oilfield Chemistry held in New Orleans, LA, USA Mar. 2-5.

Burton W.K., Cabrera N. and Frank F.C., (1951) The growth of crystals and the equilibrium structure of their surfaces. *Philos, Trans. Rol. Soc*, **243**, p. 299-358.

Christ C.L.; Hostetler P.B. and Siebert R.M. (1974) Solubility of calcite and aragonite. *J. Res. U.S. Geol. Survey*, **2**, p. 175-184.

Cicerone D.S., Regazzoni A.E. and Blesa M.A., (1992) Electrokinetic properties of the calcite/water interface in the presence of Magnesium and organic matter. *J of Colloid and Interface Science*, **154**, p. 423-433.

Compton R.G., Pritchard D.L. and Unwin P.R. (1989) The effect of carboxylic acids on the Dissolution of calcite in aqueous solution. Part I. Maleic and Fumaric acids. *J. Chem. Soc., Faraday Trans.* I, **85**, p. 4335-4366.

Compton R.G. and Unwin P.R. (1990) The dissolution of calcite in aqueous solution at pH < 4: kinetics and mechanism. *Phil. Trans. R. Soc. Lond.* **A 330**, p. 1-45.

Crowe C., McConnell S.B., Hinkel J.J. and Chapman K. (1994) Scale inhibition in wellbores, SPE 27996, The University of Tulsa Centennial Petroleum Engineering Symposium, Aug.

Davies C.W. and Jones A.L. (1955) The precipitation of silver chloride from aqueous solutions. Part 2 - Kinetics of growth of seed crystals. *Trans. Faraday*, **51**, p. 812-817.

Dawe R.A., (1990), Reservoir Physics at the Pore Scale, Seventy-five Years of Progress in Oil Field Science & Technology. Balkema, Rotterdam, p. 177-194.

Day J.R. Underwood A.L., (1991) Quantitative Analysis, 6th ed; Prentice Hall, New Jersey, p. 186.

Deer, W. A., Howie, R. A. and Zussman J., (1992) An introduction to the rock-forming minerals, 2nd ed, Harlow Longman. 2nd ed

Doerner H. A., and Hoskins W.M., (1925) The co-precipitation of radium and barium sulphates. *J of the American Chemical Society*, **47**, p. 662-675.

Dove P.M. and Hochella M.F., (1993) Calcite precipitation mechanisms and inhibition by orthophosphate: In situ observations by scanning force microscopy. *Geochimica et Cosmochimica Acta,* **57**, p. 705-714.

Dromgoole E.L. and Walter L.M., (1990a) Inhibition of calcite growth rates by Mn^{2+} in $CaCl_2$ solutions at 10, 25, and 50°C. *Geochimica et Cosmochimica Acta,* **54**, p. 2991-3000.

Dromgoole E.L. and Walter L.M., (1990b) Iron and manganese incorporation into calcite: Effects of growth kinetics, temperature and solution chemistry. *Chemical Geology*, **81**, p. 311-336.

Evans R., (1966) An introduction to crystal chemistry, Cambridge University press, p. 220-223.

Folk R.L., (1974) The natural history of crystalline calcium carbonate: Effect of magnesium content and salinity. *J. of Sedimentary Petrology*, **44**, p. 43-53

Galster H., (1991) pH Measurement - Fundamentals, Methods, Applications, Instrumentation. VCH.

Garrels R.M. and Thompson M.E. (1962) A chemical model for seawater at 25°C and one atmospheric pressure. *Amer. J. Sci.*, **260**, p. 57-68.

Garrels R.M., Thompson M.E. and Siever R., (1960) Stability of some carbonates at 25°C and one atmosphere total pressure. *Amer. J. Sci.*, **258**, p. 402-418.

Garrels R.M. and Wollast R., (1978) Discussion of: Equilibrium criteria for two-component solids reacting with fixed composition in an aqueous phase example: The magnisian calcites. *Amer. J. Sci.*, **278**, p. 1469-1474.

Garside J., (1977) Kinetics of crystallisation from solution. In Crystal Growth and Materials Kaldis E. and Scheel H.J. (Edi.) North-Holland, Amsterdam, p483 - 513.

George H and Nancollas, 1980, The formation of scales of calcium carbonate polymorphs. The influence of magnesium ion and inhibitors. SPE 8992, Oilfield Geothermal Chemistry, Stanford, California, May 28-30.

Giannimaras E.K. and Koutsoukos P.G., (1988) Precipitation of calcium carbonate in aqueous solutions in the presence of oxalate anions. *Langmuir*, **4**, p. 855-861.

Gill J.S. and Nancollas G.H., (1980) Kinetics of growth of calcium sulfate crystals at heated metal surfaces, *J. of Crystal Growth*, **48**, p. 34-40.

Gonzalez L.A., Carpenter S.J. and Lohmann K.C., (1992) Inorganic calcite morphology: Roles of fluid chemistry and fluid flow. *J of Sedimentary Petrology*, **62**, p. 382-399

Granbakken D. et al.. (1989) Scale formation in reservoir and production equipment during oil recovery-III. A kinetic model for the precipitation/dissolution reactions. SPE 19395, Unsolicited.

Gratz A.J. and Hillner P.E., (1993) Poisoning of calcite growth viewed in the atomic force microscope (AFM). *J. of Crystal Growth*, **129**, p. 789-793.

Gratz A.J., Hillner P.E. and Hansma P.K., (1993) Step dynamics and spiral growth on calcite. *Geochimica et Cosmochimica Acta*, **57**, p. 491-495.

Griffioen J. and Appelo C.A.J., (1993) Nature and extent of carbonate precipitation during aquifer thermal energy storage", *Applied Geochemistry*, **8**, p. 161-176.

Gunn D.J., (1980) "Effect of surface roughness on the nucleation and growth of calcium sulphate on metal surfaces. *J. of Crystal Growth*, **50**, p. 533-537.

Haarberg T. et al., (1989) Scale formation in reservoir and production equipment during oil recovery - II. A thermodynamic model for the solubility of scale forming minerals applied in an equilibrium approach to calculate mineral precipitation during oil recovery. SPE 19449, Unsolicited.

Hartley G. and Mucci A., (1996) The influence of pCO_2 on the partitioning of magnesium in calcite overgrowths precipitated from artificial seawater at 25°C and 1 atm total pressure, *Geochimica et Cosmochimica Acta,* **60**, p. 315-324.

Hartman P., (1973) Crystal growth : An introduction, Ed. by Hartman P., Amsterdam North-Holland Pub. Co, 1973. - (North-Holland series in crystal growth, v. 1).

Hasson D., Avriel M., Resnick W., Rozenman T. and Windreich S., (1968) Mechanism of calcium carbonate scale deposition on heat-transfer surfaces. *Industrial and Engineering Chemistry Fundamentals*, **7**, No.1, p. 59-65.

House W.A., (1981) Kinetics of crystallization of calcite from calcium bicarbonate solutions. *J. Chem. Soc., Faraday Trans.* 1, **77**, p. 341-359.

House W.A., (1987) Inhibition of calcite crystal growth by inorganic phosphate, J. *Colloid Interface Sci.*, **119**, p. 505-511.

House W.A., (1989) Reactions at the Liquid-Solid Interface, Vol. 28 of Comprehensive Chemical Kinetics, (edit by Compton R.G.), Elsevier.

House W.A. and Howson M.R., (1988) Crystallisation kinetics of calcite in the presence of magnesium ions. *J. Chem. Soc. Faraday Trans I,* **84**, p. 2723-2734.

House W.A. and Tutton J.A., (1982) An investigation of the heterogeneous nucleation of calcite. *J. of Crystal Growth*, **56**, p. 699-710.

Inskeep W.P and Bloom P.R., (1985) An evaluation of rate equations for calcite precipitation kinetics at pCO_2 less than 0.01 atm and pH greater than 8. *Geochimica et Cosmochimica Acta,* **49**, p. 2165-2180.

Inskeep W.P and Bloom P.R., (1986) Kinetics of calcite precipitation in the presence of water-soluble organic ligands. *Siol Sci. Soc. AM. J*, **50**, p. 1167-1172.

Kaasa B. and Østvold T., (1997) Alkalinity in oil field waters. What alkalinity is and how it is measured. SPE 37277, International Symposium on Olifield Chemistry held in Houston, Texas, Feb. 18-21.

Katz J.L., et al., (1993) Calcite growth inhibition by iron. *Langmuir*, **9**, p. 1423-1430.

Kazmlerczak T.F., Tomson M.B. and Nancollas G.H., (1982) Crystal growth of calcium carbonate. A controlled composition kinetic study. *J. of Phys. Chem*, **77**, p. 103-107.

Kharaka Y.K., Gunter W.D. et al., (1988) Solmineq 88: A computer program for geochemical modelling of water-rock interactions. US Geological Survey, Water-Resources Investigations Report, California, p. 88-4221.

Kharaka Y.K., Law L.M., Carothers w.W. and Gocrlitz D.F., (1986) Role of organic species dissolved in formation waters from sedimentary basins in mineral diagenesis. *SEPM*, **38**, p. 111-122.

Kotrly S. and Stanislav L., (1985) Handbook of Chemical Equilibria in Analytical Chemistry. eds by Chalmers R.A. and Masson M., Ellis Horwood, Chichester.

Koutsoukos P., Amjad, Z., Tomson, M.B. and Nancollas, G.H. (1980) Crystallization of calcium phosphates. A constant composition study. *J. Am. Chem. Soc.*, **102**, p. 1553-1557.

Lafon G.M., (1971) Calcium complexing with carbonate ion in aqueous solutions at 20°C and 1 atmosphere. *Geochimica et Cosmochimica Acta,* **34**, p. 935-942.

Langelier T.E., (1936) The analytical control of anti-corrosion water treatment. *J of A.W.W.A.*, **28**, p. 1500-1505.

Larson T.E. Sollo F.W. and McGurk F.F., (1976) Complexed affecting the solubility of calcium carbonate in water - Phase II. UILU-WRC - 76 - 0108.

Lebron I. and Suarez K.L., (1996), Calcite nucleation an precipitation kinetics as affected by dissolved organic matter at 25°C and pH > 7.5. *Geochimica et Cosmochimica Acta,* **60**, p. 2765-2776.

Lejon A.U. and Vikane O., (1996) Use of scale dissolver and scale inhibitor squeeze treatments to repair and prevent formation damage in two Statfjord field well. SPE 31126, International Symposium on Formation Damage Control, held in Lafayette.

Loewenthal R.E. and Marais C.v R., (1984) Carbonate Chemistry of Aquatic Systems, Volume 2: High Salinity Waters, Butterworths

Lovekin J.W., (1990) Control of calcium carbonate scale using concentric tubing at Coso Geothermal Field. Transactions - Geothermal Resources Council, 1990, **14**, No.2, p. 1611-1617.

MacGowan, D.B., Surdam R.C. and Ewing R.E., (1990) The effect of carboxylic acid anions on the stability of framework mineral grains in petroleum reservoirs. SPE Formation Evaluation. p. 161-165.

Markov I.V. (1995) Crystal Growth fro Beginners - Fundamentals of nucleation, crystal growth and epitaxy. World Scientific.

Momozaki K. et al., (1992) Polyacrylamide based treatment program for open recirculating cooling water system with high silica content. SPE Annual Meeting - International Water Conference, p. 84-89.

Morse J.W., (1974a) Dissolution kinetics of calcium carbonate in sea water. III. A new method for the study of carbonate reaction kinetics. *Amer. J. Sci.,* **274**, p. 97-107.

Morse J.W., (1974b) Dissolution kinetics of calcium carbonate in sea water. V. Effects of natural inhibitors and the position of the chemical lysocline. *Amer. J. Sci.,* **274**, p. 638-647.

Morse J.W,. (1978) Dissolution kinetics of calcium carbonate in sea water. VI. The near-equilibrium dissolution kinetics of calcium carbonate-rich deep sea sediments. *Amer. J. Sci.,* **278**, p. 344-353.

Morse J.W. and Mackenzie F.T., (1990) Geochemistry of Sedimentary Carbonates. Elsevier.

Mucci A. and Morse J.W. (1983) The incorporation of Mg^{2+} and Sr^{2+} into calcite overgrowths: influences of growth rate and solution composition. *Geochimica et Cosmochimica Acta,* **47**, p. 217-233.

Mucci A. and Zhong J.W. (1989) The solubility of calcite and aragonite in sulphate-free seawater and the seeded growth kinetics and composition of the precipitates at 25°C. *Chem. Geology.* **74**, p. 309-320.

Mullin J.W., (1994) Crystallisation, Butterworth Heinenann.

Nakayama F.S., (1968) Calcium activity, complex and ion pair in saturated $CaCO_3$ solutions. *Soil Sci.* **106**, p. 429-434.

Nancollas G.H. and Reddy M.M. (1971) The crystallisation of calcium carbonate. II. Calcite growth mechanism. *J. Colloid Interface Sci.* **37**, p. 824-830.

Nancollas G.H. and Reddy M.M. (1974) The kinetics of crystallisation of scale-forming minerals. *SPEJ.*, p. 117-126.

Nielsen A.E. (1984) Electrolyte crystal growth kinetics. *J. of Crystal Growth*, **67**, p. 289-310.

Nielsen A.E. and Toft J.M. (1984) Electrolyte crystal growth kinetics. *J. of Crystal Growth*, **67**, p. 278-288.

Oddo J.E., Sitz C.D., Ortiz I., Linz D.G., Lawrence A.W., Kan A.T. and Tomson M.B., (1993) NORM scale formation: a case study of the chemistry prediction, remediation, and treatment in wells of the antrim gas field. SPE 25937, SPE/EPA Exploration and Production Environmental Conference held in San Antonio, Texas, 7-10 March.

Oddo J.E., and Tomson M.B., (1982) Simplified calculation of $CaCO_3$ saturation at high temperatures and pressures in brine solutions. *J. of Petroleum Technology*, p. 1583-1590.

Oddo J.E., and Tomson M.B., (1994) Why scale forms and how to predict it. *SPEPF*, Feb., p. 47-53.

Osborne C.G., Ravenscroft P.D. and McCracken I.R., (1994) Predicted water chemistry trends in North Sea formation brines. *Marine and Petroleum Geology*, **11**, p. 20-23.

Paquette J. and Reeder R.J., (1995) Relationship between surface structure, growth mechanism, and trace element incorporation in calcite.. *Geochimica et Cosmochimica Acta,* **59**, p. 735-749.

Pankow J. F., (1991) Aquatic Chemistry Concepts. Lewis.

Pitzer K.E., (1973a) Thermodynamics of electrolytes. I. Theoretical basis and general equations. *J. of Physical Chemistry*, **77**, p. 268-277.

Pitzer K.E., (1973b) Thermodynamics of electrolytes. II. Activity and osmotic coefficients for strong electrolytes with one of both ions univalent. *J. of Physical Chemistry*, **77**, p. 2300-2308.

Pitzer K.E., (1981) Characteristics of very concentrated aqueous solution. In chemistry and geochemistry of solutions of high temperatures and pressure. *Physics and Chemistry of the Earth*, **13-14**, p. 249-272.

Pitzer K.E. (1979) Theory: Ion interaction approach In Activity Coefficients in Electrolyte Solutions, Vol. I (edit by Pytkowicz R.M.), p. 157-208.

Pitzer K.E. and Mayorga G., (1973) Thermodynamics of electrolytes. II. Activity and osmotic coefficients for strong electrolytes with one of both ions univalent. *J. of Physical Chemistry*, **77**, p. 2300-2308.

Pitzer K.E. and Silvester L.F., (1977) Thermodynamics of electrolytes. 8. High-temperature properties, including enthalpy and heat capacity, with application on sodium chloride, *J. of Physical Chemistry*, **81**, p. 1822-1829.

Pitzer K.E. and Silvester L.F., (1978) Thermodynamics of electrolytes. X. enthalpy and the effect of temperature on the activity coefficients, *J. Sol. Chem.*, **7**, p. 327-333.

Plummer L.N. and Busenbery E. (1982) The solution of calcite, aragonite and vaterite in CO_2-H_2O solution between 0 and 90°C and an evaluation of the aqueous model for the system $CaCO_3$ -CO_2-H_2O. *Geochimica et Cosmochimica Acta,* **46**, p. 1011-1040.

Plummer L.N. and Mackenzie F.T., (1974) Predicting mineral solubility from rate data: Application to the dissolution of magnesium calcites. *Amer. J. Sci.* **274**, p. 61-83.

Plummer L.N., Wigley T.M., (1976) The dissolution of calcite in CO_2 saturated solutions at 25°C and 1 atmospheric total pressure. *Geochimica et Cosmochimica Acta,* **40**, p. 191-202.

Plummer L.N., Wigley T.M. and Parkhurst D.L. (1978) The kinetics of calcite dissolution in CO_2-water systems at 5 to 60°C and 0.0 to 1.0 atm CO_2. *Amer. J. Sci.* **278**, p. 179-216.

Powell R.J., Gdanski R.D., McCabe M.A. and Buster D.C. (1995) Controlled-release scale inhibitor for use in fracturing treatments, SPE 28999, SPE International Symposium on Oilfield Chemistry.

Reddy M.M. and Gaillard W.D., (1981) Kinetics of calcium carbonate (calcite)-seeded crystallisation: influence of Solid/solution ratio on the reaction rate constant. *J of Colloid and Interface Sci.*, **80**, p. 171-177.

Reddy M.M. and Nancollas G.H., (1971) The crystallisation of calcium carbonate: I. Isotopic exchange and kinetics. *J. of Colloid and Interface Sci.*, **36** p. 166-172.

Reddy M.M. and Nancollas G.H., (1973) Calcite crystal growth inhibition by phosphonates: *Desalination*, **12** p. 61-73.

Reddy M.M., Plummer L.N. and Busenberg E., (1981) Crystal growth of calcite from calcium bicarbonate solutions at constant pCO_2 and 25°C: a test of a calcite dissolution model. *Geochimica et Cosmochimica Acta,* **45**, p. 1281-1289.

Reeder R.J., Fagioli R.O. and Meyers W.J., (1990), Oscilllatory zoning of Mn in solution-grown calcite crystals. *Earth-Science Reviews*, **29,** p. 39-46.

Reeder R.J. and Grams J.C., (1987), Sector zoning in calcite cement crystals: Implications for trace element distributions in carbonates. *Geochimica et Cosmochimica Acta,* **51**, p. 187-194.

Sandler S.I., (1994) Models for thermodynamic and phase equilibria calculations. Marcel Dekker, Inc.

Sass E., Morse J.W. and Millero F.J., (1983) Dependence of values of calcite and aragonite thermodynamic solubility products on ionic models. *Amer. J. Sci.,* **238**, p. 218-229.

Schmidt T. and Bentsen S., (1992) A method for correctly predicting the precipitation of calcium carbonate scale. Advances in solving oilfield scaling problems, conference documentation, Aberdeen.

Shiraki R. and Brantley S.L., (1995) Kinetics of near-equilibrium calcite precipitation at 100oC: An evaluation of elementary reaction-based and affinity-based rate laws. *Geochimica et Cosmochimica Acta,* **59**, p. 1457-1471.

Silvester K.S. and Pitzer K.S., (1978) Thermodynamics of electrolytes. X. Enthalpy and the effect of temperature on the activity coefficients. *J. Soln. Chem.* 7, p. 327-337.

Sjöberge E.L. and Rickard D.T., (1983) The influence of experimental-design on the rate of calcite dissolution. *Geochimica et Cosmochimica Acta,* **47**, p. 2281-2285.

Sorbie K.S. and Jiang P. et al., (1993) Effect of pH, calcium, and temperature on the adsorption of phosphonate inhibitor onto consolidated and crushed sandstone. SPE 26605, SPE Annual Technical Conference and Exhibition, Oct.

Sorbie K.S. and Yuan M.D. et al., (1993) Effect of pH on the adsorption and transport of phosphonate scale inhibitor through porous media. SPE 25165, International Symposium on Oilfield Chemistry, 1993, Mar.

Söhnel O. and Garside J., (1992) Precipitation - Basic Principles and Industrial Applications. Butterworth Heinemann.

Staudt W.J., Reeder R.J. and Schooner M.A.A., (1994), Surface structural controls on composition zoning of SO_4^{2} and SeO_4^{2-}. *Geochimica et Cosmochimica Acta,* **58**, p. 2087-2098.

Stiff H.A. and Davis L.E., (1952) A method of predicting the tendency of field waters to deposit calcium carbonate. *Pet. Trans., AIME,* **195**, p. 213-218.

Stumm W. and Morgan J.J., (1996) Aquatic chemistry - Chemical equilibria and rates in natural waters, Third edition, A Wiley - Interscience Publication, p. 69 - 76.

Sweeney F.M. and Cooper S.D. (1993), The development of a Novel scale inhibitor for severe water chemistries. SPE 25159, International Symposium on Oilfield Chemistry held in New Orleans, LA, USA Mar.

Titiloye J.O., Parker S.C., Osguthorpe D.J. and Mann S., (1991), Predicting the influence of growth additives on the morphology of ionic crystals. *J. Chem. Soc. Chem. Commun.*, p. 1494 - 1496

Tomson M.B., Matty J. and Oddo J.E., (1990) Scale inhibitor evaluations and a mechanism of inhibition of sparingly soluble salts. SPE 21571, Society of Petroleum Engineers of AIME.

Vetter O.J., (1980) Prediction of $CaCO_3$ scale under downhole conditions. SPE 8991, 5th Oilfield Geothermal Chemistry, California, May 28-30.

Vetter O.J., (1987) Calcium carbonate scale in oilfield operations. SPE 16908, 62nd Annu. Tech. Conf., Dallas, Tex. Sep. 27-30.

Warren E.A. and Smalley P.C., (1994) North Sea Formation Waters Atlas, Geological Society Memoir No. 15.

Weyl, P.K., (1958) The solution dinetics of calcite. *J. of Geology*, **66**, p. 163-176.

Wiechers, H.N.S., Sturrock, P., and Morais, G.V.R., (1975), Calcium carbonate Crystallization kinetics. Water Res., **9**, p. 835-845.

Wright R.J., Hall J.R.F. and McIntosh C.J. (1994) Scale prediction, measurement, and control in a subsea. SPE 27606, Presented in European production operations conference in Aberdeen, U.K., 12 - 17 March.

Yeboah Y.D., Somuah S.K. and Saeed M.R., (1993) A new and reliable model for predicting oilfield scale formation. SPE 25166, International symposium on Oilfield Chemistry held in New Orleans, LA, USA., March 2-5.

Zhong S. and Mucci A., (1989) Calcite and aragonite precipitation from seawater solutions of various salinities: Precipitation rates and overgrowth compositions. *Chemical Geology*, **78**, p. 283-299.

Zhong S. and Mucci A., (1993) Calcite precipitation in seawater using a constant addition technique: A new overall reaction kinetic expression. *Geochimica et Cosmochimica Acta*, **57**, p. 1409-1417.

Zuddas P. and Mucci A., (1994) Kinetics of calcite precipitation from seawater: I. A classical chemical kinetics description for strong electrolyte solutions. *Geochimica et Cosmochimica Acta*, **58**, p. 4353-4362.

Zullig J.J. and Morse J.W., (1988) Interaction of organic acids with carbonate mineral surfaces in seawater and related solutions: I. Fatty acid adsorption. *Geochimica et Cosmochimica Acta*, **52**, p. 1667-1678.